KINETIC ASSESSMENT OF THE PRODUCTION OF ACETINS VIA GLYCEROL ESTERIFICATION WITH ACETIC ACID OVER AMBERLYST-35

KAREN VANNESSA CABALLERO PÉREZ
CHEMICAL ENGINEER

UNIVERSIDAD INDUSTRIAL DE SANTANDER
FACULTAD DE INGENIERÍAS FÍSICOQUÍMICAS
ESCUELA DE INGENIERÍA QUÍMICA
MAESTRÍA EN INGENIERÍA QUÍMICA
BUCARAMANGA
2019

KINETIC ASSESSMENT OF THE PRODUCTION OF ACETINS VIA GLYCEROL ESTERIFICATION WITH ACETIC ACID OVER AMBERLYST-35

KAREN VANNESSA CABALLERO PÉREZ
CHEMICAL ENGINEER

RESEARCH WORK PRESENTED AS A REQUIREMENT TO APPLY FOR THE DEGREE OF
MAGÍSTER EN INGENIERÍA QUÍMICA

ADVISOR
PROF. VÍCTOR GABRIEL BALDOVINO MEDRANO
CHEMICAL ENGINEER, PHD

CO-ADVISOR
PROF. GUSTAVO EMILIO RAMÍREZ CABALLERO
CHEMICAL ENGINEER, PHD

UNIVERSIDAD INDUSTRIAL DE SANTANDER
FACULTAD DE INGENIERÍAS FÍSICOQUÍMICAS
ESCUELA DE INGENIERÍA QUÍMICA
MAESTRÍA EN INGENIERÍA QUÍMICA
BUCARAMANGA
2019

ACKNOWLEDGEMENTS

This work was done thanks to the financial support from the Vicerrectoría de Investigaciones UIS within the frame of the project No. 1319: Obtención de productos de alto valor agregado a partir de la glicerina cruda.

I want to thank to the professors Víctor Baldovino and Sonia Giraldo for their guidance during this research work. Likewise, thanks to all the professors that belong to the Centro de Investigaciones en Catálisis, CICAT.

I thank to the professor Carlos Omar Castillo from the Group of Chemical Engineering of the Universidad Autónoma Metropolitana – Iztapalapa, CDMX, who collaborated in this work with programing code and his good advice in the kinetic topics.

I want to express special thanks to all my laboratory partners(seb), whom I shared great experiences and stablished a true friendship.

Thanks to all my family, colleagues and friends, who spent their time and supported me during this adventure, especially in the “ugly parts”. I had not could done it without them.

This work is dedicated to:

My mom, Lucy.

CONTENTS

SUPPLEMENTARY INFORMATION

LIST OF FIGURES

INTRODUCTION

CHAPTER 1

CHAPTER 2

LIST OF TABLES

INTRODUCTION

CHAPTER 1

CHAPTER 2

LIST OF SYMBOLS

A: acetic acid. Pre-exponential factor [mmol/g h]

C: mole fraction [mmol]

D: diacetin

D_e: effective diffusivity

E_a: activation energy [kJ/mol]

G: glycerol

k_i: apparent kinetic constant of the *ith* reaction

K_i: equilibrium constant of the *ith* reaction

K_n: equilibrium adsorption constant of component n

M: monoacetin

r: reaction rate [mmol/g h]

R: acetic acid to glycerol molar ratio. Universal gas constant [kJ/mol K]. Radius of the catalyst particle [μm].

RSS: objective function

T: triacetin. temperature [K]

w: weight factor

W: water

*: active site

GREEK LETTERS

α: significance level

ΔS°: standard entropy change [kJ/mol K]

ΔH° standard enthalpy change [kJ/mol]

η: effectiveness factor

μ*: moles of active sites [mmol]

ν: stoichiometric number

φ: optimal parameter vector

Φ: Thiele modulus

Φ_{WP}: Waitz-Prater parameter

SUBSCRIPTS

ads: adsorption

exp: experiment

g: gas phase

l: liquid phase

n: component.

P: products

r: reaction

R: reactants

resp: response

SUPERSCRIPTS

B: backward

F: forward

^: calculated

*: average

RESUMEN

TÍTULO: EVALUACIÓN CINÉTICA DE LA PRODUCCIÓN DE ACETINAS VÍA ESTERIFICACIÓN DE GLICEROL CON ÁCIDO ACÉTICO SOBRE AMBERLYST-35

AUTOR: KAREN VANNESSA CABALLERO PÉREZ*[*]

PALABRAS CLAVE: ACETINAS, ESTERIFICACIÓN DE GLICEROL, AMBERLYST-35, LIMITACIONES DIFUSIONALES, CINÉTICA.

DESCRIPCIÓN:

La producción de acetinas se presenta como una alternativa de valorización de las grandes cantidades de glicerol que se encuentra en el mercado. La esterificación del glicerol con ácido acético catalizada con sólidos ácidos ha sido estudiada ampliamente en los últimos años, sin embargo, estudios cinéticos de esta reacción son escasos. Este trabajo desarrolla una metodología sistemática para el análisis estadístico de la reacción, catalizada con Amberlyst-35, controlando las variables temperatura, cantidad de sitios activos del catalizador, y relación molar de ácido acético – glicerol, en rangos de operación establecidos por la literatura. Estos mismos datos se evaluaron bajo el criterio de Madon-Boudart, el cual reveló que, bajo las actuales condiciones de reacción, el sistema catalítico trabaja con efectos de limitaciones difusionales. Luego de variar el tamaño de partícula del catalizador, se establecieron las condiciones necesarias para que el sistema de reacción trabaje en régimen cinético. El cálculo del factor de efectividad y módulo de Thiele soportan esta conclusión. Como objetivo principal, en este trabajo se desarrollan expresiones cinéticas para la formación de monoacetina, diacetina y triacetina, asumiendo un mecanismo Eley-Rideal, donde los pasos que implican reacción en superficie fueron establecidos como los RDS. En adición, los parámetros cinéticos obtenidos cumplen los criterios de Boudart y el balance termodinámico. Por lo tanto, este trabajo presenta modelos cinéticos para la formación de acetinas con capacidad predictiva del comportamiento de la reacción qué, además provee mayor conocimiento de la dinámica molecular del sistema catalítico.

---

*Proyecto de Maestría

**Facultad de Ingenierías Físicoquímicas. Escuela de Ingeniería Química. Director: Prof. Víctor Gabriel Baldovino Medrano. Codirector: Prof. Gustavo Emilio Ramírez Caballero.

ABSTRACT

TITTLE: KINETIC ASSESSMENT OF THE PRODUCTION OF ACETINS VIA GLYCEROL ESTERIFICATION WITH ACETIC ACID OVER AMBERLYST-35

AUTHOR: KAREN VANNESSA CABALLERO PÉREZ*[*]

KEYWORDS: ACETINS, GLYCEROL, AMBERLYST-35 DIFFUSION LIMITATIONS, KINETICS.

DESCRIPTION:

The acetins production is presented as an alternative of valorizing glycerol due to its large quantities in the market. The glycerol esterification with acetic acid catalyzed by solid acids have been studied extensively during the last years. Nevertheless, kinetic studies about this reaction are scarce. This work develops a systematic methodology for the statistical analysis of this reaction, which is catalyzed by Amberlyst-35, controlling the variables temperature, quantity of active sites of the catalyst, and acetic acid – glycerol molar ratio, between the ranges stablished by literature. These data were evaluated by the Madon-Boudart criterium, which showed that, at the current reaction conditions, the catalytic system works under effects of diffusion limitations. Thereby, after varying the catalyst particle size, the necessary conditions for the catalytic system works in kinetic regime were stablished. The calculation of the effectiveness factor and the Thiele modulus support the latter conclusion. As the main objective in this work, kinetic expressions for the monoacetin, diacetin and triacetin formation were developed. Eley-Rideal mechanism was assumed, where the steps involved in surface reaction are stablished as the RDS. In addition, the kinetic parameters obtained fulfill the Boudart criteria and the thermodynamic balance. Therefore, this work presents kinetic models for the acetins formation which can predict the kinetic behavior of the reaction, but also, provides more knowledge about the molecular dynamics of the catalytic system.

---

*Magister Project

**Facultad de Ingenierías Físicoquímicas. Escuela de Ingeniería Química. Advisor: Prof. Víctor Gabriel Baldovino Medrano. Co-advisor: Prof. Gustavo Emilio Ramírez Caballero.

INTRODUCTION

KINETIC ASSESSMENT OF THE PRODUCTION OF ACETINS: AN ALTERNATIVE OF VALORIZING GLYCEROL

Nowadays, the market has a huge amount of glycerol due to high demand for biodiesel. Just in Colombia there are 12 biodiesel plants with a production capacity of 986000 T/year [1]. The production of biodiesel from vegetable oils transesterification provides over 10% wt. of raw glycerol as byproduc [2]. Glycerol is a very well-known platform molecule. Nevertheless, the raw glycerin has a purity around the 80% which is not enough for conventional applications. Therefore, scores of papers dealing with its catalytic conversion have been published [3–5]. One of the multiple options to upgrade glycerol is via its liquid phase esterification to corresponding acetins [6–9]. Acetins from glycerol esterification is a mixture of esters composed by monoacetin, diacetin and triacetin. These compounds have plenty of applications in the food, pharmaceutical and biopolymeric industries, among others [10–13]. In addition, triacetin has potential as additive fuel. This oxygenate additive has the capacity to enhances the fuel properties during the engine operation, such as prevent the incomplete combustion, provide protection against corrosion, and thermal stability and viscosity of biodiesel in cool conditions. Moreover, triacetin is biodegradable and non-toxic to the environmental [6,8,14]. The Figure 1 presents the reaction of glycerol with acetic acid.

[1]FEDEBIOCOMBUSTIBLES, [online: 2018]. http://www.fedebiocombustibles.com/v3/estadistica-mostrar_info-titulo-Biodiesel.htm.
[2]M.S. Khayoon, B.H. Hameed, Bioresour. Technol. 102 (2011) 9229–9235.
[3]N. Rahmat, A.Z. Abdullah, A.R. Mohamed, Renew. Sustain. Energy Rev. 14 (2010) 987–1000.
[4]A. Gonzalez-Garay, M. Gonzalez-Miquel, G. Guillen-Gosalbez, ACS Sustain. Chem. Eng. 5 (2017) 5723–5732.
[5]H. Rastegari, H.S. Ghaziaskar, M. Yalpani, Ind. Eng. Chem. Res. 54 (2015) 3279–3284.
[6]P.S. Reddy, P. Sudarsanam, G. Raju, B.M. Reddy, Catal. Commun. 11 (2010) 1224–1228.
[7]K. Jagadeeswaraiah, M. Balaraju, P.S.S. Prasad, N. Lingaiah, Appl. Catal. A Gen. 386 (2010) 166–170.
[8]I. Dosuna-Rodríguez, C. Adriany, E.M. Gaigneaux, Catal. Today. 167 (2011) 56–63.
[9]L.N. Silva, V.L.C. Gonçalves, C.J.A. Mota, Catal. Commun. 11 (2010) 1036–1039.
[10]J. Bonet, J. Costa, R. Sire, J.M. Reneaume, A.E. Pleşu, V. Pleşu, G. Bozga, Food Bioprod. Process. 87 (2009) 171–178.
[11]X. Liao, Y. Zhu, S.G. Wang, H. Chen, Y. Li, Appl. Catal. B Environ. 94 (2010) 64–70.
[12]P. Ferreira, I.M. Fonseca, A.M. Ramos, J. Vital, J.E. Castanheiro, Catal. Commun. 12 (2011) 573–576.
[13]V.L.C. Gonçalves, B.P. Pinto, J.C. Silva, C.J.A. Mota, Catal. Today. 133–135 (2008) 673–677.
[14]M. Balaraju, P. Nikhitha, K. Jagadeeswaraiah, K. Srilatha, P.S. Sai Prasad, N. Lingaiah, Fuel Process. Technol. 91 (2010) 249–253.

Catalytic materials with acidic character favor the esterification of glycerol. Both homogeneous and heterogeneous catalysts have been employed for the reaction. As it might be expected, homogeneous catalysts rapidly achieve equilibrium conversions; i.e. 100% conversion of glycerol, and appreciable yields of the most valued triacetin product [15,16]. However, the fact that homogeneous catalysts are normally sulfuric, phosphoric or an organic acid [17–21], make them environmentally and economically problematic. Acids are frequently toxic, corrosive and hard to remove from the product. Heterogeneous catalysts avoid these inconveniencies. Solids with acidic properties such as: zeolites, sulfated metal oxides, activated carbon, heteropolyacids, and ion exchange resins, among others, have thus been subject to extensive research [6–9,14,22–25]. Among these materials, those with a high concentration of surface Brønsted acid sites are most promising since they fulfill reaction requirements [20,23].

Cation exchange resins such as Amberlyst-15 and Amberlys-35 have received especial attention due to their high acidity and chemical stability under the reaction conditions employed for glycerol valorization [5,25–28]. Reactions are typically carried out in batch reactors in liquid phase, at temperatures between 313 – 393 K, with catalyst loadings between 1 – 7%, and using acetic acid to glycerol molar ratios between 3 to 9.

[5]H. Rastegari, H.S. Ghaziaskar, M. Yalpani, Ind. Eng. Chem. Res. 54 (2015) 3279–3284.
[6]P.S. Reddy, P. Sudarsanam, G. Raju, B.M. Reddy, Catal. Commun. 11 (2010) 1224–1228.
[7]K. Jagadeeswaraiah, M. Balaraju, P.S.S. Prasad, N. Lingaiah, Appl. Catal. A Gen. 386 (2010) 166–170.
[8]I. Dosuna-Rodríguez, C. Adriany, E.M. Gaigneaux, Catal. Today. 167 (2011) 56–63.
[9]L.N. Silva, V.L.C. Gonçalves, C.J.A. Mota, Catal. Commun. 11 (2010) 1036–1039.
[15]D. Gelosa, M. Ramaioli, G. Valente, M. Morbidelli, Ind. Eng. Chem. Res. 42 (2003) 6536–6544.
[16]Z. Mufrodi, Int. J. Chem. 4 (2012) 101–107.
[17]A. Izci, F. Bodur. React. Funct. Polym. 67 (2007) 1458–1464.
[18]M.P. Pico, A. Romero, S. Rodríguez, A. Santos, Ind. Eng. Chem. Res. 51 (2012) 9500–9509.
[19]V.K.S. Pappu, V. Kanyi, A. Santhanakrishnan, C.T. Lira, D.J. Miller, Bioresour. Technol. 130 (2013) 793–797.
[20]P.U. Okoye, A.Z. Abdullah, B.H. Hameed, Renew. Sustain. Energy Rev. 74 (2017) 387–401.
[21]S. Veluturla, A. Narula, S.R. D, S.P. Shetty, Resour. Technol. 3 (2017) 337–341.
[22]J.A. Sánchez, D.L. Hernández, J.A. Moreno, F. Mondragón, J.J. Fernández, Appl. Catal. A Gen. 405 (2011) 55–60.
[23]M.S. Khayoon, S. Triwahyono, B.H. Hameed, A.A. Jalil, Chem. Eng. J. 243 (2014) 473–484.
[24]P.S. Reddy, P. Sudarsanam, G. Raju, B.M. Reddy, J. Ind. Eng. Chem. 18 (2012) 648–654.
[25]X. Liao, Y. Zhu, S.G. Wang, Y. Li, Fuel Process. Technol. 90 (2009) 988–993.
[26]A. Hasabnis, S. Mahajani, Ind. Eng. Chem. Res. 49 (2010) 9058–9067.
[27]R.P.V. Faria, C.S.M. Pereira, V.M.T.M. Silva, J.M. Loureiro, A.E. Rodrigues, Ind. Eng. Chem. Res. 52 (2013) 1538–1547.
[28]I. Dosuna-Rodríguez, E.M. Gaigneaux, Catal. Today. 195 (2012) 14–21.

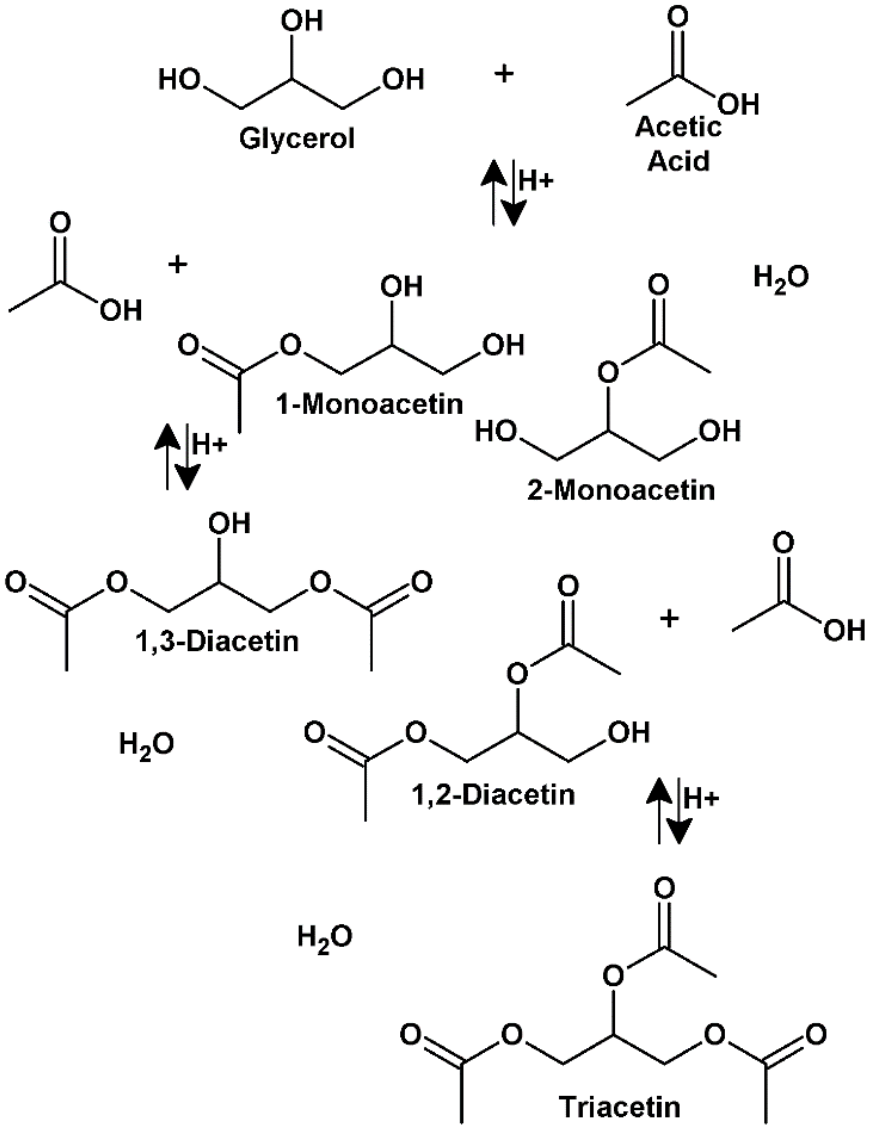

Figure 1. Reaction scheme for glycerol esterification with acetic acid to formation of acetins.

Provided the interest on both understanding the mechanism of the reaction [2,9,29] and scaling-up the process [5,10,26,30], the kinetic modeling of glycerol esterification with acetic acid over solid catalysts has been tackled in open literature [20]. Khayoon et al. [23] developed a kinetic model for glycerol esterification with acetic acid catalyzed by yttrium supported in SBA-3. They propose this reaction follow a Langmuir-Hinshelwood mechanism, where the rate limiting step is the reaction on the catalyst surface and the water adsorption is not taken into account. However, the calculations of the kinetic and thermodynamic terms are based in a pseudo-first order reaction rate model. Moreover, authors introduced a correction term in their kinetic model for mass transfer limitations. Therefore, they acknowledged that their measurements were not performed under kinetic regime. Patel & Singh [31] postulated a first order kinetic model for the reaction over MCM-41 and zirconia anchored to tungstophosphoric acid and claimd that their measurements were free of diffusion limitations after performing the test proposed by Koros & Nowak [32]. They seem to have overlooked the fact that such a test is designed for packed bed reactors with reactants in gas phase though. In addition, they reporter Turn Over Frequencies (TOF) from to relation of the Turn Over Numbers (TON)/ a time reaction. The TON is based on a “moles of products obtained/ moles of catalyst (active species)” ratio, and the time reaction is a time where the glycerol conversion is equal to all their reactions. Therefore, this methodology is not clear, and it might not be appropriate to compare with other kinetic works.

[2]M.S. Khayoon, B.H. Hameed, Bioresour. Technol. 102 (2011) 9229–9235.
[5]H. Rastegari, H.S. Ghaziaskar, M. Yalpani, Ind. Eng. Chem. Res. 54 (2015) 3279–3284.
[9]L.N. Silva, V.L.C. Gonçalves, C.J.A. Mota, Catal. Commun. 11 (2010) 1036–1039.
[10]J. Bonet, J. Costa, R. Sire, J.M. Reneaume, A.E. Pleşu, V. Pleşu, G. Bozga, Food Bioprod. Process. 87 (2009) 171–178.
[20]P.U. Okoye, A.Z. Abdullah, B.H. Hameed, Renew. Sustain. Energy Rev. 74 (2017) 387–401.
[23]M.S. Khayoon, S. Triwahyono, B.H. Hameed, A.A. Jalil, Chem. Eng. J. 243 (2014) 473–484.
[26]A. Hasabnis, S. Mahajani, Ind. Eng. Chem. Res. 49 (2010) 9058–9067.
[29]L. Zhou, T.H. Nguyen, A.A. Adesina, Fuel Process. Technol. 104 (2012) 310–318.
[30]S.K. Hung, C.C. Lee, H.Y. Lee, C.L. Lee, I.L. Chien, Ind. Eng. Chem. Res. 53 (2014) 11989–12002.
[31]A. Patel, S. Singh, Fuel. 118 (2014) 358–364.
[32]R.M. Koros, E.J. Nowak, Chem. Eng. Sci. 22 (1967) 470.

Gelosa et al. [15] developed a first order reaction rate expression for glycerol esterification with acetic acid over an acidic polymeric resin as catalyst. The authors discarded the occurrence of mass transport limitations by making tests at different stirring rates and comparing catalytic results. According to their analysis, overlapping of curves representing mass fraction of the reactants and products of the reaction allowed discarding “interphase mass transport resistances”. For “intraphase mass transport resistances”, authors used a “nonreactive experiment”. A small quantity of water was added to the reactor with a mixture of catalyst and glycerol and its concentration was monitored. The transport process took about 10 min. Thence, the authors admitted this resistance has a significant effect on the kinetics. However, such methodologies are not conclusive enough for discarding mass transport limitations [33]. On the other hand, Zhou et al. [29] developed a kinetic study of glycerol esterification over an Amberlyst-15 catalyst. In the experimental section of their paper, these authors stated: “The solid was then grounded into finer particles and fractions in the size range of 90 – 200 μm were selected for experiment. It was found that in this range the size of the catalysts has almost no effect on glycerol conversion and the product distribution”. Under the conditions employed in their experiments, authors determined activation energies equal to 57.26, 31.87 and 13.90 kJ/mol, for the consecutive transformation of glycerol to triacetin. The statement made by the authors in the experimental section of the paper; i.e. “almost no effect”, and the fact that they report an activation energy below 21 kJ/mol [34] cast serious doubts on whether their measurements were carried out under a kinetic regime. Rane et al. present a kinetic study for glycerol esterification catalyzed by SO_4^{2-}/ɣ-Al_2O_3. They developed the kinetics models of pseudo-first order and pseudo-second order for this reaction. The activation energy values are 47.13 and 106 kJ/mol, respectively.

[15]D. Gelosa, M. Ramaioli, G. Valente, M. Morbidelli, Ind. Eng. Chem. Res. 42 (2003) 6536–6544.
[29]L. Zhou, T.H. Nguyen, A.A. Adesina, Fuel Process. Technol. 104 (2012) 310–318.
[33]C. Sievers, Y. Noda, L. Qi, E.M. Albuquerque, R.M. Rioux, S.L. Scott, ACS Catal. 6 (2016) 8286–8307.
[34]E. Santacesaria, Catal. Today. 34 (1997) 393–400.

However, the authors indicate the pseudo-second order reaction rate expression has the best adjustment to the experimental data. Nevertheless, the authors no present a diffusion limitations assessment, they just mention the glycerol conversion increase with the increment from 0.2 to 2 M of the SO_4^{2-} groups over the support. The author declares this behavior is explained by kinetic effect. Contrary, when the SO_4^{2-} concentration is increased from 2 to 4.8 M the conversion decrease. Thus, the authors say the activity decreases might be due to the internal diffusion limitation in the catalyst. Therefore, the 2 M SO_4^{2-}/γ-Al_2O_3 is selected to performed the reaction tests [35]. The Table 1 summarizes the kinetic models developed in these studies.

Besides, a search in Scopus using the string: “TITLE-ABS-KEY (glycerol AND esterification AND acetic AND acid AND kinetics)” produces 20 documents (Date accessed: November 18, 2018) . Among them, none showed strict evaluation of transport limitations. In Table 1, one may notice that though Khayoon et al. [23], Patel & Singh [31], and Gelosa et al. [15] reported some measurements to assess transport limitations, their analyses seemed not systematic enough as to rigorously discard them.

Prior to any kinetic study, researchers must ensure some conditions to propose a kinetic modeling. Vannice [36] has summarized the Boudart’s philosophy about kinetics and catalysis to tackle in an appropriate way this kind of studies:

i. The experimental data ought to be reproducible.
ii. The reaction conditions have been tested to guaranty the absence of artifacts, i.e. mass and heat transfer limitations.
iii. The proposed reaction mechanism should be composed of a series of elementary steps that picture a catalytic cycle.

[15]D. Gelosa, M. Ramaioli, G. Valente, M. Morbidelli, Ind. Eng. Chem. Res. 42 (2003) 6536–6544.
[23]M.S. Khayoon, S. Triwahyono, B.H. Hameed, A.A. Jalil, Chem. Eng. J. 243 (2014) 473–484.
[31]A. Patel, S. Singh, Fuel. 118 (2014) 358–364.
[35]S.A. Rane, S.M. Pudi, P. Biswas, Chem. Biochem. Eng. Q. J. 30 (2016) 33–45.
[36]M.A. Vannice, Kinetics of Catalytic Reactions, 2005.

iv. Necessary assumptions are made about dominant species and relative rates of the elementary steps to enable the derivation of a kinetic expression according to the data.
v. The kinetic and adsorption equilibrium constants of the kinetic expression might be physically reasonable and thermodynamically consistent.
vi. If possible, additional tests can be proposed and conducted to verify the kinetic model.
vii. The catalyst should be characterized to determine the active surface area. If possible, the active sites should be count. The additional information about the chemical state of the catalyst is also desirable.

Thereupon, one of these points that is common to overlook is the assessment of mass and heat transport limitations. Liquid phase reactions with solid catalysis are particularly sensitive to mass transfer limitations while heat transfer is usually not a problem. One may picture that indeed the transport of a reactant in liquid phase into an active site located inside the pore of a solid catalyst is a very demanding process hindered by the multiple interactions established between the molecules of the reactant themselves and those of the surrounding fluid. Conversely, the latter circumstance enhances thermal conductivity hence buffering temperature gradients which facilitate heat transport. External (i.e. interphase) mass transfer limitations can be avoided by varying the rate of mechanical stirring while, internal (i.e. intraphase) mass transfer limitations can be avoid by using suitable catalyst particle size. Notwithstanding, these efforts to evade the mass transfer limitations may have not result.

Table 1. Literature review of kinetic studies for glycerol esterification with acetic acid and solid catalysts in batch reactors.

Catalyst	E_a [kJ/mol]	Reaction Conditions	Kinetic Model
Y/SBA-3 [23]	21.54	T = 353 – 393 K R = 4 Wt_{Cat} = 0.05 g V = 100 cm^3	$r_s = \frac{\overline{C_v^2}}{\overline{C_m}}\left(K_G K_B C_G C_B - \frac{k_d(C_M + C_D + C_T)}{K_s}\right)$
TPA_3/MCM-41 TPA_3/ZrO_2 [31]	22.3 25.2	T= 333 – 393 K R = 6 Wt_{Cat} = 0.15 g V = 100 cm^3	$-r = kC_G$
Amberlyst-15 [15]	62.76 17.57 18.41	T = 333 – 373 K R = 2.3 – 3.9 Wt_{Cat} = 27 – 135 g V = 600 cm^3	$r_1 = k_1\Gamma_{glycerine}\Gamma_{acetic\ acid}\left[1 - \prod_{i=1}^{N}\frac{(\Gamma_{EQ,i})^{v_{i,1}}}{K_{EQ,1}^{\Gamma}}\right]$ $r_2 = k_2\Gamma_{monoacetine}\Gamma_{acetic\ acid}\left[1 - \prod_{i=1}^{N}\frac{(\Gamma_{EQ,i})^{v_{i,2}}}{K_{EQ,2}^{\Gamma}}\right]$ $r_3 = k_3\Gamma_{diacetine}\Gamma_{acetic\ acid}\left[1 - \prod_{i=1}^{N}\frac{(\Gamma_{EQ,i})^{v_{i,3}}}{K_{EQ,3}^{\Gamma}}\right]$
Amberlyst-15 [29]	57.26 31.87 13.90	T = 353 – 393 K R = 3 – 9 Wt_{Cat} = 2.65 g V = 150 cm^3	$k_1 = 2.07 * 10^6\beta^{0.274}exp\left(-\frac{6890}{T}\right)$ $k_2 = 18.66\beta^{1.82}exp\left(-\frac{3830}{T}\right)$ $k_2 = 1.16\beta^{-0.474}exp\left(-\frac{1670}{T}\right)$
$SO_4^{2-}/\gamma\text{-}Al_2O_3$ [35]	47.13 106	T = 383 K R = 9 Wt_{Cat} = 0.25 g V = 30 cm^3	$-r = kC_G$ $-r = kC_G^2$

[15]D. Gelosa, M. Ramaioli, G. Valente, M. Morbidelli, Ind. Eng. Chem. Res. 42 (2003) 6536–6544.
[23]M.S. Khayoon, S. Triwahyono, B.H. Hameed, A.A. Jalil, Chem. Eng. J. 243 (2014) 473–484.
[29]L. Zhou, T.H. Nguyen, A.A. Adesina, Fuel Process. Technol. 104 (2012) 310–318.
[31]A. Patel, S. Singh, Fuel. 118 (2014) 358–364.
[35]S.A. Rane, S.M. Pudi, P. Biswas, Chem. Biochem. Eng. Q. J. 30 (2016) 33–45.

Through the years, both theoretical and experimental tests for mass transfer limitations have been developed [37]. Among the theoretical criteria, the Weisz-Prater criterion [38] is commonly applied. The Weisz-Prater parameter <3.0 is acceptable for the absence of the mass transport limitations. However, for applying it, a calculation of the effective diffusivity of the fluid through the pore must be carried out. The required data for the latter is scantly found. In general, the application of theoretical criteria is limited to estimating physical properties often absent from literature. Therefore, approximations leading to error deviations are unavoidable. Experimental methods are the most reliable. The Madon-Boudart criterion [39] is a graphic method for assessing mass and heat transfer limitations which was developed following the concepts proposed by Koros & Nowak [32]. This criterion is independent the phase of fluid reaction with the catalyst.

Another example to assess the mass transfer limitations is the effectiveness factor, η, calculation. The effectiveness factor is the relation between the observable reaction rate and the real reaction rate achieve on the catalyst surface. The effectiveness factor has values between 0 and 1. Then, $\eta \rightarrow 1$ indicates the observable reaction rate is the intrinsic reaction rate of the system. Contrary, $\eta \rightarrow 0$, the measured reaction rates have transport artifacts. The effectiveness factor can be defined in terms of the Thiele modulus, Φ. This definition represents the quotient between the superficial reaction rate and the internal diffusion through the catalyst. The Thiele modulus calculation depends on the dimensions of the catalyst and the order of the reaction rate. Thiele modulus with high values indicates the reaction is carried out over the external surface and a meager amount of reactive goes through the pores of the catalyst. Meanwhile, Thiele modulus with low values points to the internal diffusion through the catalyst is huge. The Table 2 summarizes these mass transfer evaluation methods, and their pros and cons of each one.

---

[32]R.M. Koros, E.J. Nowak, Chem. Eng. Sci. 22 (1967) 470.
[37]C.N. Satterfield, Heterogeneous catalysis in industrial practice, 2nd Ed. Ed. 51 (1991) 447.
[38]P.B. Weisz, C.D. Prater, Adv. Catal. 6 (1954) 143–196.
[39]R.J. Madon, M. Boudart, Ind Eng Chem Fundam. (1982) 438–447.

Table 2. Summary of selected criteria employed for the assessment of mass transport limitations.

Method	Definition	*Pro*	*Contra*
Waisz-Prater criterion	$\Phi_{WP} = \frac{-rR_p^2}{C_{As}D_e} < 0.3$ $-r$: reaction rate. R: radius of the catalyst particles. D_e: effective diffusivity. C_{As}: reagent *A* concentration at external surface.	Only one reaction rate measurement is necessary to apply the criterion.	i) The effective diffusivity should be predicted. ii) The criterion is valid for spherical particles of the catalyst
Madon-Boudart criterion	The reaction rate is measured in a series of tests at the same reaction conditions but different concentration of active sites. A plot of the logarithm of the reaction rate versus the logarithm of the concentration of active sites is constructed. When the slope is ~1, mass transport limitations are discarded. If the plots at different temperatures maintained the slope ~1, heat transport limitations are also discarded.	The conclusions of the criterion are based on real data of the reaction system.	Resource consumption is necessary for deriving the necessary data.
Effectiveness factor and Thiele modulus calculation	$\eta = \frac{-r_{obs}}{-r_s} = \frac{3}{\Phi^2}(\Phi coth\Phi - 1)$ $\Phi = \frac{-r'_s R^2 \rho_c}{D_e C_s}$ $-r_{obs}$: observable reaction rate. $-r_s$: Reaction rate on the surface. R, ρ_c: radius and density from catalyst particles. D_e: effective diffusivity. C_s: concentration of reagent at the external surface of the catalyst.	It indicates how significant is the internal diffusion over the real reaction rate.	Real reaction rate data and physical properties should be known.

Usually, rate models are tested and checked when the experimental data is fixed to a mathematical expression. Nonetheless, the physicochemical consistency is not considered. Even if the rate models are based in a Langmurian expression where the adsorption – desorption processes are accounting, the kinetic parameters could have not physical sense either thermodynamic consistency. Considering the van't Hoff equation, (Equation 1) which relates the adsorption equilibrium constant in thermodynamic terms, these kinetic parameters can be assessed. Vannice [36] are

[36]M.A. Vannice, Kinetics of Catalytic Reactions, 2005.

collected criteria from the Boudart' works and other authors to test the physicochemical consistency of the parameters of the models. These rules and guidelines are defined as follow:

i. The adsorption of the molecules on the catalyst surface is an exothermic process.
ii. After adsorption, the entropy must be decrease. Then, the entropy change should be greater than cero but less than the standard total entropy in gas phase of the corresponding specie.
iii. The adsorbed species must lose at least one degree of translational freedom. Then, a calculation for a typical gas at reasonable temperature the entropy change is higher than 41.8 kJ/mol K. Also, an empirical correlation between entropy and enthalpy of adsorption on carbons is stablish. These guidelines are less rigid than the rules above.

$$K = \frac{\Delta S_{ad}^{o}}{R} - \frac{\Delta H_{ad}^{o}}{RT} \quad \text{(Equation 1)}$$

Table 3. Criteria for adsorption equilibria constant assessment in a Langmurian rate expression.

Rule 1	$-\Delta H_{ad}^{o} > 0$
Rule 2 & 3	$0 < -\Delta S_{ad}^{o} < S_{g}^{o}$
Guidelines	$41.8 < -\Delta S_{ad}^{o} < 51.04 - 1.4\Delta H_{ad}^{o}\ [kJ/mol]$

Moreover, the Equation 2 presents a relation between thermodynamics and chemical kinetics, where, the standard enthalpy of the reaction should be equal to the difference between the change of energy of the adsorption – desorption processes and the difference between the forward and backward activation energies of the reaction proces.

$$\Delta H_{r}^{o} = (\Delta H_{R}^{o} - \Delta H_{P}^{o}) + (E_{a}^{F} - E_{a}^{B}) \quad \text{(Equation 2)}$$

In a chemical reaction catalyzed by a solid material, there are energy changes due to the activated barriers, but also due to the several adsorption – desorption

processes. They are determined by the steps of the reaction mechanism. This energy balance is picture in a potential energy diagram (Figure 2)

In a heterogeneous reaction with a solid catalyst can occur several adsorption – desorption processes and presents many activated barriers. It is determined by the steps of the reaction mechanism. This thermodynamic criterion is pictured in a potential energy diagram (Figure 2).

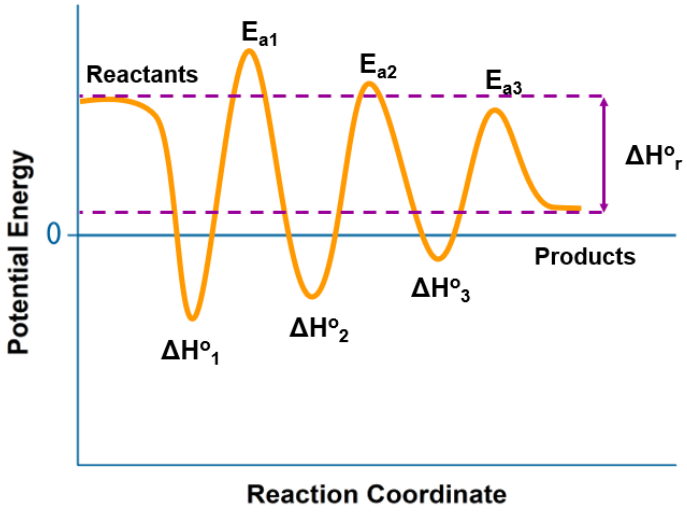

Figure 2. Energy changes in a reaction with heterogeneous catalysis.

Considering the above circumstances, this work presents a re-visit of the reactivity of the glycerol esterification in liquid phase catalyzed by Amberlyst-35, and a kinetic modeling of its mechanism. In the next chapter, the experimental data recollected allowed the analysis of the catalytic activity on statistical ground, and the assessment of the mass and heat transport limitations following the Madont-Boudart criterion. This revision introduces the accurate conditions to guaranty the acquisition of experimental data free of transport artifacts. Consequently, the last chapter presents the kinetic modeling of the glycerol esterification. From the Langmuir-Hinshelwood-Hougen-Watson formalism, three rate expressions are developed to model the production of acetins. In addition, the kinetic parameters found are assessed by physicochemical tests founded on thermodynamic grounds.

CHAPTER 1

REVISITING GLYCEROL ESTERIFICATION WITH ACETIC ACID OVER AMBERLYST-35 VIA STATISTICALLY DESIGNED EXPERIMENTS

In this chapter, the usual reaction conditions encountered in published literature were applied in a systematic analysis. Results for this experiments not only allowed for the analysis of the catalytic reactivity on statistical ground, but also for the assessment of mass and heat transfer limitations following the Madon-Boudart criterion. The collected experimental evidence showed that such conditions are subjected to transport artifacts. Particularly, intraphase mass transport limitations were found. Subsequently, reaction conditions free of diffusion limitations are stablished.

1.1 EXPERIMENTAL SECTION

1.1.1 Catalytic tests: The liquid phase esterification of glycerol (99.5%, Laboratorios León) with acetic acid (100%, Merck) was carried out in a 100 ml round flask reactor provided with a magnetic stirrer and reflux system at atmospheric pressure. A stirring speed of 1400 rpm was fixed for all tests. The reaction temperature was controlled by heat exchange with a mineral oil bath. Figure 3 presents a sketch of the reaction set-up. Samples of the reaction products were normally taken at 6, 9, 16, 29 and 46 min. Before analysis, any trace of catalyst contained in these samples was separated from the liquid medium using a 0.45 µm pore size nylon filter membrane (Agilent) and withheld there. Reaction products were analyzed by gas chromatography using a GC Agilent 6890 instrument provided with an automatized robot arm for injection and a flame ionization detector (FID). An HP-1 column (100 m x 0.25 mm x 0.5 µm, J&W Scientific) was used for molecules separation and helium (99.99%, Linde Colombia S.A.) was employed as carrier gas. For the chromatographic analysis, 10 µl of the sample taken from the reaction tests were diluted in 1000 µl of ethanol (99.9%, Merck) and 10 µl of 1,4-dioxane (99%,

Baker). Where, dioxane was used as an internal standard. Samples of 1 µl of the aforementioned dilution were injected to the GC and further vaporized by the instrument. The oven of the GC was programed with a temperature ramp starting at 363 K for 1 min. Temperature was further raised to 503 K using a heating rate of 5 K/min. The latter temperature was held for 1 min.

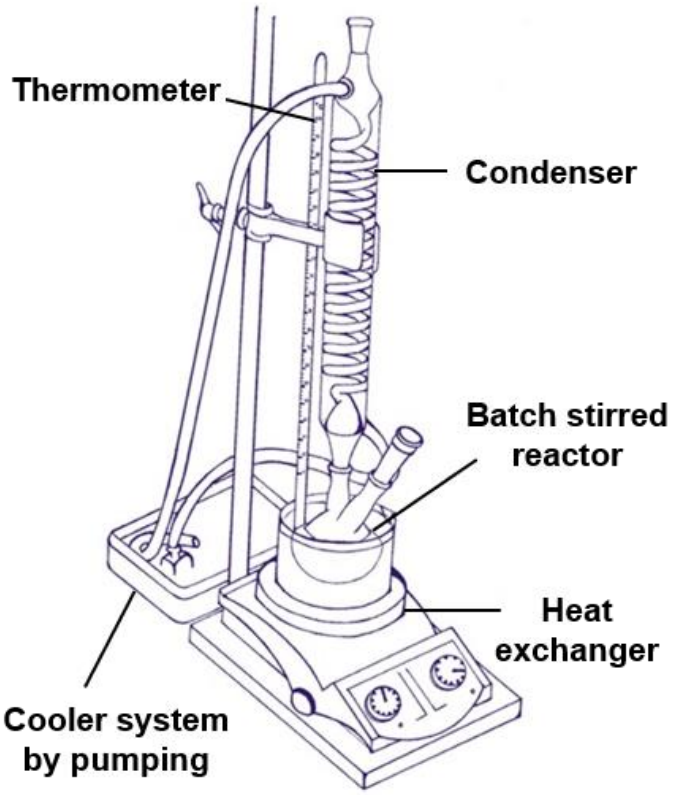

Figure 3. Experimental reaction set-up for the liquid phase glycerol esterification with acetic acid.

Catalytic tests over Amberlyst-35 (Rohm and Hass) were statistically designed for assessing the effects of temperature and of the quantity of moles of active sites of the Amberlyst-35 catalyst over the turnover rates of glycerol consumption. The number of active sites of Amberlyst-35 was assumed to correspond to the number of SO_3H^+ acid sites, i.e. $5.0*10^{-3}$ mol eq/g_{cat}, reported by the manufacturer [40].

[40]Rohm and Haas, Amberlyst 35dry - Industrial Grade Strongly Acidic Catalyst, (2006) 1–2.

Two sets of reactions tests were carried out. For the first set, Amberlyst-35 was used as provided by the manufacturer after sieving its particles sizes between 600 – 1180 μm. Three blocks of experiments were planned and executed following a 3^2 full factorial experimental design (FFED). The first block of experiments was made with temperatures (T) of 345, 353, and 361 K and varying the number of moles of active sites (μ^*) with values of 1.14, 3.75, and 6.37 mmol of SO_3H^+. The temperatures mentioned above were also employed for the remaining two blocks of experiments. In this way, the full set of experiments provided rich data on the influence of the number of active sites over the catalytic reactivity. For the second block of experiments, only μ^* was changed using 0.82, 2.70, and 4.58 mmol of SO_3H^+. μ^* was set to 0.62, 2.04, and 3.45 mmol of SO_3H^+ for the third block of catalytic experiments. An additional variable that was assessed between the experimental blocks was the acetic acid to glycerol molar ratio. Therefore, R was set to 1.8, 3.0, and 4.4 for the first, second, and third experimental blocks, respectively. For the second set of catalytic tests, the Amberlyst-35 catalyst was crushed and sieved to obtain particles within a particle size range between 25 – 75 μm. Using this particle size, a new 3^2 FFED was carried out to reassess the effects of the T and μ^*. The values of temperatures and moles of active sites were the same as for the third block of the previous experimental design. The acetic acid to glycerol molar ratio was kept constant at 4.4. The aforementioned quantities of moles of active sites correspond to 0.7, 2.3, and 3.9 wt.% of Amberlyst-35 as in regard to the weight of glycerol in the reactor. Two replicates of the above described experimental designs were run. The order of execution of the experiments was randomized using the Excel® RANDBETWEEN function.

The results of each experimental design were statistically analyzed by both graphical and numerical methods. Main effects and interaction plots were built to analyze the effects of the variables on the catalytic performance [41,42].

[41]G.P. Quinn, M.J. Keough, Experimental Design Data Analysis for Biologists, Cambridge, 2002.
[42]C.F.J. Wu, M.S. Hamada, Experiments: Planning, Analysis, and Optimitation, Second edi, 2009.

For the sake of convenience, some of these plots are presented using the reciprocal number of moles of active sites; i.e. μ^{*-1}. A quantitative statistical assessment of the observed effects was further achieved by carrying out analysis of variance (ANOVA) tests with the aid of a Microsoft Excel® 2016 spreadsheet. For the ANOVA tests, the Type-I error (α) was fixed at 0.01; i.e. a confidence of 99% was set. The value of α for the significance of each factor was readjusted following the criterion derived from Kimball's inequality [43,44]. In every instance, an analysis of residuals was performed for checking the validity of the assumptions of normality, constant variance and independence of the ANOVA model following the procedures presented in the textbooks by Montgomery et al. [45], Quinn et al. [41], and Kutner et al. [44].

The evolution of the catalytic results with time was followed from glycerol conversion and from the yield to acetins. These quantities were defined according to IUPAC definitions [46]. Reaction rates were calculated by the initial rates method [47]. The derived rates were further transformed into turnover frequencies following Boudart's definition (Equation 3) [48], and taking into consideration the recommendations made by Kozuch & Martin [49]. Accordingly, the calculation of turnover frequencies was carried out from reaction samples taken near to the 10% of the glycerol consumption.

$$Turnover\ [s^{-1}] = \frac{measured\ reaction\ rate\ [mol{*}g_{cat}^{-1}{*}s^{-1}]}{active\ sites\ concentration\ [mol\ eq{*}g_{cat}^{-1}]} \quad \text{(Equation 3)}$$

[41]G.P. Quinn, M.J. Keough, Experimental Design Data Analysis for Biologists, Cambridge, 2002.
[43]A.W. Kimball, On Dependent Tests of Significance in the Analysis of Variance, Ann. Math. Stat. 22 (1951) 600–6002.
[44]M.H. Kutner, C.J.J. Nachtsheim, J. Neter, W. Li, Applied Linear Statistical Models, Fifth Edit, 2004.
[45]D.C. Montgomery, G.C. Runger, Applied Statistics and Probability for Engineers, John Wiley & Sons, Inc., 2013.
[46]J. Haber, Pure Appl. Chem. 63 (1991) 1227–1246.
[47]H.S. Fogler, Elements of Chemical Reaction Engineering, Third Edit, 1999.
[48]M. Boudart, Kinetics of Chemical Processes, Butterworth-Heinemann, 1991.
[49]S. Kozuch, J.M.L. Martin, ACS Catal. 2 (2012) 2787–2794.

1.1.2 Estimation of the apparent activation energy: Apparent activation energies (E_a) were estimated by plotting the logarithm of the apparent kinetic constant (k) as a function of the reciprocal of the temperature as from a standard linearization of the Arrhenius equation (Equation 4):

$$lnk = lnA - \frac{E_a}{RT} \quad \text{(Equation 4)}$$

The apparent kinetic constant was calculated following the integral method [47] and assuming a pseudo-homogeneous second order reaction (Equation 5) with respect to glycerol concentration, C_G.

$$-r = kC_G^2 \quad \text{(Equation 5)}$$

1.1.3 Surface area and porosity of Amberlyst-35: The surface area and porosity of Amberlyst-35 were estimated from N_2 adsorption – desorption isotherms preformed at 77 K in a 3FLEX apparatus (Micromeritics). Measurements were carried out within a range of relative pressures between 0.001 to 0.999. Prior to the analysis, samples of 0.2 g were degassed at 393 K during 12 h reaching a final vacuum pressure of 3 Pa. The data analysis program 3FLEX V.3.02 provided with the instrument was used to estimate surface area; by the BET method [50], and pores volume and size distribution; by the BJH method [51].

1.1.4 Catalyst stability and recyclability tests: In order to corroborate the stability of the catalyst with its particle size reduced in a range of 25 – 75 µm, a set of tests was carried out in a similar way as Dosuna & Gaigneaux present in their work [28]. Firstly, a regular reaction was executed at temperature of 347 K, acetic acid to glycerol molar ratio of 9 and the quantity of moles of active sites of 0.85 mmol. Samples of the products were taken at 0, 0.5 and 1 h of the reaction.

---

[28]I. Dosuna-Rodríguez, E.M. Gaigneaux, Catal. Today. 195 (2012) 14–21.
[47]H.S. Fogler, Elements of Chemical Reaction Engineering, Third Edit, 1999.
[50]S. Brunauer, P.H. Emmett, E. Teller, J. Am. Chem. Soc. 60 (1938) 309–319.
[51]E.P. Barrett, L.G. Joyner, P.P. Halenda, J. Am. Chem. Soc. 73 (1951) 373–380.

Later, the reaction was stopped, and the catalyst was separated from the reaction mixture by centrifugation. The liquid medium obtained was filtered, then it was put in reaction conditions once again. New samples of the products were taken every hour starting from 0 until complete 6 h of reaction.

To compare the evolution of the earlier reaction and check the absence of leached species of the catalyst, another reaction at the same conditions but without catalyst was carried out for 10 h. Hence, the starting point of the reaction from the liquid medium was displaced to the point in the curve of the reaction without catalyst with a similar composition. Finally, the catalyst recovered for the first reaction was put in a fresh reaction medium. Therefore, the reaction was accomplished at the same reaction conditions for 1 h. The catalytic activities of the first and the last reaction were compared to observe the recyclability of the catalyst.

To avoid future confusion with the references of these tests, each reaction in this part are named: first reaction, homogeneous reaction, blank reaction and recycle reaction, respectively.

1.2 ASSESSMENT OF TRANSPORT LIMITATIONS

1.2.1 Madon-Boudart Criterion: The Madon-Boudart criterion [39] was applied to assess the influence of mass and heat transport limitations. This criterion is based on the Koros-Nowak test [32] which indicates that the system works without transport limitations when the increase of the reaction rate is proportional to the increment of the number of active sites in the reaction medium. The methodology consists on measuring the reaction rate at constant reaction conditions but varying the concentration of active sites. The reaction is said to be run in a kinetic regime when the ratio of the reaction rate related to active sites concentration is maintained invariant.

[32]R.M. Koros, E.J. Nowak, Chem. Eng. Sci. 22 (1967) 470.
[39]R.J. Madon, M. Boudart, Ind Eng Chem Fundam. (1982) 438–447.

Madon & Boudart developed a graphical approximation to this criterion in which a plot of the logarithm of the reaction rate versus the logarithm of the concentration of active sites is constructed. When the slope of the plotted curve is ~1, mass transport limitations are discarded. Furthermore, if the plots are constructed at different temperatures and a slope ~1 is maintained, heat transport limitations can also be ruled out.

1.2.2 Effectiveness factor and Thiele modulus approximation: Besides the Madon-Boudart criterion, calculation of effectiveness factor (η) and of Thiele modulus (Φ) was carried out. The methodology for the corresponding calculations was based on procedures presented by Fogler [47] and detailed in the Figure 4.

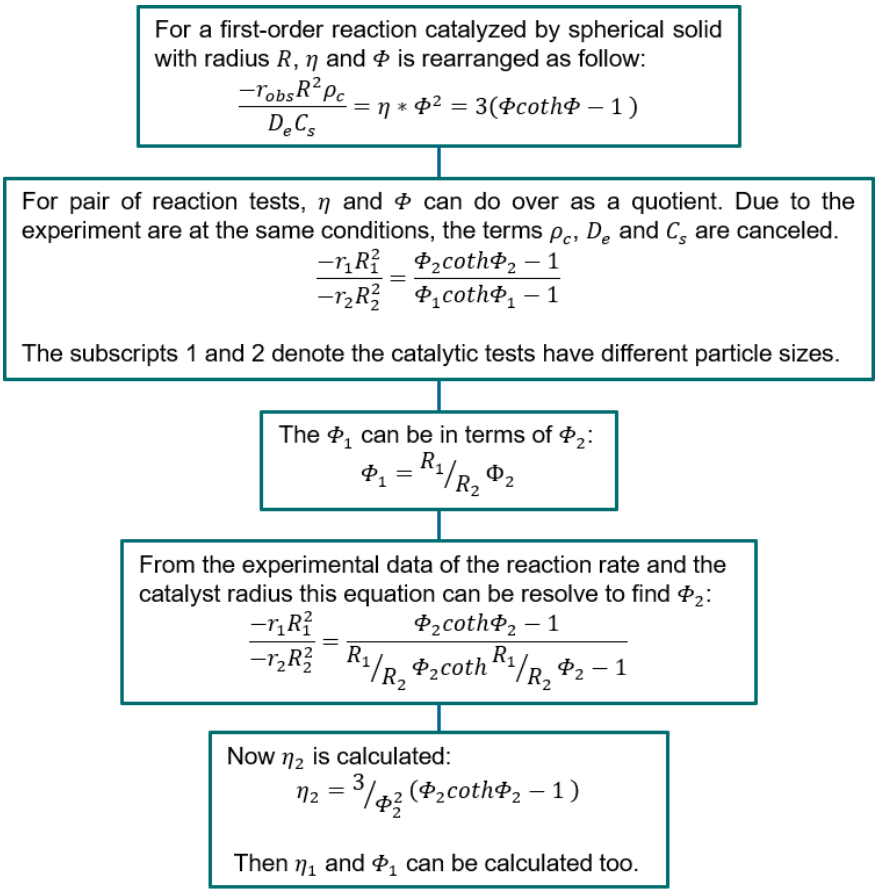

Figure 4. Effectiveness factor and Thiele modulus approximation. The subscripts 1 and 2 are referred to the data from the first and second set of experiments.

[47]H.S. Fogler, Elements of Chemical Reaction Engineering, Third Edit, 1999.

1.3. RESULTS AND DISCUSSION

1.3.1 Statistical assessment of the reactivity data for the first set of experiments: The turnover frequencies calculated from the catalytic conversion of glycerol over Amberlyst-35 for the first set of statistically designed experiments are presented in Tables 4 to 6; each table corresponds to an experimental block. As stated in the Experimental section, experimental blocks were defined for three values of R; namely; 1.8; 3.0; and 4.4. Also, all blocks were performed using particles of Amberlyst-35 within a range: 600 – 1180 μm. These conditions comprise those reported in the literature survey conducted in this work and summarized in Table 1. The interested reader may consult data for the evolution of the catalytic performance as function of time in the Supplementary Information (Table S1).

Table 4. Summary of Turnover frequencies for glycerol esterification with acetic acid over Amberlyst-35 as obtained from reaction tests executed according to a 3^2 full factorial experimental design. Acetic acid to glycerol molar ratio of 1.8. Amberlyst-35 particle size of 600 – 1180 μm.

Reaction	μ* [mmol]	T [K]	Turnover frequency *10^2 [s^{-1}]
1_i	1.14	345	6.49
2_i	3.75	345	2.24
3_i	6.37	345	2.02
4_i	1.14	353	6.54
5_i	3.75	353	2.65
6_i	6.37	353	2.44
7_i	1.14	361	6.44
8_i	3.75	361	2.87
9_i	6.37	361	2.37
10_i	1.14	345	6.35
11_i	3.75	345	2.28
12_i	6.37	345	2.31
13_i	1.14	353	6.72
14_i	3.75	353	2.97
15_i	6.37	353	2.43
16_i	1.14	361	6.25
17_i	3.75	361	3.26
18_i	6.37	361	2.92

Table 5. Summary of Turnover frequencies for glycerol esterification with acetic acid over Amberlyst-35 as obtained from reaction tests executed according to a 3^2 full factorial experimental design. Acetic acid to glycerol molar ratio of 3.0. Amberlyst-35 particle size of 600 – 1180 μm.

Reaction	μ* [mmol]	T [K]	Turnover frequency *10^2 [s^{-1}]
1_{ii}	0.82	345	9.98
2_{ii}	2.70	345	4.46
3_{ii}	4.58	345	2.48
4_{ii}	0.82	353	7.71
5_{ii}	2.70	353	3.29
6_{ii}	4.58	353	2.74
7_{ii}	0.82	361	12.87
8_{ii}	2.70	361	3.97
9_{ii}	4.58	361	2.92
10_{ii}	0.82	345	10.66
11_{ii}	2.70	345	4.36
12_{ii}	4.58	345	2.89
13_{ii}	0.82	353	6.13
14_{ii}	2.70	353	3.70
15_{ii}	4.58	353	2.24
16_{ii}	0.82	361	13.29
17_{ii}	2.70	361	4.84
18_{ii}	4.58	361	3.21

Table 6. Summary of Turnover frequencies for glycerol esterification with acetic acid over Amberlyst-35 as obtained from reaction tests executed according to a 3^2 full factorial experimental design. Acetic acid to glycerol molar ratio of 4.4. Amberlyst-35 particle size of 600 – 1180 μm.

Reaction	μ* [mmol]	T [K]	Turnover frequency *10^2 [s^{-1}]
1_{iii}	0.62	345	10,41
2_{iii}	2.04	345	5,43
3_{iii}	3.45	345	2,11
4_{iii}	0.62	353	14,58
5_{iii}	2.04	353	3,60
6_{iii}	3.45	353	3,19
7_{iii}	0.62	361	12,54
8_{iii}	2.04	361	3,77
9_{iii}	3.45	361	3,42
10_{iii}	0.62	345	14,19
11_{iii}	2.04	345	5,21
12_{iii}	3.45	345	2,45
13_{iii}	0.62	353	14,98
14_{iii}	2.04	353	3,40
15_{iii}	3.45	353	2,90
16_{iii}	0.62	361	11,89
17_{iii}	2.04	361	4,97
18_{iii}	3.45	361	3,49

The first step for a proper statistical analysis of any set of data derived from statistically designed experiments is to make a graphic assessment of the data [41,42,52]. For factorial experimental designs, this is most adequately made by means of the so-called main and interaction effects plots [41,42,44,45]. These plots are shown in Figures 5; main effects, and 6; interaction plots.

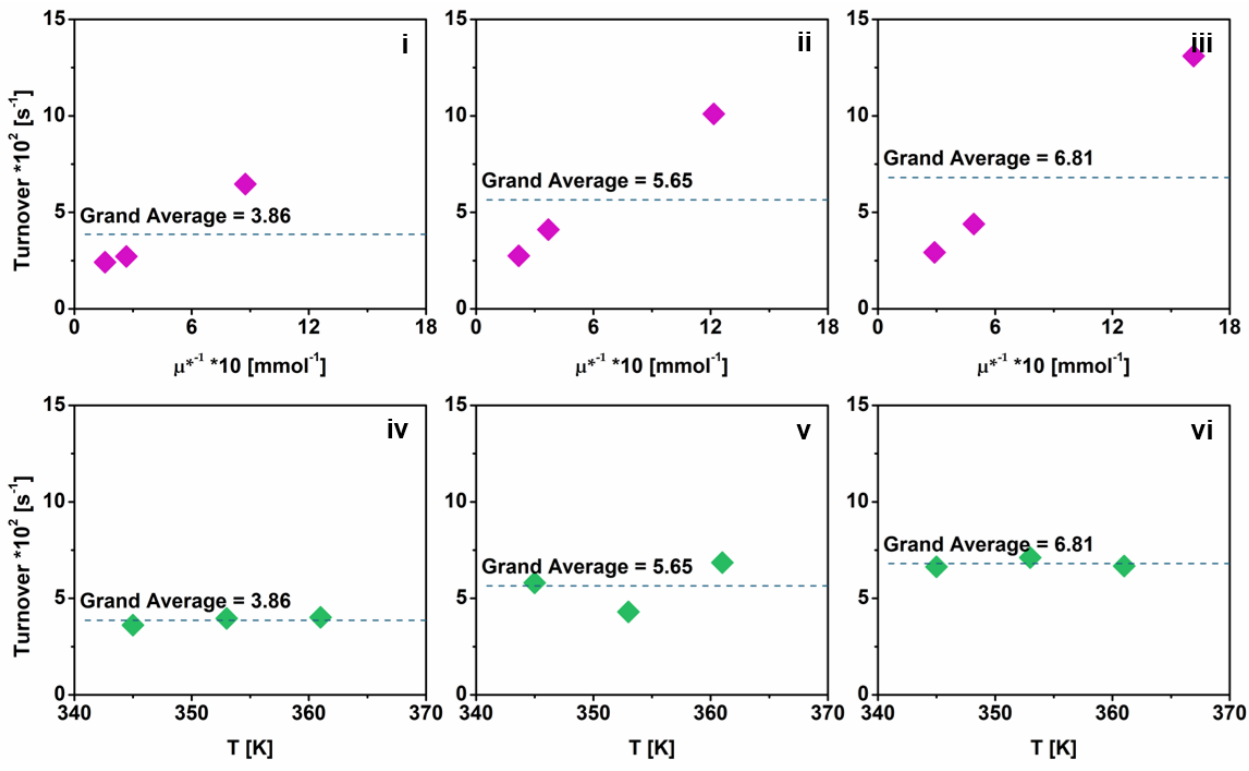

Figure 5. Main effect plots for results from the designed blocks of a 3^2 full factorial experimental designs at the selected acetic acid to glycerol molar ratios (R) set-up for the blocks of R. Variation of the Turnover frequencies for glycerol with the reciprocal of moles of active sites (μ^{*-1}) at: i) R = 1.8, μ^* = 1.14, 3.75 and 6.37 mmol; ii) R = 3.0, μ^* = 0.82, 2.70 and 4.58 mmol; and iii) R = 4.4, μ^* = 0.62, 2.04 and 3.45 mmol. Variation of the Turnover of the glycerol consumption with the reaction temperature (T) at: iv) R = 1.8; v) R = 3.0; and vi) R = 4.4. T = 345, 353, and 361 K. Amberlyst-35 particle size of 600 – 1180 μm.

[41]G.P. Quinn, M.J. Keough, Experimental Design Data Analysis for Biologists, Cambridge, 2002.
[42]C.F.J. Wu, M.S. Hamada, Experiments: Planning, Analysis, and Optimitation, Second edi, 2009.
[44]M.H. Kutner, C.J.J. Nachtsheim, J. Neter, W. Li, Applied Linear Statistical Models, Fifth Edit, 2004.
[45]D.C. Montgomery, G.C. Runger, Applied Statistics and Probability for Engineers, John Wiley & Sons, Inc., 2013.
[52]G.E. Box, J.S. Hunter, W.G. Hunter, Statistics for Experimenters Design, Innovation, and Discovery, Second Edi, 2005.

Main effects plots were elaborated for the temperature and for the (reciprocal) quantity of active sites within the experimental blocks. The plots were built by averaging the obtained turnover frequencies at each factor level within the experimental blocks. For facilitating the qualitative assessment of the effect of the variables, the grand average of all the turnovers from the experimental design was also plotted. According to the trends registered in the main effect plots, Figures 5i to 5iii, the (reciprocal) quantity of catalytic sites of Amberlyst-35 had a positive effect on the catalytic activity with the averages crossing the line traced for the grand average every time. This effect followed a linear trend for each one of the experimental blocks; i.e. regardless of acetic acid to glycerol molar ratio. Conversely, temperature, Figures 5iv to 5vi, did not seem to influence the turnover frequency for the blocks executed with R = 1.8 and 4.4. This was evidenced by the fact that the calculated averages were distributed around the grand average of the turnovers as in contrast to what was found for the quantity of active sites commented earlier. The only exception for this trend was found for the block with R = 3.0, where the line of the grand average was crossed. Finally, comparing the grand averages obtained for each experimental block, the increase in the acetic acid to glycerol molar ratio had a positive effect over the catalytic activity.

Concerning interaction plots, these were elaborated by taking the averages of the turnovers at each level of one of two main variables and then connecting these averages with a curve comprising one of the levels of the other main variable. In consequence, each interaction plot features three curves; one for each level of the variable selected as secondary. Interaction plots for a two factor; e.g. A and B, FFED might thus be of two types: A×B and B×A [42]. Therefore, Figure 6 features the interaction plots for the (reciprocal) quantity of active sites times temperature; i.e. μ^{*-1}×T, Figures 6i to 6iii and temperature times the (reciprocal) quantity of active sites: i.e. T×μ^{*-1}, Figures 6iv to 6vi. In these plots, interactions are said to occur if the curves in both A×B and B×A plots intersect each other.

[42]C.F.J. Wu, M.S. Hamada, Experiments: Planning, Analysis, and Optimitation, Second edi, 2009.

Conversely, the presence of interactions between variables is ruled out when these curves are completely parallel [53,54]. Finally, the existence of the interaction is dubious if the intersection of the plots occurs at the borders of the curves or if, for three level experiments, they are present between only two levels of the studied variables. It may also occur that an interaction is observed when each one of the variables that comprise it are statistically significant. Considering the above arguments, the interpretation of the interaction plots presented in Figure 6 is not straightforward since clear intersections of the curves in both $\mu^{*-1}\times T$ and $T\times\mu^{*-1}$ plots were not observed, regardless of the experimental blocks as referred to values of R.

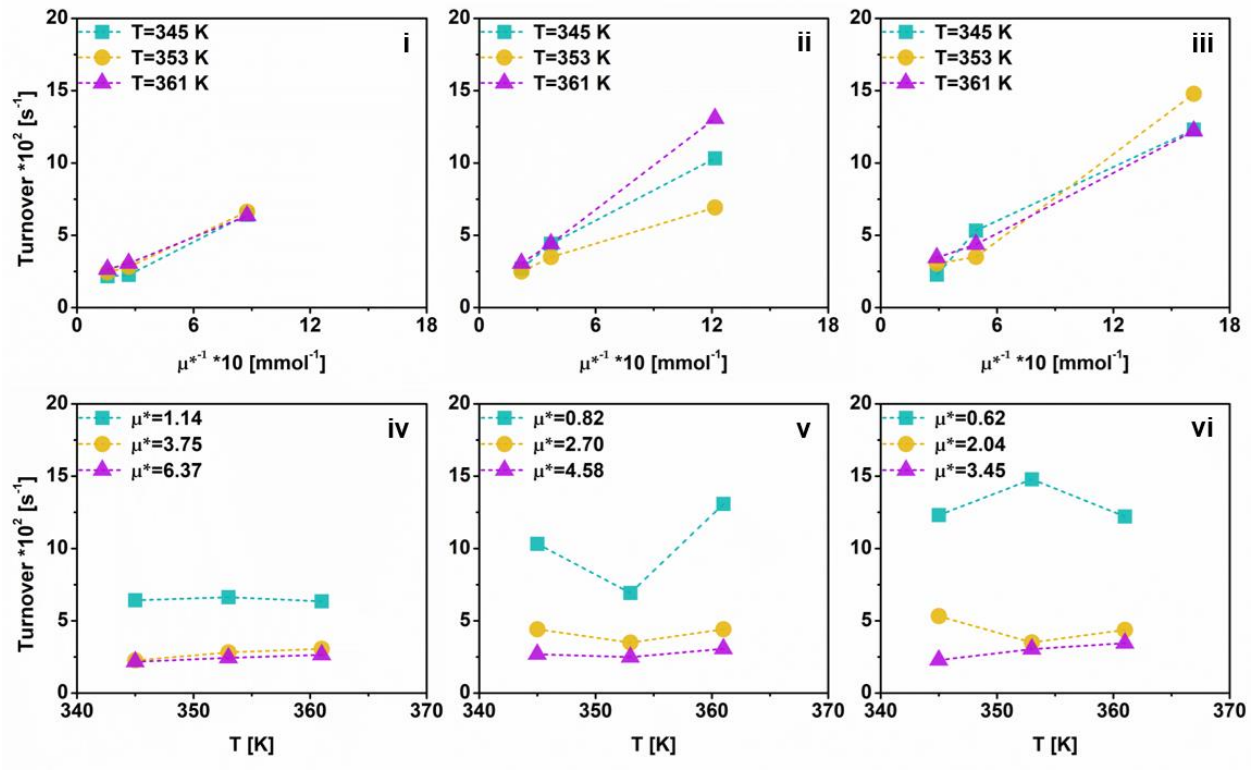

Figure 6. Interaction plots for the results from the designed blocks of a 3^2 full factorial experimental designs at the selected acetic acid to glycerol molar ratios (R) set-up for the blocks of R. $\mu^{*-1}\times T$ interactions at: i) R = 1.8, μ^* = 1.14, 3.75 and 6.37 mmol; ii) R = 3.0, μ^* = 0.82, 2.70 and 4.58 mmol; and iii) R = 4.4, μ^* = 0.62, 2.04 and 3.45 mmol. $T\times\mu^{*-1}$ interactions at: iv) R = 1.8, μ^* = 1.14, 3.75 and 6.37 mmol; v) R = 3.0, μ^* = 0.82, 2.70 and 4.58 mmol; and vi) R = 4.4, μ^* = 0.62, 2.04 and 3.45 mmol. Reaction temperatures of 345, 353, and 361 K. Amberlyst-35 particle size of 600 – 1180 μm.

[53]G.R. Loftus, On interpretation of interactions, 6 (1978) 312–319.
[54]E.J. Wagenmakers, A.M. Krypotos, A.H. Criss, G. Iverson, Mem. Cogn. 40 (2012) 145–160.

To complement the graphical analysis discussed above, independent ANOVA tests were performed for each one of the experimental blocks. Tables 7 to 9 present the results of these tests.

Table 7. ANOVA test for assessing the effects of the different factors: μ^{*-1}, T and μ^{*-1}×T over the Turnover frequency considered in the 3^2 full factorial experimental design executed for glycerol esterification with acetic acid over Amberlyst-35 with particle size of 600 – 1180 µm, and acetic acid to glycerol molar ratio of 1.8.

Factor	SS	υ	MS	F-value	p-value	S
μ^{*-1}	61.10	2	30.55	742.73	1.02E-10	YES
T	0.56	2	0.28	6.83	1.57E-02	NO
μ^{*-1}×T	0.43	4	0.11	2.64	1.04E-01	NO
Error	0.37	9	0.04			
Total	62.46	17				

SS: sum of squares. υ: degrees of freedom. MS: mean squares. S: significance.

Table 8. ANOVA test for assessing the effects of the different factors: μ^{*-1}, T and μ^{*-1}×T over the Turnover frequency considered in the 3^2 full factorial experimental design executed for glycerol esterification with acetic acid over Amberlyst-35 with particle size of 600 – 1180 µm, and acetic acid to glycerol molar ratio of 3.0.

Factor	SS	υ	MS	F-value	p-value	S
μ^{*-1}	184.04	2	92.02	361.99	2.52E-09	YES
T	19.69	2	9.85	38.73	3.79E-05	YES
μ^{*-1}×T	19.84	4	4.96	19.51	1.85E-04	YES
Error	2.29	9	0.25			
Total	225.86	17				

SS: sum of squares. υ: degrees of freedom. MS: mean squares. S: significance.

Table 9. ANOVA test for assessing the effects of the different factors: μ^{*-1}, T and μ^{*-1}×T over the Turnover frequency considered in the 3^2 full factorial experimental design executed for glycerol esterification with acetic acid over Amberlyst-35 with particle size of 600 – 1180 µm, and acetic acid to glycerol molar ratio of 4.4.

Factor	SS	υ	MS	F-value	p-value	S
μ^{*-1}	362.82	2	181.41	196.42	3.77E-08	YES
T	0.83	2	0.41	0.45	6.52E-01	NO
μ^{*-1}×T	12.40	4	3.10	3.36	6.07E-02	NO
Error	8.31	9	0.92			
Total	384.35	17				

SS: sum of squares. υ: degrees of freedom. MS: mean squares. S: significance.

When preforming an ANOVA test, it is mandatory to check the fulfillment of the assumptions of the ANOVA model; namely, (1) the assumption of constant variance among the levels of the considered factors, (2) the assumption of variance

independence from the order of execution of the experiments, and, (3) the assumption of normality of the data [41,42,44,45]. Assumptions (1) and (2) were checked by plotting the residuals of the ANOVA model as a function of the levels of the experimental factors and of the execution order of the experiments, respectively. Assumption (3) was checked by plotting z-scores [41,42,44,45] as a function of residuals of the model. Plots illustrating the verification of these assumptions for every performed ANOVA test are presented in the Supplementary Information (Figures S2, S4 and S6, and Sections S3, S5 and S7). For the assumption of constant variance to be fulfilled, funnel shaped patterns should not be observed in the corresponding plots. Figures S2, S4 and S6 show that this was not the case for some of the plots of residuals as a function of the levels for the quantity of active sites. The origin of such a trend can be related to the uncontrolled error from the chromatographic method which could increase when measuring smaller differences in the concentration of glycerol. One may notice that larger residuals were found for the tests with lower catalytic activities. The plots prepared for the other two assumptions of the ANOVA model did not raise further reasons for concern. Considering these findings, the interpretation of the results of the ANOVA tests must be done with some caution. Despite such a warning, the collected data are not in any way erroneous. Results for the ANOVA test presented in Table 7 show that only the quantity of active sites was statistically relevant for the catalytic performance under the conditions of the first experimental block; i.e. R = 1.8. Such a finding agrees well with the graphical analysis of the data of this block performed earlier, Figure 5i. Therefore, despite the concerns of the validity of the ANOVA model expressed above, it seems relatively safe to conclude that only the quantity of active sites played a role on the catalytic activity registered under R = 1.8. A similar conclusion can be reached from the results of both the graphical analysis and the ANOVA test for the third block of experiments; i.e. R = 4.4, Table 9.

[41]G.P. Quinn, M.J. Keough, Experimental Design Data Analysis for Biologists, Cambridge, 2002.
[42]C.F.J. Wu, M.S. Hamada, Experiments: Planning, Analysis, and Optimitation, Second edi, 2009.
[44]M.H. Kutner, C.J.J. Nachtsheim, J. Neter, W. Li, Applied Linear Statistical Models, Fifth Edit, 2004.
[45]D.C. Montgomery, G.C. Runger, Applied Statistics and Probability for Engineers, John Wiley & Sons, Inc., 2013.

For the experimental block executed at R = 3.0, the ANOVA test, Table 8, indicated that all the considered factors have a statistically significant effect on the catalytic activity. However, the graphical analysis for the factor representing the interaction between the studied input variables showed a high degree of uncertainty for its statistical interpretation; namely, the plot for μ^{*-1}×T showed borderline interactions [53,54]. Whereas the reciprocal T×μ^{*-1} displayed curves with inflections points that did not crossed themselves at any point. Therefore, and also taking into account that the constant variance assumption of the ANOVA model showed signs of violation (Figures S2, S4 and S6) and that when two individual factors have an effect on the response variable the ANOVA test would tend to indicate that their interaction is statistically significant [53–55], one better abstains of claiming the existence of an interaction between the two variables within this experimental block.

1.3.2 Phenomenological assessment of the reactivity data for the first set of experiments: The statistical analysis of the reactivity data led to the following conclusions: (1) both the quantity of active sites and the acetic acid to glycerol molar ratio have a positive effect on the glycerol turnover frequency; (2) temperature has either a weak or statistically negligible effect on the measured glycerol turnover frequency; (3) the existence of statistical interactions between the quantity of active sites and temperature were dubious in all instances. Previous studies [2,3,7,20,24] on the esterification of glycerol with acetic acid in batch reactors have proposed that the parameters influencing the performance of heterogeneous catalysts in this reaction are: the catalyst loading, the reaction temperature, the acetic acid to glycerol molar ratio, the surface acidity, and the agitation speed. Among the latter, the catalyst loading, and the surface acidity are better represented by the quantity and quality of the catalyst active sites.

[2]M.S. Khayoon, B.H. Hameed, Bioresour. Technol. 102 (2011) 9229–9235.
[3]N. Rahmat, A.Z. Abdullah, A.R. Mohamed, Renew. Sustain. Energy Rev. 14 (2010) 987–1000
[7]K. Jagadeeswaraiah, M. Balaraju, P.S.S. Prasad, N. Lingaiah, Appl. Catal. A Gen. 386 (2010) 166–170.
[20]P.U. Okoye, A.Z. Abdullah, B.H. Hameed, Renew. Sustain. Energy Rev. 74 (2017) 387–401.
[24]P.S. Reddy, P. Sudarsanam, G. Raju, B.M. Reddy, J. Ind. Eng. Chem. 18 (2012) 648–654.
[53]G.R. Loftus, On interpretation of interactions, 6 (1978) 312–319.
[54]E.J. Wagenmakers, A.M. Krypotos, A.H. Criss, G. Iverson, Mem. Cogn. 40 (2012) 145–160.
[55]R.L. Rosnow, R. Rosenthal, Psychol. Sci. 6 (1995) 3–9.

In this case, we assumed that the quantity of active sites corresponds to the number of surface SO_3H^+ acid sites and that the quality of these sites is homogenous; i.e. they are homogenously distributed on the surface of the catalyst and they all have the same acidic strength. The analysis is further simplified by considering that acetic acid is absorbed on these sites following a 1:1 stoichiometry. Such a proposal is consistent with studies on the mechanism of the reaction [3,9,20,56–58] that postulates that the reaction initiates with the transfer of a proton from the active site the carboxylic acid henceforward creating a carbocation that is susceptible to nucleophilic attack by one of the hydroxyls of glycerol. Concerning the influence of the agitation speed, if such an effect exists, the catalytic measurements are influenced by interparticle mass transport limitations. The literature reports that this is the case for most of the studies conducted at agitation speeds within the range 300 – 1200 rpm [20,59,60]. Herein, the experiments were carried out a fixed agitation speed of 1400 rpm hence imposing a stronger hydrodynamic regime around the catalyst particles. Therefore, the three variables selected in this study; quantity of active sites, temperature, and acetic acid to glycerol molar ratio, are aimed to evaluate the intrinsic kinetics of the esterification reaction. Moreover, the methodology selected for calculating the turnover frequencies was chosen as to warranty statistically reliable data with physical meaning [49]. Accordingly, the conclusions reached from the statistical assessment of the data can also be interpreted from the kinetic point of view. It was thus not surprising that the quantity of active sites and the acetic acid to glycerol molar ratio had a positive effect on the turnover. However, the weal effect of temperature drew attention into the possible interference of mass and heat transport limitations in turnover rates.

[3]N. Rahmat, A.Z. Abdullah, A.R. Mohamed, Renew. Sustain. Energy Rev. 14 (2010) 987–1000.
[9]L.N. Silva, V.L.C. Gonçalves, C.J.A. Mota, Catal. Commun. 11 (2010) 1036–1039.
[20]P.U. Okoye, A.Z. Abdullah, B.H. Hameed, Renew. Sustain. Energy Rev. 74 (2017) 387–401.
[49]S. Kozuch, J.M.L. Martin, ACS Catal. 2 (2012) 2787–2794.
[56]G.A. Bedogni, C.L. Padró, N.B. Okulik, J. Mol. Model. 20 (2014).
[57]S.R. Kirumakki, N. Nagaraju, K.V.R. Chary, Appl. Catal. A, Gen. 299 (2006) 185–192.
[58]J. Lilja, D.Y. Murzin, T. Salmi, J. Aumo, P. Maäki-Arvela, M. Sundell, J. Mol. Catal. A Chem. 182 (2002) 555–563.
[59]J. Liu, B. Yang, C. Yi, Ind. Eng. Chem. Res. 52 (2013) 3742–3751.
[60]M.R. Nanda, Z. Yuan, W. Qin, H.S. Ghaziaskar, M. Poirier, Fuel. 117 (2014) 470–477.

Therefore, a systematic assessment of these effects, by means of the Madon-Boudart method, on the catalytic results is henceforward presented. Figure 7 presents plots corresponding to the Madon-Boudart test for the three experimental blocks carried out. The plots feature the natural logarithm of the turnover frequencies as a function of the natural logarithm of the reciprocal of the quantity of active sites at the three different temperatures tested. To facilitate their interpretation, the curves for 353 K and 361 K were shifted from the origin by adding 0.5 and 1.0 unit, respectively, to the original values of turnover.

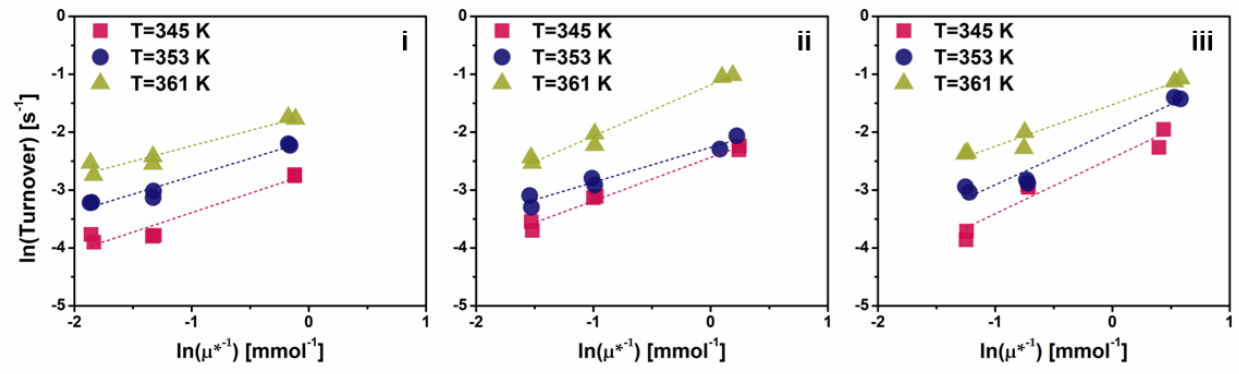

Figure 7. Logarithmic plots of Turnover frequencies as a function of the reciprocal of the number of active sites (μ^{*-1}) for assessing mass and heat transport limitation via the Madon-Boudart in the esterification of glycerol with acetic acid over Amberlyst-35 with particle size of 600 – 1180 μm. Values of moles of active sites (μ^*) at the different acetic acid to molar ratios (R): i) R = 1.8, μ^* = 1.14, 3.75 and 6.37 mmol; ii) R = 3.0, μ^* = 0.82, 2.70 and 4.58 mmol; and iii) R = 4.4, μ^* = 0.62, 2.04 and 3.45 mmol. Reaction temperatures of 345, 353, and 361 K.

The Madon-Boudart criterion indicates the presence of intraparticle mass transport limitations if the slope of the constructed plots is around 0.5. Likewise, if the plots at different temperatures display non parallel slopes, the influence of heat transport cannot be discarded either [39]. From Figure 7, the slopes of the prepared plots were indicative of the presence of both intraparticle and heat transfer limitations in the system. Therefore, the data obtained under these reaction conditions did not correspond to the intrinsic kinetic regime.

[39]R.J. Madon, M. Boudart, Ind Eng Chem Fundam. (1982) 438–447.

A calculation of the corresponding effectiveness factor and Thiele modulus further supported this conclusion; From the experimental data, 18 pairs of reactions were compared from both experimental sets with the same reaction conditions but different particle sizes. Hence, the systems catalyzed by Amberlyst-35 with a particle size of 600 – 1180 µm, the average value of the effectiveness factor was 0.663. For convenience, the complete calculations of the effectiveness factor and Thiele modulus are presented in the Supplementary Information (Table S11).

In addition, an estimation of the apparent activation energy for the registered data sets from the Arrhenius linearization of the apparent pseudo-second order kinetic rate constant, Figure 8i, led to values of 53.3, 54.0 and 45.7 kJ/mol for the first, second and third experimental blocks, respectively, which are representative of intrinsic kinetic measurements [34]. Therefore, the latter criterium is not self-sufficient for running out the absence of mass and heat transport limitations.

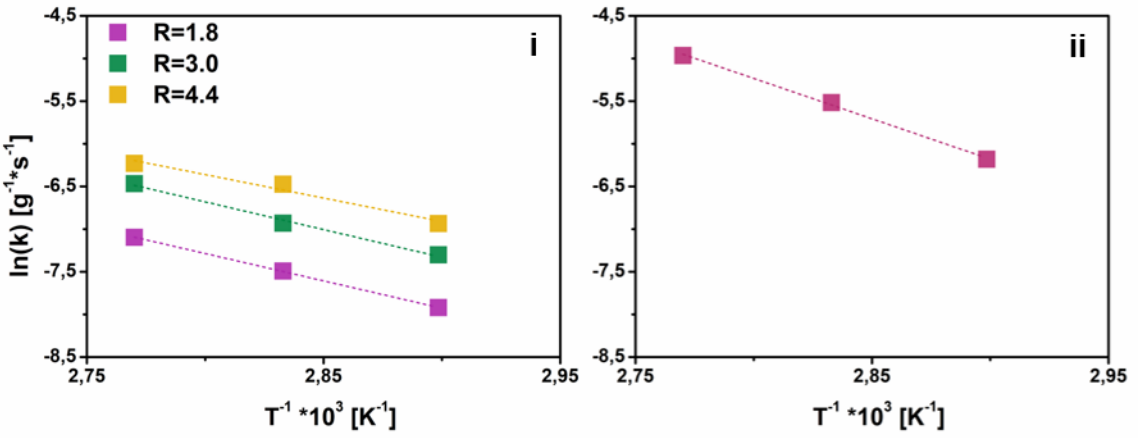

Figure 8. Arrhenius plots for the glycerol esterification with acetic acid catalyzed by Amberlyst-35. i) Catalyst particle size of 600 – 1180 µm, with values of moles of active sites (µ*) at the different acetic acid to glycerol molar ratios (R): R = 1.8, µ* = 1.14, 3.75 and 6.37 mmol; R = 3.0, µ* = 0.82, 2.70 and 4.58 mmol; and R = 4.4, µ* = 0.62, 2.04 and 3.45 mmol. ii) Catalyst particle size of 25 – 75 µm, with values of moles of active sites (µ*) at the acetic acid to glycerol molar ratio of 4.4, µ* = 0.62, 2.04 and 3.45 mmol. Reaction temperatures of 345, 353, and 361 K.

[34]E. Santacesaria, Catal. Today. 34 (1997) 393–400.

According to our literature survey, Table 1 and references [20,57,58], the data reported by several authors were also influenced by this type of artifacts. In the case of the work by Patel et al. [31], who discarded transport limitations from the results of a Koros-Nowak test, the reported turnover frequencies were estimated directly from the ratio of moles of obtained products to the “moles of catalyst” hence lacking true kinetic value [49]. Several kinetics studies for the esterification of alcohols with carboxylic acids over ion exchange resins have disregarded the presence of the intraparticle transport limitations without providing concrete experimental evidence of their absence [61–64]. Otherwise, the Weisz-Prater criterion [38] has been usually applied to analyze this kind of reaction systems [19,65,66] despite the known limitations of the method; namely, the assumption of several physicochemical parameters not available for reactions in the liquid phase. Particularly, predictions of the effective diffusivity tend to be extremely inaccurate because of the assumption of a Knudsen regime of diffusion.

Usually, it is considered that ion exchange resins are non-porous materials. Such a conception is misleading and make think researchers that intraparticle mass transport effects for reactions preformed over these solids should be absent *per se*. In view of the effects detected herein, it was decided to analyze the porosity of the Amberlyst-35 employed in this study. Figure 9 shows the N_2 adsorption – desorption isotherms recorded for two samples of the material; one corresponds to the particles employed in the current set of experiments and another to particles recovered after crushing and sieving the material down to a particle size range between 25 – 75 μm. Both isotherms correspond to type IV(a) and exhibited H1 type hysteresis loops [67].

[19]V.K.S. Pappu, V. Kanyi, A. Santhanakrishnan, C.T. Lira, D.J. Miller, Bioresour. Technol. 130 (2013) 793–797.
[20]P.U. Okoye, A.Z. Abdullah, B.H. Hameed, Renew. Sustain. Energy Rev. 74 (2017) 387–401.
[31]A. Patel, S. Singh, Fuel. 118 (2014) 358–364.
[38]P.B. Weisz, C.D. Prater, Adv. Catal. 6 (1954) 143–196.
[49]S. Kozuch, J.M.L. Martin, ACS Catal. 2 (2012) 2787–2794.
[61]M. Rıza, A. Çıtak, Appl. Catal. A Gen. 239 (2003) 141–148.
[62]S.H. Ali, O. Al-Rashed, F.A. Azeez, S.Q. Merchant, Bioresour. Technol. 102 (2011) 10094–10103.
[63]W. Osorio-Viana, M. Duque-Bernal, J. Fontalvo, I. Dobrosz-Gómez, Chem. Eng. Sci. 101 (2013) 755–763.
[64]H.T.R. Teo, B. Saha, J. Catal. 228 (2004) 174–182.
[65]M.J. Wulfers, R.F. Lobo, Appl. Catal. A Gen. 505 (2015) 394–401.
[66]A. Orjuela, A.J. Yanez, A. Santhanakrishnan, C.T. Lira, Chem. Eng. J. 188 (2012) 98–107.
[67]M. Thommes, K. Kaneko, A. V. Neimark, J.P. Olivier, F. Rodriguez-Reinoso, J. Rouquerol, K.S.W. Sing, Pure Appl. Chem. 87 (2015) 1051–1069.

These results point out that Amberlyst-35 is a mesoporous material possibly with cylindrical pores. The estimated surface area calculated by the BET method was 38 m^2/g_{cat} [50] and the average values for the total pore volume and for the pore diameter were 0.3 cm^3/g_{cat} and 31 nm, respectively, as calculated by the BJH method [51]. (See inset in Figure 9 displaying the corresponding pore size distribution). These results evidence that a significant portion of active sites might be located inside the pores of Amberlyst-35 where the transport of a bulky molecule such as glycerol should be slow.

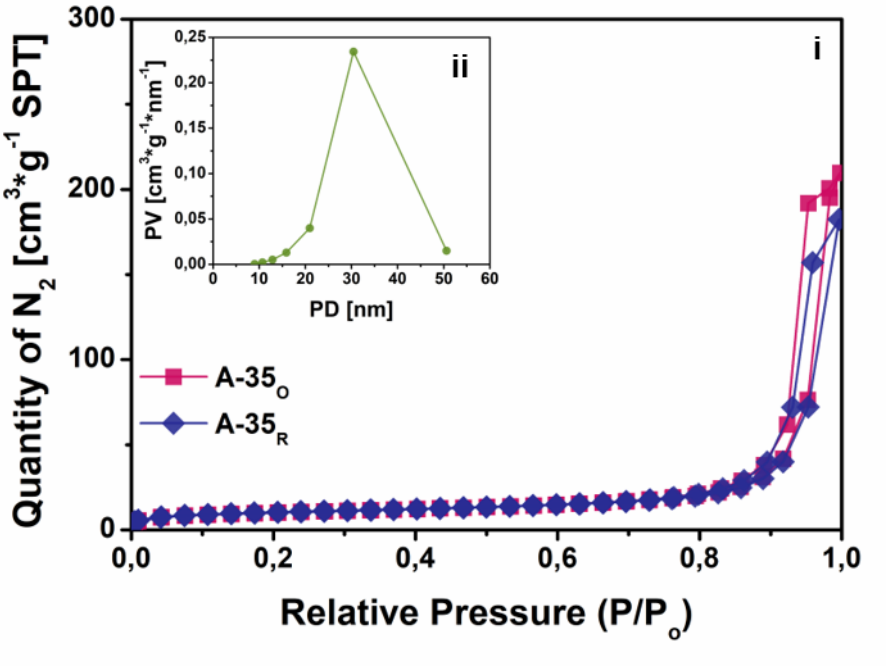

Figure 9. i) Plot of the N_2 adsorption – desorption isotherms for Amberlyst-35 recorded at 77 K, P/P_0 = 0.001 to 0.999. A-35_O: Amberlyst-35 with particle size between 600 – 1180 µm. A-35_R: Amberlyst-35 with particle size between 25 – 75 µm. ii) Pore size distribution plot for Amberlyst-35 as derived from the BJH method. PV: pore volume. PD: pore diameter.

[50]S. Brunauer, P.H. Emmett, E. Teller, J. Am. Chem. Soc. 60 (1938) 309–319.
[51]E.P. Barrett, L.G. Joyner, P.P. Halenda, J. Am. Chem. Soc. 73 (1951) 373–380.

1.3.3 Statistical assessment of the reactivity data for the second set of experiments: Provided the existence of intraparticle mass transport limitations for the reaction under the conditions of the first set of experiments, a second 3^2 FFED was carried out for testing the effect of temperature and of the quantity of active sites over the catalytic performance after reducing the particle size of Amberlyst-35 to a range between 25 – 75 μm. In this case, the acetic acid to glycerol molar ratio was fixed at R = 4.4. Table 10 summarizes the turnover frequencies obtained from these experiments. Curves illustrating the evolution of the conversion and products yield are presented in the Supplementary Information (Table S8).

Table 10. Summary of Turnover frequencies for glycerol esterification with acetic acid over Amberlyst-35 as obtained from reaction tests executed according to a 3^2 full factorial experimental design. Acetic acid to glycerol molar ratio of 4.4. Amberlyst-35 particle size of 25 – 75 μm.

Reaction	μ* [mmol]	T [K]	Turnover frequency *10^2 [s^{-1}]
1	0.62	345	18.38
2	2.04	345	5.54
3	3.45	345	3.99
4	0.62	353	18.58
5	2.04	353	6.54
6	3.45	353	4.32
7	0.62	361	22.54
8	2.04	361	6.21
9	3.45	361	5.04
10	0.62	345	17.15
11	2.04	345	5.65
12	3.45	345	3.42
13	0.62	353	17.26
14	2.04	353	6.11
15	3.45	353	4.27
16	0.62	361	22.68
17	2.04	361	5.38
18	3.45	361	4.63

For the statistical analysis of the data, Figure 10 shows the main effect plots for the outcomes of the experimental design. The first thing to be noticed is that the grand average for the turnovers of this FFED was higher (0.0987 s^{-1}) than the one obtained for the corresponding experimental block from the first set of experiments (0.0681 s^{-1}) at the same value of R (R = 4.4), Figure 10. In general, both variables showed a positive effect on the catalytic activity. From the plots, it can be inferred that this effect of the quantity of active sites was stronger as compared to the effect of

temperature. On the other hand, Figure 11 displays the interaction plots produced from the data of these experiments. The curves in these plots exhibited border line crosses and inflexions. However, just as in the case of the first set of experiments, the interactions suggested by these trends are dubious; particularly because both variables had an effect on the output of the experiment.

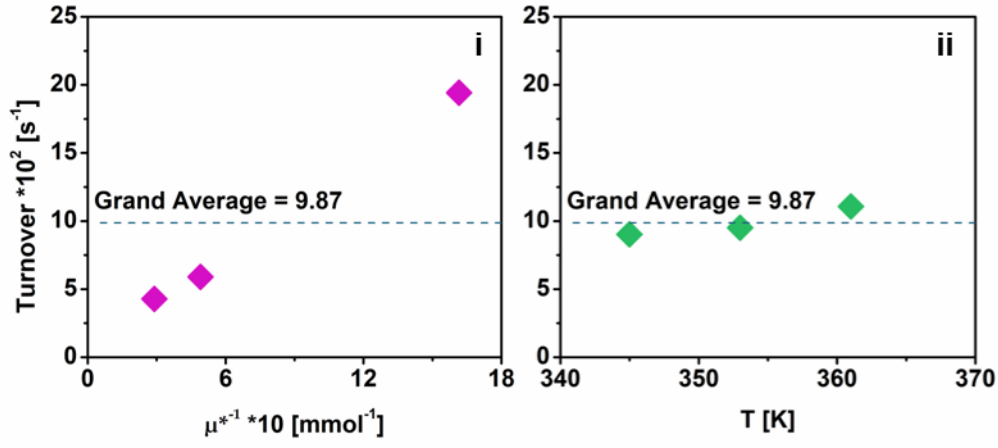

Figure 10. Main effect plots for results from a 3^2 full factorial experimental design with acetic acid to glycerol molar ratio of 4.4. i) Turnover frequencies for glycerol with the reciprocal of moles of active sites (μ^{*-1}). Values of moles of active sites (μ^*) of 0.62, 2.04 and 3.45 mmol. ii) Variation of the Turnover of the glycerol consumption with the reaction temperature (T). T = 345, 353, and 361 K. Amberlyst-35 particle size of 25 – 75 μm.

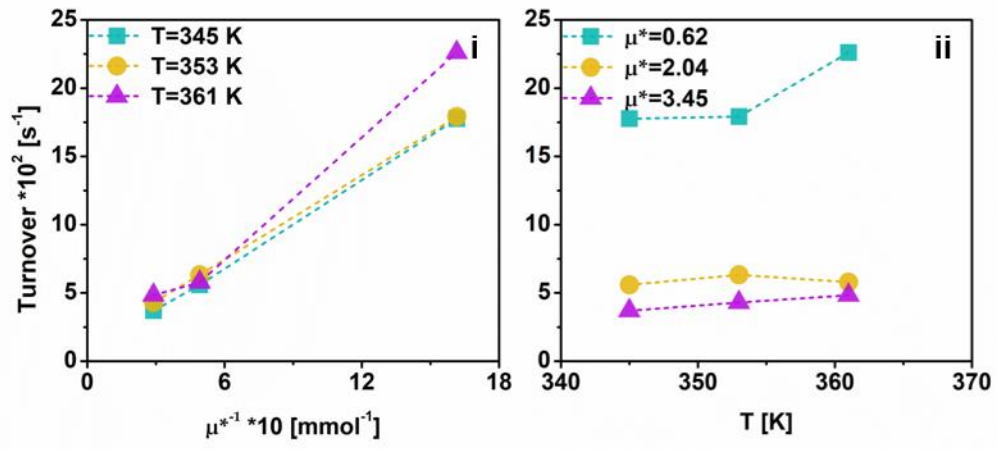

Figure 11. Interaction plots for results from a 3^2 full factorial experimental design with acetic acid to glycerol molar ratio of 4.4. i) $\mu^{*-1}\times T$ interactions. ii) $T\times\mu^{*-1}$ interactions. Values of moles of active sites (μ^*) of 0.62, 2.04 and 3.45 mmol. Reaction temperatures (T) of 345, 353, and 361 K. Amberlyst-35 particle size of 25 – 75 μm.

To complement the above analysis, the results of an ANOVA test for the data is shown in Table 11. The analysis of the residuals from the ANOVA model (Figure S9 and Section S10) did not show tendencies that represent major concerns regarding the assumptions of the model. Therefore, the conclusions from the analysis are more statistically robust than those attained for the first set of catalytic experiments (Section 3.2). In this instance, the ANOVA test indicated that all the factors had a statistically significant effect over the turnover frequency. However, as evidenced from the graphic analysis of the data, the statistical significance of the factor representing the interaction between temperature and quantity of active sites may be a consequence of them having an effect on the catalytic turnover. Therefore, despite that the statistically interaction might not be removable from the ANOVA model [53–55], this factor might not convey physical meaning.

Table 11. ANOVA test for assessing the effects of the different factors: μ^{*-1}, T and μ^{*-1}×T over the Turnover frequency considered in the 3^2 full factorial experimental design executed for glycerol esterification with acetic acid over Amberlyst-35 with particle size of 25 – 75 μm, and acetic acid to glycerol molar ratio of 4.4.

Factor	SS	υ	MS	F-value	p-value	S
μ^{*-1}	830.27	2	415.14	1599.07	3.29E-12	YES
T	13.84	2	6.92	26.66	1.65E-04	YES
μ^{*-1}×T	18.30	4	4.57	17.62	2.76E-04	YES
Error	2.34	9	0.26			
Total	864.75	17				

SS: sum of squares. υ: degrees of freedom. MS: mean squares. S: significance.

1.3.4 Phenomenological assessment of the reactivity data for the second set of experiments: To evaluate the possible influence of transport limitations under the conditions of the second set of experiments, Madon-Boudart plots were produced from the data once again. Figure 12 shows these plots; where, for the sake of the convenience, the curves for 353 and 361 K were again shifted by 0.5 and 1 units from the axis origin. In general, the obtained curves were parallel and had slopes close to 1. These outcomes permitted establishing that this set of data are free of mass and heat transfer effects.

[53]G.R. Loftus, On interpretation of interactions, 6 (1978) 312–319.
[54]E.J. Wagenmakers, A.M. Krypotos, A.H. Criss, G. Iverson, Mem. Cogn. 40 (2012) 145–160.
[55]R.L. Rosnow, R. Rosenthal, Psychol. Sci. 6 (1995) 3–9.

Further support for the latter conclusion was achieved by calculating the corresponding Thiele modulus and effectiveness factor. In this case, for the reaction systems catalyzed by Amberlyst-35 with particle size in a range of 25 – 75 μm, the average value of the effectiveness factor was 0.998. (Table S11).

In addition, from the Arrhenius linearization of the apparent pseudo-second order kinetic rate constant, Figure 8ii, and apparent activation energy of 78.7 kJ/mol was estimated this time. According to the review of Okoye et al. [20], for the esterification of glycerol over Amberlyst-15 catalysts, apparent activation energies around 60 kJ/mol have been estimated. However, the two studies reviewed by Okoye correspond to the works of Gelosa and Zhou [15,29] whose original papers showed evidence suggesting the influence of transport limitations. Similar remarks can be made for the work of Kim et al. [68] who reported activation energy values within the range from 59.2 to 80.1 kJ/mol after calculating turnover rates at constant glycerol conversion of ca. 0.30 and without referring them to the quantity of catalytic active sites of their solids. On the other hands, Khayoon et al [23] reported the value of 21.5 kJ/mol over yttria modified mesoporous silica catalysts, where the authors recognized that their system does not work under kinetic regime. Otherwise, if the results presented in this work for the experimental blocks with the acetic acid to glycerol molar ratio set-up in 4.4 are compared, when the Amberlyst-35 particle size is reduced, the value of the apparent activation energy increase from 45.7 to 78.7 kJ/mol which further confirms how transport limitations influence apparent activation energies.

[15]D. Gelosa, M. Ramaioli, G. Valente, M. Morbidelli, Ind. Eng. Chem. Res. 42 (2003) 6536–6544.
[20]P.U. Okoye, A.Z. Abdullah, B.H. Hameed, Renew. Sustain. Energy Rev. 74 (2017) 387–401.
[23]M.S. Khayoon, S. Triwahyono, B.H. Hameed, A.A. Jalil, Chem. Eng. J. 243 (2014) 473–484.
[29]L. Zhou, T.H. Nguyen, A.A. Adesina, Fuel Process. Technol. 104 (2012) 310–318.
[68]I. Kim, J. Kim, D. Lee, "Applied Catal. B, Environ. 148–149 (2014) 295–303.

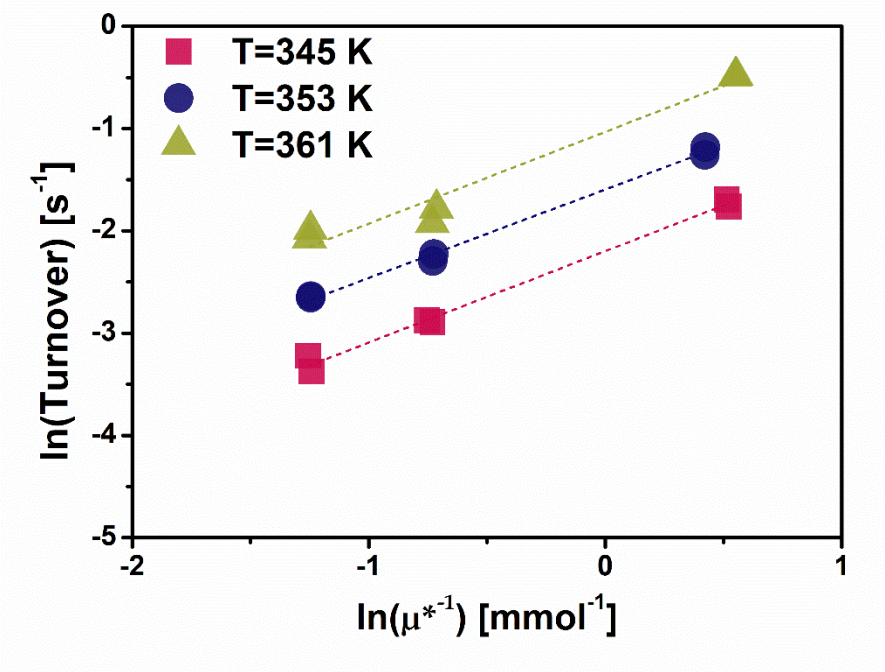

Figure 12. Logarithmic plots of Turnover frequencies as a function of the reciprocal to the number of active sites (μ^{*-1}) for assessing mass and heat transport limitation via the Madon-Boudart in the esterification of glycerol with acetic acid over Amberlyst-35 with particle size of 25 – 75 µm. Values of moles of active sites (μ^*) of 0.62, 2.04 and 3.45 mmol. Reaction temperatures (T) of 345, 353, and 361 K.

1.3.5 Catalyst stability and recyclability tests: The result of the stability test for the Amberlyst-35 with particle size in a range of 25 – 75 µm is presented in the Figure 13. Subsequently, the catalyst is removed from the liquid medium of the first reaction, the evolution of the homogeneous reaction is very similar to the activity of the blank reaction. Therefore, this test supports the stability of the Amberlyst-35 and the absence of the leached species, even when its particle size is reduced to a fine powder. The result of the recyclability test is presented in the Figure 14. As was expected, the catalytic activities from the first reaction and the recycle reaction are overlapped. Once again, the chemical stability of the Amberlyst-35 at the current reaction conditions is confirmed.

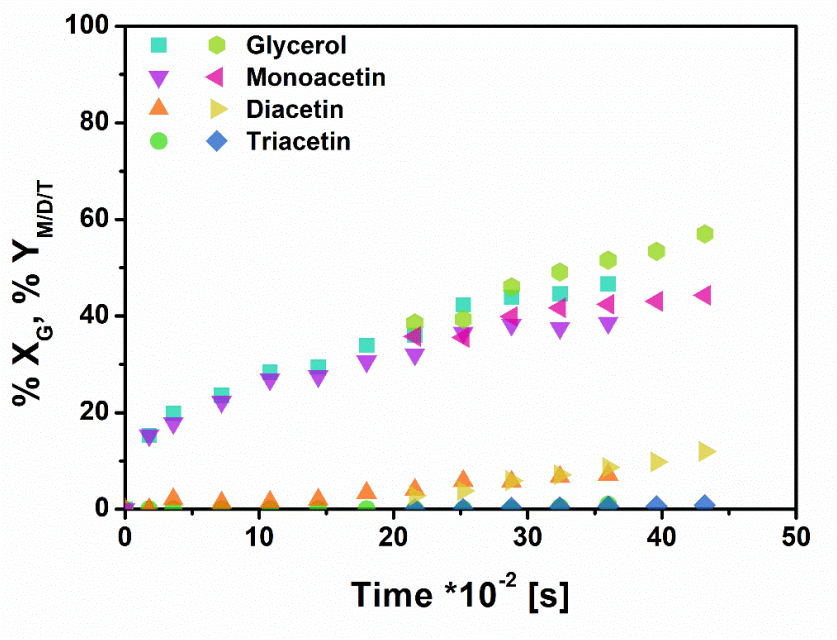

Figure 13. Stability test for the Amberlyst-35 with a particle size of 25 – 75 µm. Glycerol esterification with initial acetic acid to glycerol molar ratio of 9, temperature of 343 K, and quantity of moles of active sites of 0.85 mmol.

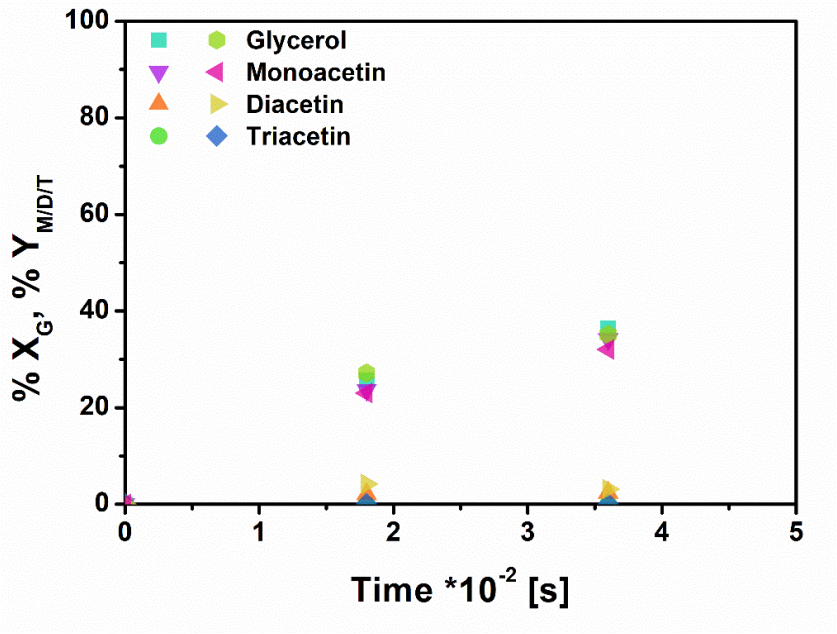

Figure 14. Recycle test for the Amberlyst-35 with a particle size of 25 – 75 µm. Glycerol esterification with initial acetic acid to glycerol molar ratio of 9, temperature of 343 K, and quantity of moles of active sites of 0.85 mmol.

1.4 CONCLUSIONS

This work revisited the esterification of glycerol with acetic acid over Amberlyst-35 employing sequential statistically designed experiments. Thanks to this approach, the collected data were statistically robust and provided meaningful insight into the catalytic reaction. The influence of the quantity of active sites; assumed herein as the number of SO_3H^+ sites, temperature, and of the acetic acid to glycerol molar ratio on turnover frequencies was clearly established. On the one hand, results showed that under the typical conditions employed in most open literature, the reported catalytic trends are influence by mass and heat transport limitations. Particularly, the application of the Madon-Boudart criterion along with calculations of Thiele modulus, effectiveness factor, and apparent activation energies allowed establishing that though Amberlyst-35 has large pores (average size ~30 nm) intraparticle transport limitations influence the catalytic results when employing particle sizes larger than 600 μm. Such limitations became negligible when reducing the particle size of the material to a range between 25 and 75 μm. The latter conditions allowed establishing a straightforward relationship between the concentration of surface SO_3H^+ active sites and the turnover rates. Conversely, under the studied conditions, the reaction temperature had a rather weak effect on the glycerol consumption. In general, this new conditions allow the acquisition of kinetically relevant data.

CHAPTER 2

KINETIC MODELING OF THE PRODUCTION OF ACETINS VIA GLYCEROL ESTERIFICATION WITH ACETIC ACID OVER AMBERLYST-35

This chapter presents a kinetic modeling of the production of acetins via glycerol esterification. Starting from the Fischer esterification and the Langmuir-Hinshelwood-Hougen-Watson (LHHW) formalism, rate expressions for monoacetin, diacetin and triacetin formation are developed. Three sets of experiments were carried out to collect enough experimental data to find the corresponding kinetic parameters. Then, the kinetic models were submitted to regression analyses with the reparametrized form of the Arrhenius and van't Hoff equations. Finally, the parameters were assessed by physicochemical tests founded on thermodynamic grounds.

2.1 EXPERIMENTAL SECTION

2.1.1 Catalytic tests: The catalytic tests and the analysis of the reaction samples were performed as described in the previous chapter. The Amberlyst-35 particle size was fixed in a range of 25 – 75 µm for all tests to avoid transport limitations. Three experimental sets were carried out to estimate the parameters from the developed kinetic model. The first set of catalytic tests was executed following a 3^2 FFED. Temperatures employed were 347, 361 and 373 K, the acetic acid to glycerol molar ratio (R) was set to 5.0, 7.0 and 9.0, and the catalyst loading was kept constant at 1 wt.%. This percentage is referred to the weight of glycerol in the reactor. For this set of experiments, three replicates at the center point were taken to monitor the repeatability of the results. The repeatability test is presented in the Supplementary Information (Figure S12). The second set of catalytic tests was a 2x2x3 factorial experimental design (FED), temperatures were set at 361 and 373 K, acetic acid to glycerol molar ratios were fixed at 7.0 and 9.0, and catalyst loadings were set at 0.5, 2.3 and 3.9 wt.%. The third set of catalytic tests was designed with a 2^2 FFED using

temperatures of 361 and 373 K, and the catalyst loading values of 0.5 and 2.3 wt.%. The acetic acid to glycerol molar ratio was kept constant at 5.0 in this occasion. In order to follow the evolution in the production of acetins, samples of the reaction products were taken at defined times starting from 0.0, 0.5, 1 h, and each hour to complete 10 h of reaction. In total, 27 reactions were carried out.

2.2 KINETIC MODELING

2.2.1 Fischer esterification mechanism: Fischer esterification is a reaction in which a carboxylic acid interacts with an alcohol in presence of an acid catalyst. The mechanism of this reaction has several steps. Firstly, the proton from the catalyst is transferred to the carbonyl oxygen. Therefore, the electrophilicity of the carbonyl carbon increases. Then, the oxygen atom of the hydroxyl group produces a nucleophilic attack on the protonated carbonyl group of the acid. The proton is transferred to the alcohol molecule to form an activated complex where a C-O bond is given between the carbon from the carbonyl group and the oxygen from the hydroxyl group. This complex is called tetrahedral intermediate. From this, a water molecule is produced along with the corresponding ester. To close the cycle, the proton is recovered for the catalyst [69,70].

In the heterogeneous reaction system of glycerol, acetic acid and Amberlyst-35, a mechanism similar to the Fischer esterification has been proposed [3,9,20,56–58]. The reaction requires, of course, steps for the adsorption – desorption of the reactants and products, respectively.

[3]N. Rahmat, A.Z. Abdullah, A.R. Mohamed, Renew. Sustain. Energy Rev. 14 (2010) 987–1000.
[9]L.N. Silva, V.L.C. Gonçalves, C.J.A. Mota, Catal. Commun. 11 (2010) 1036–1039.
[20]P.U. Okoye, A.Z. Abdullah, B.H. Hameed, Renew. Sustain. Energy Rev. 74 (2017) 387–401.
[56]G.A. Bedogni, C.L. Padró, N.B. Okulik, J. Mol. Model. 20 (2014).
[57]S.R. Kirumakki, N. Nagaraju, K.V.R. Chary, Appl. Catal. A, Gen. 299 (2006) 185–192.
[58]J. Lilja, D.Y. Murzin, T. Salmi, J. Aumo, P. Maäki-Arvela, M. Sundell, J. Mol. Catal. A Chem. 182 (2002) 555–563.
[69]J. McMurry, Química Orgánica, Octava Edi, 2012.
[70]F.A. Carey, R.J. Sundberg, Fifth Edit, 2007.

The protonation of the carbonyl group is assumed to occur on the catalyst surface producing the acetic acid – active site complex. The surface reaction is carried out between a glycerol molecule in the liquid medium and the acetic acid – active site complex. Then, one water molecule is lost to the liquid medium while one monoacetin molecule is desorbed. These steps are repeated until each hydroxyl group from glycerol is replaced to form the diacetin and triacetin molecules. This mechanism is pictured in the Figure 15.

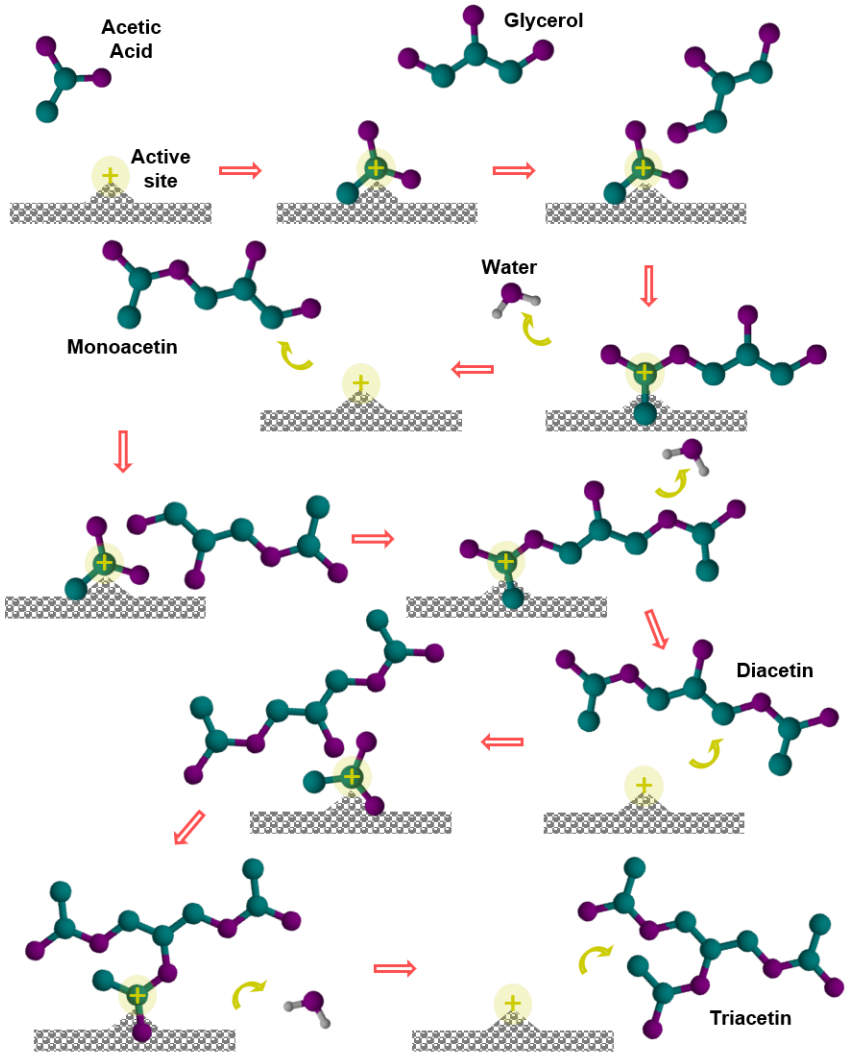

Figure 15. Illustration of the mechanism of the production of acetins via glycerol esterification catalyzed by Amberlys-35. Purple and green balls represent oxygen and carbon atoms, respectively.

2.2.2 Langmuir-Hinshelwood-Hougen-Watson kinetics: The LHHW formalism is a strategy to determine a kinetic expression for a reaction heterogeneous system. It is based in the insights by Langmuir [71], Hinshelwood [72], and Hougen & Watson [73]. This method presents adsorption, surface reaction and desorption processes as a consecutive reaction sequence, for both gas or liquid phases. The assumptions are that the adsorbed species are recognized as reaction intermediates, and that the coverage of the active sites is related with reactant and product species. The reaction mechanism is described as a series of elementary steps. Depending on how the molecule adsorption is achieved, the series of elementary steps is named Eley-Rideal or Langmuir-Hinshelwood mechanism when adsorption occurs on one or two active sites, respectively. Then, each step is defined with a law of mass action expression for a reversible reaction in terms of the concentrations. The step with the lowest rate is considered the rate determining step (RDS) [36,74,75]. Usually, the step which involves reaction on the catalyst surface is settled as the RDS. The other steps are very fast compared to the RDS. Hence, they are assumed to be in a quasi-steady state; i.e. the change in the rates forward and backward is very small and the net rate is supposed to be near zero [36,74,75]. Accordingly, these expressions are rearranged to eliminate terms that depend on the coverage of active sites. Consequently, the overall reaction rate is the RDS expression in terms of the measurable concentrations.

2.2.3 Parameter estimation: Kinetic parameters are estimated by minimizing an objective function $RSS(\varphi)$, which includes the residual sum of squares of the concentration of the different species.

$$RSS(\varphi) = \sum_{n=1}^{n_{resp}} w_n \sum_{k=1}^{n_{exp}} \left(C_{k,n} - \hat{C}_{k,n}\right)^2 \xrightarrow{\varphi_1,\varphi_2,\ldots,\varphi_n} minimum \quad \text{(Equation 6)}$$

[36]M.A. Vannice, Kinetics of Catalytic Reactions, 2005.
[71]I. Langmuir, J. Am. Chem. Soc. 40 (1918) 1361–1403.
[72]C.N. Hinshelwood, The kinetics of chemical change, 1940.
[73]O.A. Hougen, K.M. Watson, Ind. Eng. Chem. 35 (1943) 529–541.
[74]E.M. Davis, R.J. Davis, Fundamentals of Chemical Reaction Engineering, 2003.
[75]I. Chorkendorff, J.W. Niemantsverdriet, Concepts of Modern Catalysis and Kinetics, 2003.

In the above equation, φ is the optimal parameter vector; n_{exp} and n_{resp} are the number of independent experiments and number of responses, respectively; $C_{k,n}$ and $\hat{C}_{k,n}$ are the mole fraction of the nth experimental and predicted responses for the kth observation; and w_n is the weight factor assigned to the nth response.

The subroutine VODE is used to solve the corresponding set of ordinary differential equations (ODEs) [76]. The initial minimization of the objective function (Equation 6), in the model regression is carried out using the Rosenbrock method [77]. The ODRPACK software is used for fitting the corresponding experimental data points [78]. This set of subroutines can perform either weight orthogonal distance regression or nonlinear least squares problems for explicit and implicit models using multi-response data with an implementation of Levenberg-Marquard method [79].

The kinetic constant of the ith reaction, k_i, and the equilibrium adsorption constant of the component n, K_n, are reparametrized from the Arrhenius and van't Hoff equations (Equation 7 and 8). Therefore, these kinetic parameters are in terms of the values of activation energies, pre-exponential factors, and standard adsorption enthalpies and entropies.

$$k_i = exp\left[A'_i - \frac{E_{a,i}}{R}\left(\frac{1}{T} - \frac{1}{T^*}\right)\right] \quad \text{(Equation 7)}$$

$$K_n = exp\left[\frac{\Delta S_n^o}{R} - \frac{\Delta H_n^o}{R}\left(\frac{1}{T} - \frac{1}{T^*}\right)\right] \quad \text{(Equation 8)}$$

For the ith reaction, A'_i is the natural logarithm of the pre-exponential factor and $E_{a,i}$ is the activation energy. ΔS_n^o and ΔH_n^o are the standard entropy and enthalpy of the component n, respectively. For both equations, T and T^* are the reaction temperature and the average reaction temperatures, respectively, and R is the universal gas constant.

---

[76]P.N. Brown, G.D. Byrne, A.C. Hindmarsh, SIAM J Sci Stat Comput. 10 (1989) 1038–1051.
[77]H.H. Rosenbrock, Computer (Long. Beach. Calif). 3 (1960) 175–184.
[78]P.T. Boggs, J.R. Donaldson, R. h. Byrd, R.B. Schnabel, ACM Trans. Math. Softw. 15 (1989) 348–364. [79] D. Marquardt, An Algorithm for least-squares estimation of nonlinear parameters, J. Soc. Indust. Appl. Math. 11 (1963) 431–441.
[79]D. Marquardt, J. Soc. Indust. Appl. Math. 11 (1963) 431–441.

Once the parameters are estimated, the significance of the overall regression for each model is tested by means of an F-test. The F-value for the global significance of the regression is defined as the ratio between sum of squares of the regression and the residual sum of squares divided by their respective number of degrees of freedom. The significance of the individual parameters is assessed by a t-test. The resulting t-value is compared with a tabulated value obtained for degrees of freedom and the probability level of $1-\propto$, i.e. $\propto = 0.05$.

The programming code for parameter estimation was fed with initial values of the parameters, and a database consisting of the conditions of each reaction: temperature, catalyst loading, and the initial and intermediate concentrations of the reactants. And products as measured during the experiments. In total, there are 324 rows of data. The new parameters found by the program are used to recalculate the concentration of all compounds in each reaction time. This process is repeated until the calculated parameters show a good mathematical fit in the kinetic model. In practice, one parameter estimation run last almost two minutes.

The mathematical fit of the recalculated data was evaluated from the construction of parity diagrams for the mole fractions of each component comparing the experimental values from the experimental designs and the calculated values from the developed kinetic models. With the aid of a Microsoft Excel 2016 spreadsheet, prediction intervals were calculated for the related data in the parity diagrams using the Equation 9 [44,80].

$$Prediction\ interval = C_{pred} \pm t_{\alpha} SE \sqrt{1 + \frac{1}{n} + \frac{\left(C_{exp} - \bar{C}_{exp}\right)^2}{SS}} \quad \text{(Equation 9)}$$

[44]M.H. Kutner, C.J.J. Nachtsheim, J. Neter, W. Li, Applied Linear Statistical Models, Fifth Edit, 2004.
[80]W. Navidi, Statistics for Engineers and Scientists, Fourth Edi, 2015.

Therein, C_{pred} is the predicted mole fraction value from the linear regression. C_{exp}, and $\bar{C}_{exp}$ are the mole fraction and the average mole fraction from the experimental data, respectively. The Student's t-distribution (t_{α}) has a probability level of $90\% = (1-\propto) * 100$, i.e. $\propto = 0.1$. SE and SS are the standard error and the sum of squares deviations of data points, respectively. n is the total number of data, i.e. 324.

2.2.4 Physicochemical tests on the parameters of the models: The parameters obtained after the above calculations are evaluated with the rules and guidelines proposed by Boudart et al. [36,48], namely:

$$-\Delta H_{ad}^{o} > 0 \quad \text{(Equation 10)}$$

$$0 < -\Delta S_{ad}^{o} < S_{g}^{o} \quad \text{(Equation 11)}$$

$$41.8 < -\Delta S_{ad}^{o} < 51.04 - 1.4\Delta H_{ad}^{o}\ [kJ/mol] \quad \text{(Equation 12)}$$

The upper limit in Equation 11 corresponds to the standard total entropy in gas phase, S_{g}^{o}. This constraint implies that the entropy change in a given step cannot be higher than the entropy of its highest energetic state. These criteria were originally developed for reactions in gas phase. However, the reaction system studied herein in liquid phase. Therefore, the entropy for the highest energetic state must be referred to the liquid state, S_{l}^{o}. Table 12 lists the S_{l}^{o} values for the species involved in the esterification system as obtained from the CRC data base [81]. The S_{l}^{o} values for monoacetin and diacetin are not reported. Considering their structure and chemical nature, these values are expected between the glycerol and triacetin S_{l}^{o} values, nonetheless.

[36]M.A. Vannice, Kinetics of Catalytic Reactions, 2005.
[48]M. Boudart, Kinetics of Chemical Processes, Butterworth-Heinemann, 1991.
[81]Crc, STANDARD THERMODYNAMIC PROPERTIES OF CHEMICAL SUBSTANCES (continued), CRC Handb. Chem. Phys. 13 (2012) 5.4-5.41.

Table 12. Standard total entropy in liquid phase (S_l^o) values for each compound of the reaction system.

Component	S_l^o [J*mol^{-1}*K^{-1}]
Glycerol	206.3
Acetic acid	159.8
Monoacetin	~ 290
Diacetin	~ 374
Triacetin	458.3
Water	70

Moreover, the thermodynamic criterion which relates the standard enthalpy for the ith reaction with all contributions of the energy changes is taken into account. The reaction enthalpies used in this work were calculated from the thermodynamic equilibrium experimental data presented in the work by Gelosa et al. [15]. Therefore, this reaction enthalpies were supplied to the programming code to evaluate the parameters with thermodynamic criterion.

$$\Delta H_{r,i}^{o} = \left(\Delta H_{R,i}^{o} - \Delta H_{P,i}^{o}\right) + \left(\Delta E_{a,i}^{F} - \Delta E_{a,i}^{B}\right) \quad \text{(Equation 13)}$$

2.3 RESULTS AND DISCUSSION

The catalytic test with Amberlyst-35 were carried out as mentioned in the experimental section. The outcomes are presented in Table 13. For sake of brevity, curves showing the evolution of the catalytic activity as a function of time are presented in the Supplementary Information (Figure S13 to Figure S39).

From the LHHW formalism and considering the formation of the active complex in a single active site. i.e. an Eley-Rideal mechanism, the steps assumed for glycerol esterification over Amberlyst-35 are presented in Table 14. Therein, the symbol $\boldsymbol{\nu_i}$ is the stoichiometric number for each step necessary to complete one catalytic cycle. Glycerol esterification is a consecutive reaction, wherefore the global reaction is achieved when all the hydroxyl groups of the glycerol are reacted.

[15]D. Gelosa, M. Ramaioli, G. Valente, M. Morbidelli, Ind. Eng. Chem. Res. 42 (2003) 6536–6544.

Table 13 shows the turnover frequency for each acetin formation. In comparison with the rate of monoacetin formation, the rate for the second and third acetin formation vary by one and two orders of magnitude, respectively. The diacetin and triacetin formation are very slow. Therefore, the evolution of the intermediate acetins must be analyzed. The steps which involve the surface reaction are assumed as RDS, i.e. 2, monoacetin formation; 4, diacetin formation; and 6, triacetin formation. For this mechanism, all the active sites have similar nature. In addition, the Amberlyst-35 has high affinity to adsorb water, hence, the water adsorption – desorption processes are recognized in the mechanism.

Table 13. Summary of Turnover frequencies for glycerol esterification with acetic acid over Amberlyst-35 as obtained from reaction tests executed according to three sets of experiments designed. Amberlyst-35 particle size of 25 – 75 μm.

Reaction	μ* [mmol]	R	T [K]	Turnover frequency [s^{-1}]		
				M *10^2	D*10^3	T *10^4
1	1.33	5	347	1.08	2.63	1.72
2	1.01	7	347	2.12	3.30	2.43
3	0.81	9	347	1.66	3.17	3.00
4	1.33	5	361	2.32	5.84	4.10
5	1.01	7	361	2.01	5.41	5.37
6	1.01	7	361	2.28	7.55	6.47
7	1.01	7	361	2.37	6.61	5.39
8	0.81	9	361	2.34	7.51	7.48
9	1.33	5	373	4.20	11.93	9.93
10	1.01	7	373	4.34	10.45	10.98
11	0.81	9	373	4.20	11.38	13.40
12	0.51	7	361	7.83	8.19	19.47
13	2.33	7	361	2.65	5.17	12.91
14	3.95	7	361	1.70	5.26	14.19
15	0.41	9	361	5.30	8.76	19.61
16	1.87	9	361	2.56	4.89	7.90
17	3.18	9	361	1.57	5.07	11.29
18	0.51	7	373	11.69	31.01	49.61
19	2.33	7	373	2.73	10.43	20.65
20	3.95	7	373	0.57	7.42	16.51
21	0.41	9	373	9.95	17.21	46.02
22	1.87	9	373	2.73	11.08	17.54
23	3.18	9	373	1.58	7.12	17.32
24	0.67	5	373	5.60	13.29	43.24
25	0.67	5	361	4.41	7.89	21.05
26	3.07	5	373	2.57	8.49	21.29
27	3.07	5	361	2.48	4.82	12.14

*M: monoacetin. D: diacetin. T: triacetin.

Table 14. Reaction mechanism for the glycerol esterification with acetic acid catalyzed by Amberlyst-35.

Mechanism	ν_i	Step
$A + * \leftrightarrows A*$	3	**1.** Acetic acid adsorption
$A* + G \leftrightarrows M* + W$	1	**2.** Monoacetin and water formation
$M* \leftrightarrows M + *$	1	**3.** Monoacetin desorption
$A* + M \leftrightarrows D* + W$	1	**4.** Diacetin and water formation
$D* \leftrightarrows D + *$	1	**5.** Diacetin desorption
$A* + D \leftrightarrows T* + W$	1	**6.** Triacetin and water formation
$T* \leftrightarrows T + *$	1	**7.** Triacetin desorption
$W + * \leftrightarrows W*$	1	**8.** Water adsorption
$W* \leftrightarrows W + *$	1	**9.** Water desorption
Global Reaction		
$3A + G \leftrightarrows M \leftrightarrows D \leftrightarrows T + 3W$		

With the aforementioned, three kinetic models are developed for the formation of each acetin. The mathematical formulation of these models leads to the following expressions for the reaction rates:

- Rate of monoacetin formation:

$$r_{M*} = \frac{k_2\left[K_A C_A C_G - \frac{K_M C_M C_W}{K_2}\right]}{1 + K_A C_A + K_M C_M + K_D C_D + K_T C_T + K_W C_W} \quad \text{(Equation 14)}$$

- Rate of diacetin formation:

$$r_{D*} = \frac{k_4\left[K_A C_A C_M - \frac{K_D C_D C_W}{K_4}\right]}{1 + K_A C_A + K_M C_M + K_D C_D + K_T C_T + K_W C_W} \quad \text{(Equation 15)}$$

- Rate of triacetin formation:

$$r_{T*} = \frac{k_6\left[K_A C_A C_D - \frac{K_T C_T C_W}{K_6}\right]}{1 + K_A C_A + K_M C_M + K_D C_D + K_T C_T + K_W C_W} \quad \text{(Equation 16)}$$

Where, the terms k_2, k_4, and k_6 are the kinetic constants for the formation of monoacetin, diacetin and triacetin, respectively. K_2, K_4, and K_6 are the equilibrium constants for each reaction step. K_{A}, K_{M}, K_{D}, K_{T}, and K_{W} are the equilibrium adsorption constants, and C_n is the concentration in mole fraction (mmol/mol) of the corresponding species.

Table 15. Values of the kinetic parameters for the models of the monoacetin, diacetin and triacetin formation.

Parameter	Estimated value	Unit
A_2^F	2.000	[mmol/g h]
A_4^F	0.999	
A_6^F	0.001	
E_{a2}^F	119.814	[kJ/mol]
E_{a4}^F	100.124	
E_{a6}^F	150.373	
A_2^B	1.583	[mmol/g h]
A_4^B	0.001	
A_6^B	0.001	
E_{a2}^B	125.795	[kJ/mol]
E_{a4}^B	87.950	
E_{a6}^B	117.663	
$-\Delta H_A^\circ$	114.860	[kJ/mol]
$-\Delta H_M^\circ$	15.012	
$-\Delta H_D^\circ$	15.007	
$-\Delta H_T^\circ$	15.001	
$-\Delta H_W^\circ$	70.029	
$-\Delta S_A^\circ$	50.090	[kJ/mol K]
$-\Delta S_M^\circ$	49.932	
$-\Delta S_D^\circ$	50.069	
$-\Delta S_T^\circ$	49.179	
$-\Delta S_W^\circ$	49.797	

After executing with the programming code in an iterative process, the values for the activation energy and the pre-exponential factors, and the standard adsorption enthalpies and entropies were found from the Arrhenius and van't Hoff equations (Equations 7 and 8), and these data is displayed in Table 15. In the Supplementary Information is presented the Scheme S40 that it pictures the iterative process, and

the kinetic constants and the equilibrium adsorption constants in terms of the kinetic parameter founds, Sections S41 to S54.

The backward activation energy values were calculated from the following equation that relates the backward and forward activation energies with reaction enthalpy:

$$E_{a,i}^{B} = E_{a,i}^{F} - \Delta H_{r,i} \quad \text{(Equation 17)}$$

As mentioned in the earlier section, the reaction enthalpies were calculated from the thermodynamic equilibrium experimental data presented by Gelosa et al. [15]. Accordingly, the values of the reaction enthalpies for monoacetin, diacetin and triacetin formation were -5.98, 12.17, and 32.71 [kJ/mol], respectively.

The computer program uses the new parameter to recalculate the concentration of all compounds in each reaction time. Figure 16 shows parity diagrams for each component. Where, the experimental mole fractions of the reaction products are compared with the calculated mole fractions. From the three models developed for the acetins formation, an acceptable fitting was obtained for the experimental observations. Likewise, the compositions of the glycerol, acetic acid and water were calculated by considering the stoichiometry of the reaction. Prediction bands are made from the calculated values of 90% prediction intervals for data points related in each parity diagram. Which means, 90% of the calculated mole fraction ($x_{Calculated}$) for a certain experimental mole fraction ($x_{Experimental}$) will be predicted within the interval range around the linear regression line.

[15]D. Gelosa, M. Ramaioli, G. Valente, M. Morbidelli, Ind. Eng. Chem. Res. 42 (2003) 6536–6544.

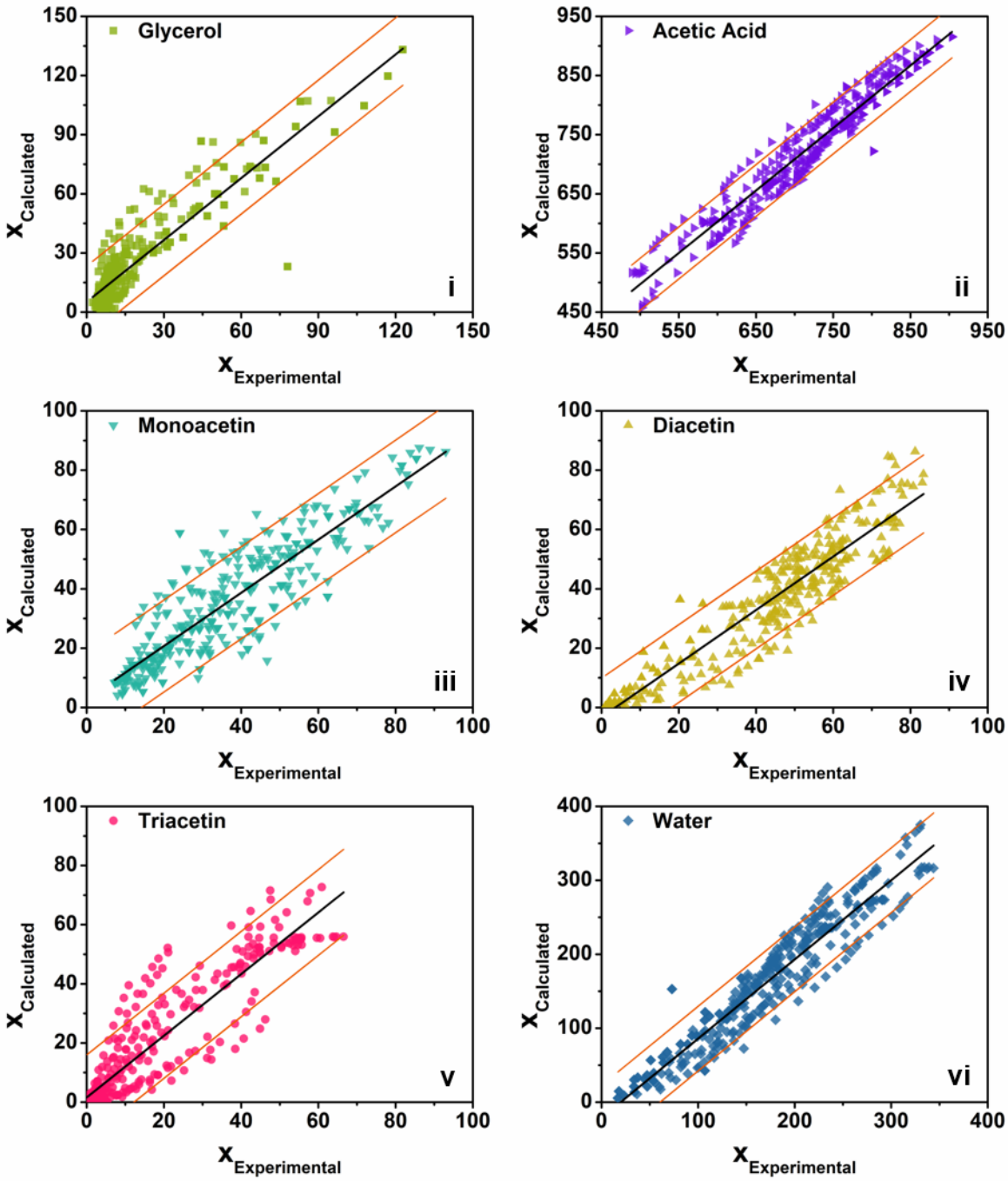

Figure 16. Parity diagrams for comparing the experimental and calculated mole fraction from the developed kinetic models. i) Glycerol. ii) Acetic acid. iii) Monoacetin. iv) Diacetin. v) Triacetin. vi) Water. The space between orange lines represents the prediction bands.

The calculated values of the adsorption enthalpies and entropies satisfied the Boudart et al. [36,48] rules. The values of the change in entropy were also within the range fixed by the criteria (Equation 10 to 12). Likewise, the activation energies obtained are within the range proposed by Santacesaria [34]. Figures 17 to 20 present the predictive capacity of the kinetic models developed for one of the reaction evaluated in this work. For comparison purposes, all the evolution curves in the reaction time from both experimental and calculated data are presented in the Supplementary Information (Figure S13 to Figure S39).

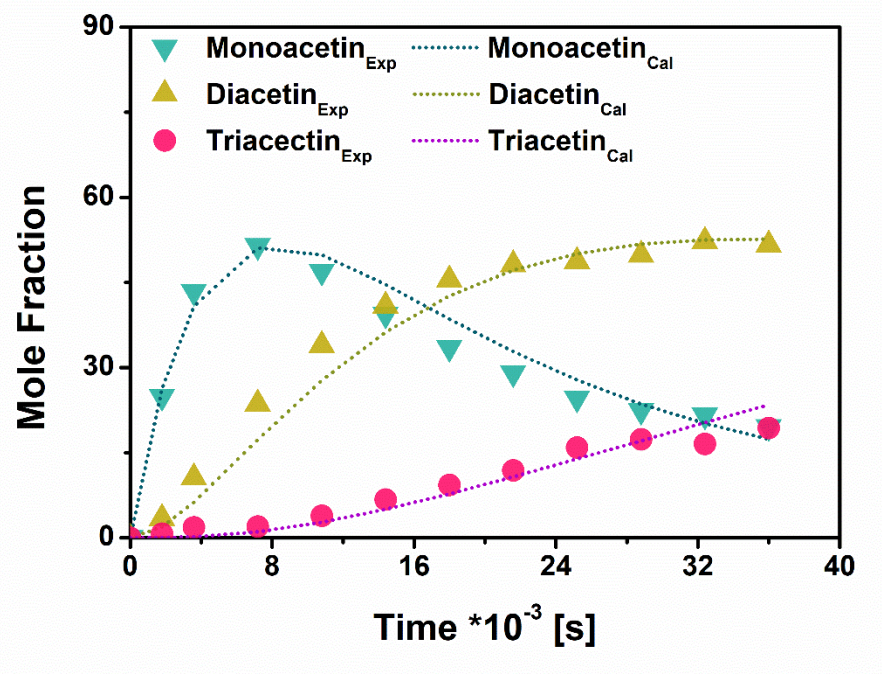

Figure 17. Evolution plot of the acetins formation. Glycerol esterification catalyzed by Amberlyst-35 with particle size of 25 – 75 µm. Initial acetic acid to glycerol molar ratio of 7, temperature of 361 K, and quantity of moles of active sites of 1.01 mmol. Exp: experimental values from the experimental designs. Cal: calculated values from the developed kinetic models.

[34]E. Santacesaria, Catal. Today. 34 (1997) 393–400.
[36]M.A. Vannice, Kinetics of Catalytic Reactions, 2005.
[48]M. Boudart, Kinetics of Chemical Processes, Butterworth-Heinemann, 1991.

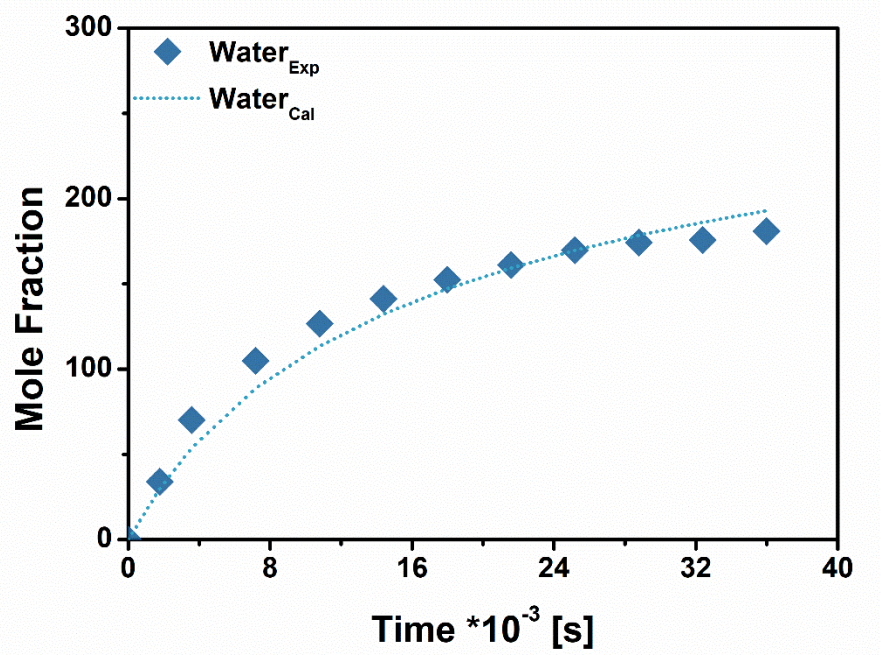

Figure 18. Evolution plot of the water formation. Glycerol esterification catalyzed by Amberlyst-35 with particle size of 25 – 75 μm. Initial acetic acid to glycerol molar ratio of 7, temperature of 361 K, and quantity of moles of active sites of 1.01 mmol. Exp: experimental values from the experimental designs. Cal: calculated values from the developed kinetic models.

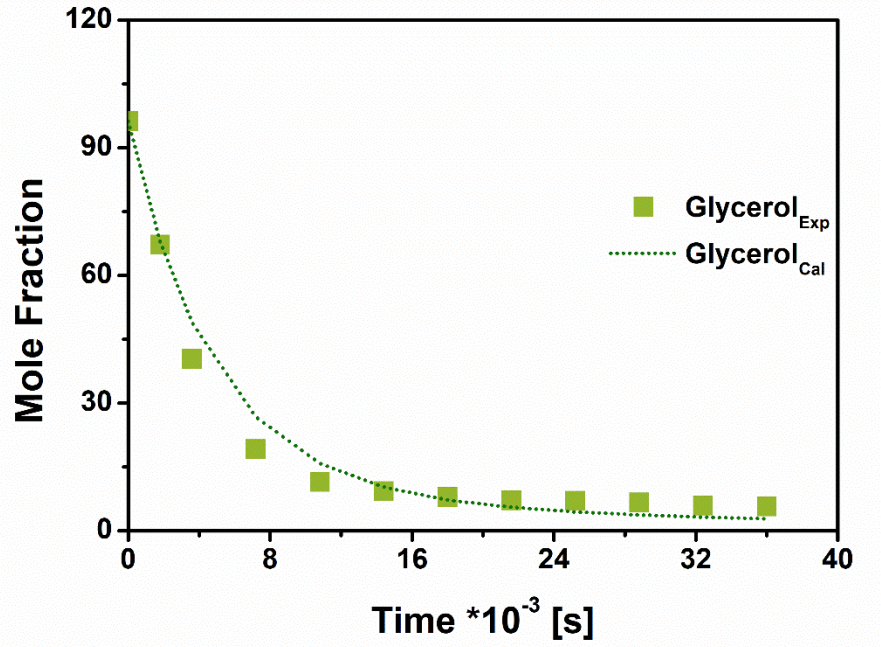

Figure 19. Evolution plot of the glycerol consumption. Glycerol esterification catalyzed by Amberlyst-35 with particle size of 25 – 75 μm. Initial acetic acid to glycerol molar ratio of 7, temperature of 361 K, and quantity of moles of active sites of 1.01 mmol. Exp: experimental values from the experimental designs. Cal: calculated values from the developed kinetic models.

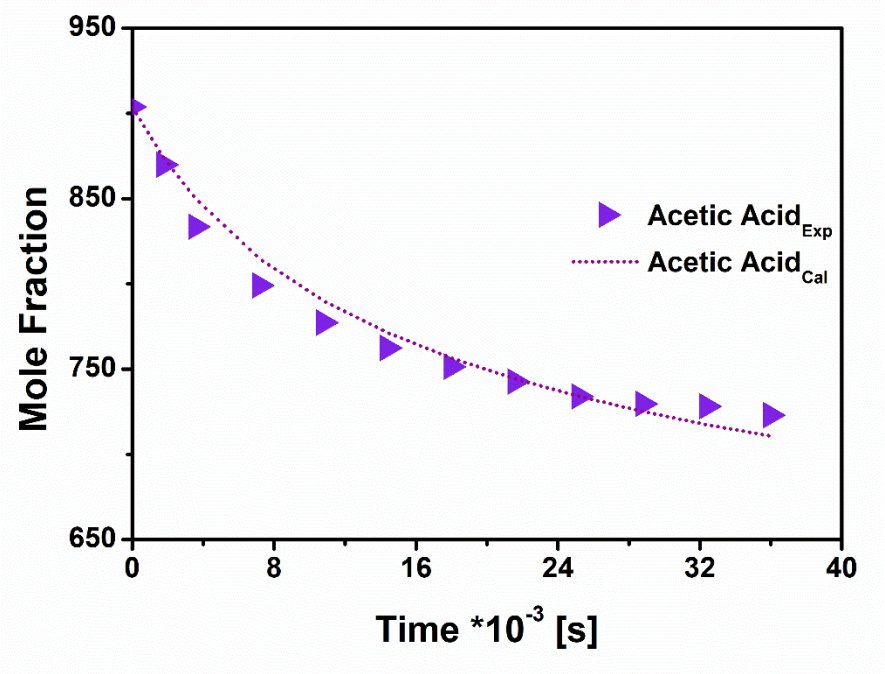

Figure 20. Evolution plot of the acetic acid consumption. Glycerol esterification catalyzed by Amberlyst-35 with particle size of 25 – 75 μm. Initial acetic acid to glycerol molar ratio of 7, temperature of 361 K, and quantity of moles of active sites of 1.01 mmol. Exp: experimental values from the experimental designs. Cal: calculated values from the developed kinetic models.

2.4 CONCLUSIONS

This kinetic study developed rate expressions for monoacetin, diacetin and triacetin formation, an Eley-Rideal mechanism was assumed, where the acetic acid is adsorbed on the catalyst surface to form an intermediate complex, which react with glycerol molecules in the liquid medium. The steps where involve reaction on catalyst surface were considered as the RDS. Consequently, this models were able to predict the kinetic behavior of the glycerol esterification under the reaction conditions applied. Moreover, the parameters obtained fulfill both the thermodynamic balance and the Boudart criteria. Hence, this work provides more knowledge about this heterogeneous catalytic system in liquid phase.

BIBLIOGRAPHY

ALI S.H., AL-RASHED O., AZEEZ F.A., MERCHANT S.Q., Potential biofuel additive from renewable sources - Kinetic study of formation of butyl acetate by heterogeneously catalyzed transesterification of ethyl acetate with butanol, Bioresour. Technol. 102 (2011) 10094–10103.

BALARAJU M., NIKHITHA P., JAGADEESWARAIAH K., SRILATHA K., SAI PRASAD P.S., LINGAIAH N., Acetylation of glycerol to synthesize bioadditives over niobic acid supported tungstophosphoric acid catalysts, Fuel Process. Technol. 91 (2010) 249–253.

BARRETT E.P., JOYNER L.G., HALENDA P.P., The Determination of Pore Volume and Area Distributions in Porous Substances. I. Computations from Nitrogen Isotherms, J. Am. Chem. Soc. 73 (1951) 373–380.

BEDOGNI G.A., PADRÓ C.L., OKULIK N.B., A combined experimental and computational study of the esterification reaction of glycerol with acetic acid, J. Mol. Model. 20 (2014).

BOGGS P.T., DONALDSON J.R., BYRD R. h., SCHNABEL R.B., Algorithm 676 ODRPACK: software for weighted orthogonal distance regression, ACM Trans. Math. Softw. 15 (1989) 348–364.

BONET J., COSTA J., SIRE R., RENEAUME J.M., A.E. Pleşu, V. Pleşu, G. Bozga, Revalorization of glycerol: Comestible oil from biodiesel synthesis, Food Bioprod. Process. 87 (2009) 171–178.

BOUDART M., Kinetics of Chemical Processes, Butterworth-Heinemann, 1991.

BOX G.E., HUNTER J.S., HUNTER W.G., Statistics for Experimenters Design, Innovation, and Discovery, Second Edi, 2005.

BROWN P.N., BYRNE G.D., HINDMARSH A.C., VODE, A variable coefficient ODE solver, SIAM J Sci Stat Comput. 10 (1989) 1038–1051.

BRUNAUER S., EMMETT P.H., TELLER E., Adsorption of Gases in Multimolecular Layer, J. Am. Chem. Soc. 60 (1938) 309–319.

CAREY F.A., SUNDBERG R.J., Advanced Organic Chemistry Part A: Structure and Mechanisms, Fifth Edit, 2007.

CHORKENDORFF I., NIEMANTSVERDRIET J.W., Concepts of Modern Catalysis and Kinetics, 2003.

CRC, Standard thermodynamic properties of chemical substances (continued), CRC Handb. Chem. Phys. 13 (2012) 5.4-5.41.

DAVIS E.M., DAVIS R.J., Fundamentals of Chemical Reaction Engineering, 2003.

DOSUNA-RODRÍGUEZ I., ADRIANY C., GAIGNEAUX E.M., Glycerol acetylation on sulphated zirconia in mild conditions, Catal. Today. 167 (2011) 56–63.

DOSUNA-RODRÍGUEZ I., GAIGNEAUX E.M., Glycerol acetylation catalysed by ion exchange resins, Catal. Today. 195 (2012) 14–21.

FARIA R.P.V., PEREIRA C.S.M., SILVA V.M.T.M., LOUREIRO J.M., RODRIGUES A.E., Glycerol valorization as biofuel: Thermodynamic and kinetic study of the acetalization of glycerol with acetaldehyde, Ind. Eng. Chem. Res. 52 (2013) 1538–1547.

FEDEBIOCOMBUSTIBLES, Biodiésel de palma de aceite, Inf. Estadística Sect. Biocombustibles. (2018). http://www.fedebiocombustibles.com/v3/estadistica-mostrar_info-titulo-Biodiesel.htm.

FERREIRA P., FONSECA I.M., RAMOS A.M., VITAL J., Castanheiro J.E., Acetylation of glycerol over heteropolyacids supported on activated carbon, Catal. Commun. 12 (2011) 573–576.

FOGLER H.S., Elements of Chemical Reaction Engineering, Third Edit, 1999.

GELOSA D., RAMAIOLI M., VALENTE G., MORBIDELLI M., Chromatographic Reactors: Esterification of Glycerol with Acetic Acid Using Acidic Polymeric Resins, Ind. Eng. Chem. Res. 42 (2003) 6536–6544.

GONÇALVES V.L.C., PINTO B.P., SILVA J.C., MOTA C.J.A., Acetylation of glycerol catalyzed by different solid acids, Catal. Today. 133–135 (2008) 673–677.

GONZALEZ-GARAY A., GONZALEZ-MIQUEL M., GUILLEN-GOSALBEZ G., High-Value Propylene Glycol from Low-Value Biodiesel Glycerol: A Techno-Economic and Environmental Assessment under Uncertainty, ACS Sustain. Chem. Eng. 5 (2017) 5723–5732.

HABER J., Manual on Catalyst Characterization, Pure Appl. Chem. 63 (1991) 1227–1246.

HASABNIS A., MAHAJANI S., Entrainer-based reactive distillation for esterification of glycerol with acetic acid, Ind. Eng. Chem. Res. 49 (2010) 9058–9067.

HINSHELWOOD C.N., The kinetics of chemical change, 1940.

HOUGEN O.A., WATSON K.M., General Principles, Ind. Eng. Chem. 35 (1943) 529–541.

HUNG S.K., LEE C.C., LEE H.Y., LEE C.L., CHIEN I.L., Improved design and control of triacetin reactive distillation process for the utilization of glycerol, Ind. Eng. Chem. Res. 53 (2014) 11989–12002.

IZCI A., BODUR F., Liquid-phase esterification of acetic acid with isobutanol catalyzed by ion-exchange resins, React. Funct. Polym. 67 (2007) 1458–1464.

JAGADEESWARAIAH K., BALARAJU M., PRASAD P.S.S., LINGAIAH N., Selective esterification of glycerol to bioadditives over heteropoly tungstate supported on Cs-containing zirconia catalysts, Appl. Catal. A Gen. 386 (2010) 166–170.

KHAYOON M.S., HAMEED B.H., Acetylation of glycerol to biofuel additives over sulfated activated carbon catalyst, Bioresour. Technol. 102 (2011) 9229–9235.

KHAYOON M.S., TRIWAHYONO S., HAMEED B.H., JALIL A.A., Improved production of fuel oxygenates via glycerol acetylation with acetic acid, Chem. Eng. J. 243 (2014) 473–484.

KIM I., KIM J., LEE D., A comparative study on catalytic properties of solid acid catalysts for glycerol acetylation at low temperatures, "Applied Catal. B, Environ. 148–149 (2014) 295–303.

KIMBALL A.W., On Dependent Tests of Significance in the Analysis of Variance, Ann. Math. Stat. 22 (1951) 600–6002.

KIRUMAKKI S.R., NAGARAJU N., CHARY K.V.R., Esterification of alcohols with acetic acid over zeolites Hβ, HY and HZSM5, Appl. Catal. A, Gen. 299 (2006) 185–192.

KOROS R.M., NOWAK E.J., A diagnostic test of the kinetic regime in a packed bed reactor, Chem. Eng. Sci. 22 (1967) 470.

KOZUCH S., MARTIN J.M.L., “Turning over” definitions in catalytic cycles, ACS Catal. 2 (2012) 2787–2794.

KUTNER M.H., Nachtsheim C.J.J., Neter J., Li W., Applied Linear Statistical Models, Fifth Edit, 2004.

LANGMUIR I., The adsorption of gases on plane surfaces of glass, mica and platinum, J. Am. Chem. Soc. 40 (1918) 1361–1403.

LIAO X., ZHU Y., WANG S.G., CHEN H., LI Y., Theoretical elucidation of acetylating glycerol with acetic acid and acetic anhydride, Appl. Catal. B Environ. 94 (2010) 64–70.

LIAO X., ZHU Y., WANG S.G., LI Y., Producing triacetylglycerol with glycerol by two steps: Esterification and acetylation, Fuel Process. Technol. 90 (2009) 988–993.

LILJA J., MURZIN D.Y., SALMI T., AUMO J., MAÄKI-ARVELA P., SUNDELL M., Esterification of different acids over heterogeneous and homogeneous catalysts and correlation with the taft equation, J. Mol. Catal. A Chem. 182 (2002) 555–563.

LIU J., YANG B., YI C., Kinetic study of glycerol etherification with isobutene, Ind. Eng. Chem. Res. 52 (2013) 3742–3751.

LOFTUS G.R., On interpretation of interactions, 6 (1978) 312–319.

MADON R.J., BOUDART M., Experimental Criterion for the Absense of Artifacts in the Measurements of Rates of Heterogeneous Catalytic Reactions, Ind Eng Chem Fundam. (1982) 438–447.

MARQUARDT D., An Algorithm for least-squares estimation of nonlinear parameters, J. Soc. Indust. Appl. Math. 11 (1963) 431–441.

MCMURRY J., Química Orgánica, Octava Edi, 2012.

MONTGOMERY D.C., Runger G.C., Applied Statistics and Probability for Engineers, John Wiley & Sons, Inc., 2013.

MUFRODI Z., Chemical Kinetics for Synthesis of Triacetin from Biodiesel Byproduct, Int. J. Chem. 4 (2012) 101–107.

NANDA M.R., YUAN Z., QIN W., GHAZIASKAR H.S., POIRIER M., CHARLES C., Thermodynamic and kinetic studies of a catalytic process to convert glycerol into solketal as an oxygenated fuel additive, Fuel. 117 (2014) 470–477.

NAVIDI W., Statistics for Engineers and Scientists, Fourth Edi, 2015.

OKOYE P.U., ABDULLAH A.Z., HAMEED B.H., A review on recent developments and progress in the kinetics and deactivation of catalytic acetylation of glycerol—A byproduct of biodiesel, Renew. Sustain. Energy Rev. 74 (2017) 387–401.

ORJUELA A., YANEZ A.J., SANTHANAKRISHNAN A., LIRA C.T., MILLER D.J., Kinetics of mixed succinic acid/acetic acid esterification with Amberlyst 70 ion exchange resin as catalyst, Chem. Eng. J. 188 (2012) 98–107.

OSORIO-VIANA W., DUQUE-BERNAL M., FONTALVO J., DOBROSZ-GÓMEZ I., GÓMEZ-GARCÍA M.Á., Kinetic study on the catalytic esterification of acetic acid with isoamyl alcohol over Amberlite IR-120, Chem. Eng. Sci. 101 (2013) 755–763.

PAPPU V.K.S., KANYI V., SANTHANAKRISHNAN A., LIRA C.T., MILLER D.J., Butyric acid esterification kinetics over Amberlyst solid acid catalysts: The effect of alcohol carbon chain length, Bioresour. Technol. 130 (2013) 793–797.

PATEL A., SINGH S., A green and sustainable approach for esterification of glycerol using 12-tungstophosphoric acid anchored to different supports: Kinetics and effect of support, Fuel. 118 (2014) 358–364.

PICO M.P., ROMERO A., RODRÍGUEZ S., SANTOS A., Etherification of Glycerol by tert -Butyl Alcohol: Kinetic Model, Ind. Eng. Chem. Res. 51 (2012) 9500–9509.

QUINN G.P., KEOUGH M.J., Experimental Design Data Analysis for Biologists, Cambridge, 2002.

RAHMAT N., ABDULLAH A.Z., MOHAMED A.R., Recent progress on innovative and potential technologies for glycerol transformation into fuel additives: A critical review, Renew. Sustain. Energy Rev. 14 (2010) 987–1000.

RANE S.A., PUDI S.M., BISWAS P., Esterification of Glycerol with Acetic Acid over Highly Active and Stable Alumina-based Catalysts: A Reaction Kinetics Study, Chem. Biochem. Eng. Q. J. 30 (2016) 33–45.

RASTEGARI H., GHAZIASKAR H.S., YALPANI M., Valorization of biodiesel derived glycerol to acetins by continuous esterification in acetic acid: Focusing on high selectivity to diacetin and triacetin with no byproducts, Ind. Eng. Chem. Res. 54 (2015) 3279–3284.

REDDY P.S., SUDARSANAM P., RAJU G., REDDY B.M., Selective acetylation of glycerol over CeO2-M and SO42-/CeO2-M (M=ZrO2and Al2O3) catalysts for synthesis of bioadditives, J. Ind. Eng. Chem. 18 (2012) 648–654.

REDDY P.S., SUDARSANAM P., Raju G., Reddy B.M., Synthesis of bio-additives: Acetylation of glycerol over zirconia-based solid acid catalysts, Catal. Commun. 11 (2010) 1224–1228.

RIZA M., ÇITAK A., Kinetics study of esterification of acetic acid with isobutanol in the presence of amberlite catalyst, Appl. Catal. A Gen. 239 (2003) 141–148.

ROHM AND HAAS, Amberlyst 35dry - Industrial Grade Strongly Acidic Catalyst, (2006) 1–2.

ROSENBROCK H.H., An automatic method for finding the greatest or least value of a function, Computer (Long. Beach. Calif). 3 (1960) 175–184.

ROSNOW R.L., ROSENTHAL R., “Some Things You Learn Aren’t So”: Cohen’s Paradox, Asch’s Paradigm, and the Interpretation of Interaction, Psychol. Sci. 6 (1995) 3–9.

SÁNCHEZ J.A., HERNÁNDEZ D.L., MORENO J.A., MONDRAGÓN F., FERNÁNDEZ J.J., Alternative carbon based acid catalyst for selective esterification of glycerol to acetylglycerols, Appl. Catal. A Gen. 405 (2011) 55–60.

SANTACESARIA E., Kinetics and transport phenomena, Catal. Today. 34 (1997) 393–400.

SATTERFIELD C.N., Heterogeneous catalysis in industrial practice, 2Nd Ed. Ed. 51 (1991) 447.

SIEVERS C., NODA Y., QI L., ALBUQUERQUE E.M., RIOUX R.M., SCOTT S.L., Phenomena Affecting Catalytic Reactions at Solid–Liquid Interfaces, ACS Catal. 6 (2016) 8286–8307.

SILVA L.N., GONÇALVES V.L.C., MOTA C.J.A., Catalytic acetylation of glycerol with acetic anhydride, Catal. Commun. 11 (2010) 1036–1039.

TEO H.T.R., SAHA B., Heterogeneous catalysed esterification of acetic acid with isoamyl alcohol: Kinetic studies, J. Catal. 228 (2004) 174–182.

THOMMES M., KANEKO K., NEIMARK A. V., OLIVIER J.P., RODRIGUEZ-REINOSO F., ROUQUEROL J., SING K.S.W., Physisorption of gases, with special reference to the evaluation of surface area and pore size distribution (IUPAC Technical Report), Pure Appl. Chem. 87 (2015) 1051–1069.

VANNICE M.A., Kinetics of Catalytic Reactions, 2005.

VELUTURLA S., NARULA A., S.R. D, SHETTY S.P., Kinetic study of synthesis of bio-fuel additives from glycerol using a hetropolyacid, Resour. Technol. 3 (2017) 337–341.

WAGENMAKERS E.J., KRYPOTOS A.M., CRISS A.H., IVERSON G., On the interpretation of removable interactions: A survey of the field 33 years after Loftus, Mem. Cogn. 40 (2012) 145–160.

WEISZ P.B., PRATER C.D., Interpretation of Measurements in Experimental Catalysis, Adv. Catal. 6 (1954) 143–196.

WU C.F.J., HAMADA M.S., Experiments: Planning, Analysis, and Optimitation, Second edi, 2009.

WULFERS M.J., LOBO R.F., Assessment of mass transfer limitations in oligomerization of butene at high pressure on H-beta, Appl. Catal. A Gen. 505 (2015) 394–401.

ZHOU L., NGUYEN T.H., ADESINA A.A., The acetylation of glycerol over amberlyst-15: Kinetic and product distribution, Fuel Process. Technol. 104 (2012) 310–318.

SUPPLEMENTARY INFORMATION

Supplementary Information A. Reactions outcomes corresponding to the first experimental set to assess the transport limitations in glycerol esterification at the usual reaction conditions.

Table S1. Summary of the curves of glycerol conversion (X_G) and yield of each acetin ($Y_{M/D/T}$) in the reaction time from the first set of experiments, catalyzed by Amberlyst-35 with particle size of 600 – 1180 μm. The subscripts i, ii and iii are appointed to the tests for each block of a 3^2 full factorial experimental designs at the values of acetic acid to glycerol molar ratio of 1.8, 3.0 and 4.4, respectively. These results are presented in order of execution.

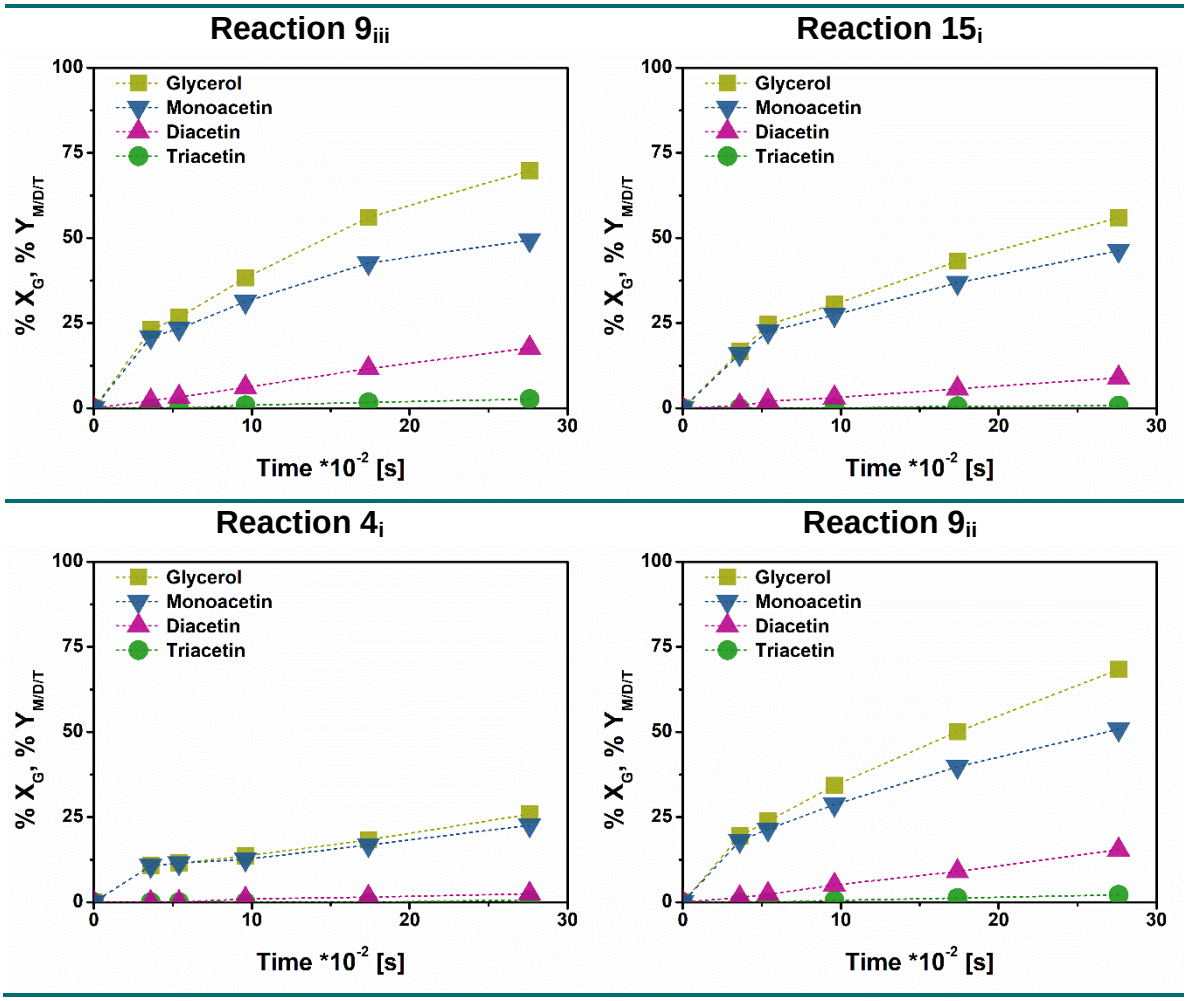

Reaction 16_{iii}

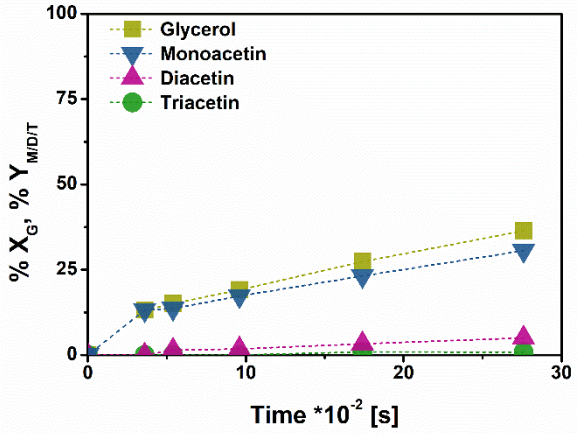

Reaction 10_{ii}

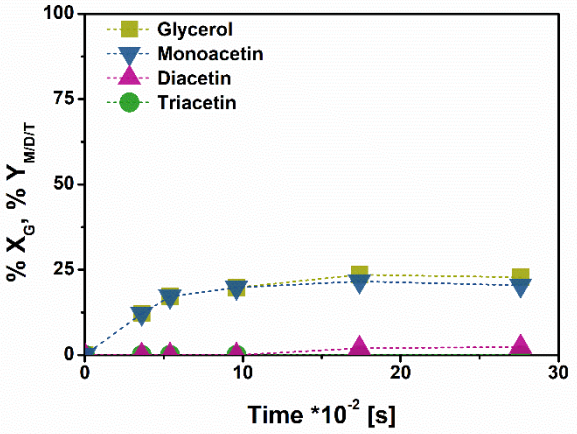

Reaction 17_{iii}

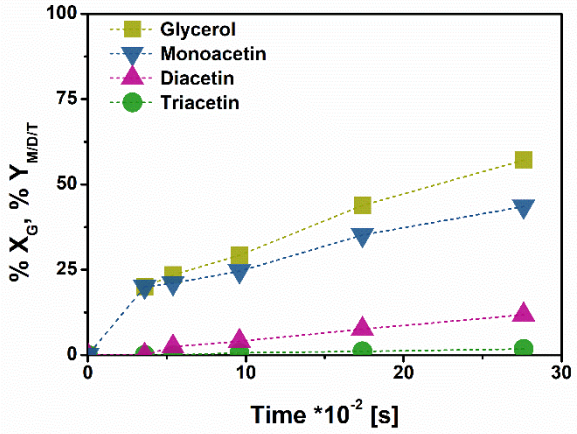

Reaction 6_{ii}

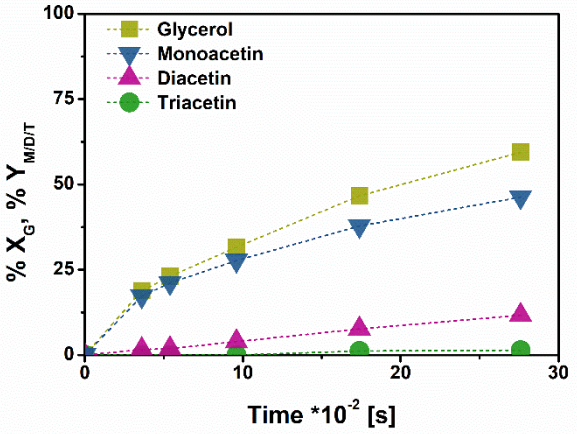

Reaction 18_{ii}

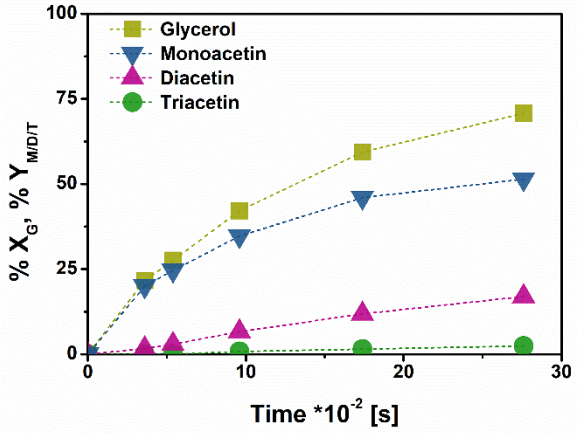

Reaction 2_{ii}

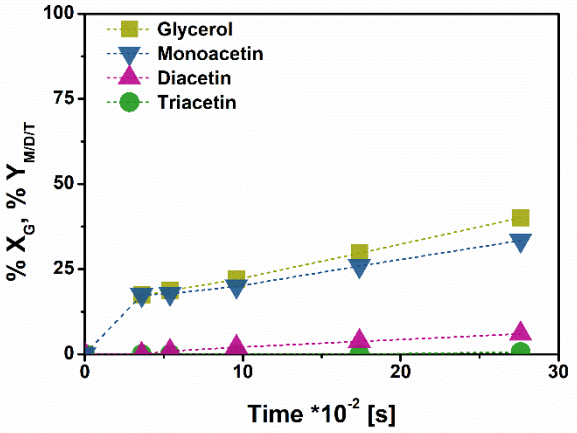

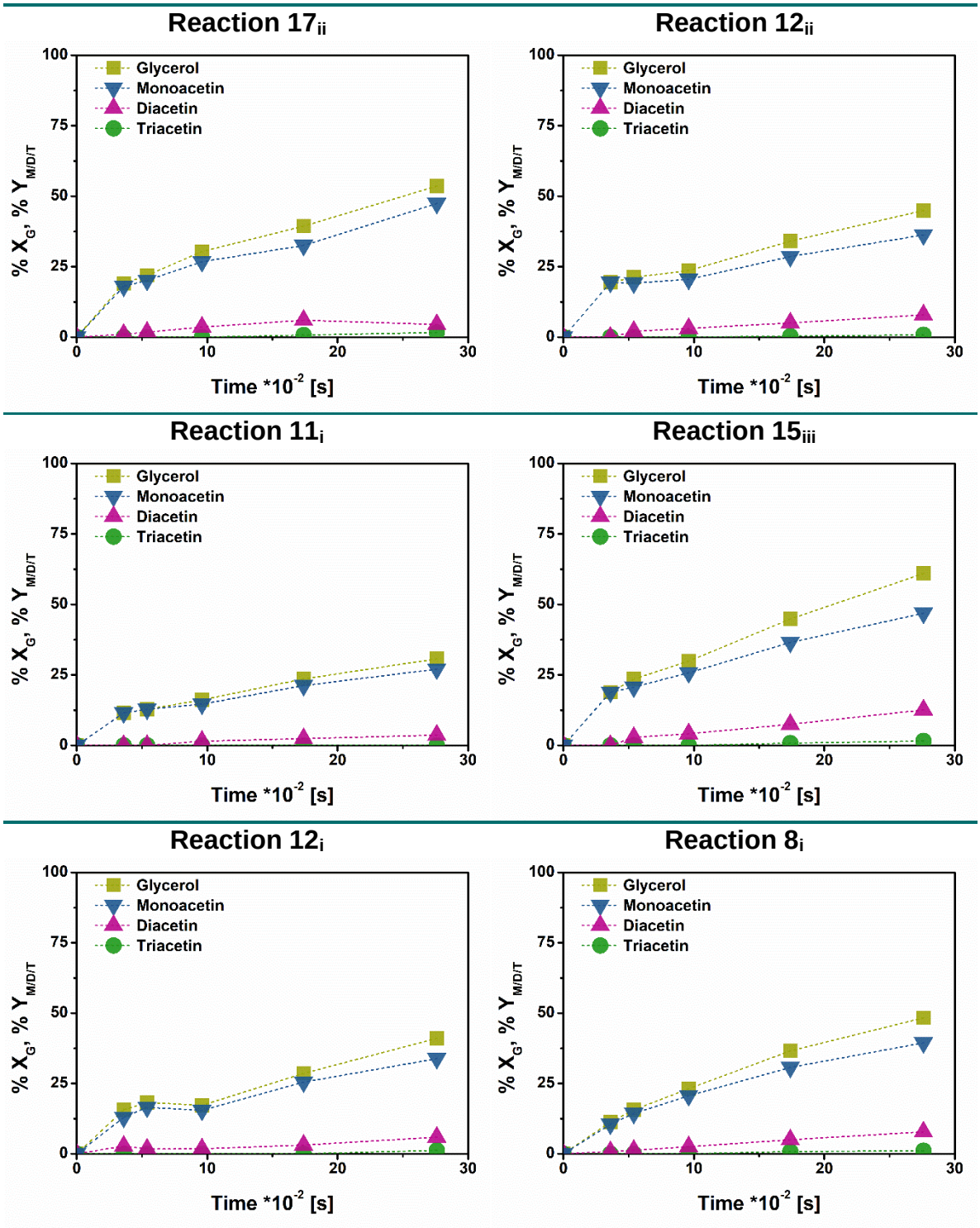
Reaction 17ii
Reaction 12ii
Reaction 11i
Reaction 15iii
Reaction 12i
Reaction 8i
Glycerol
Monoacetin
Diacetin
Triacetin
% XG, % YM/D/T
Time *10-2 [s]
0
25
50
75
100
0
10
20
30

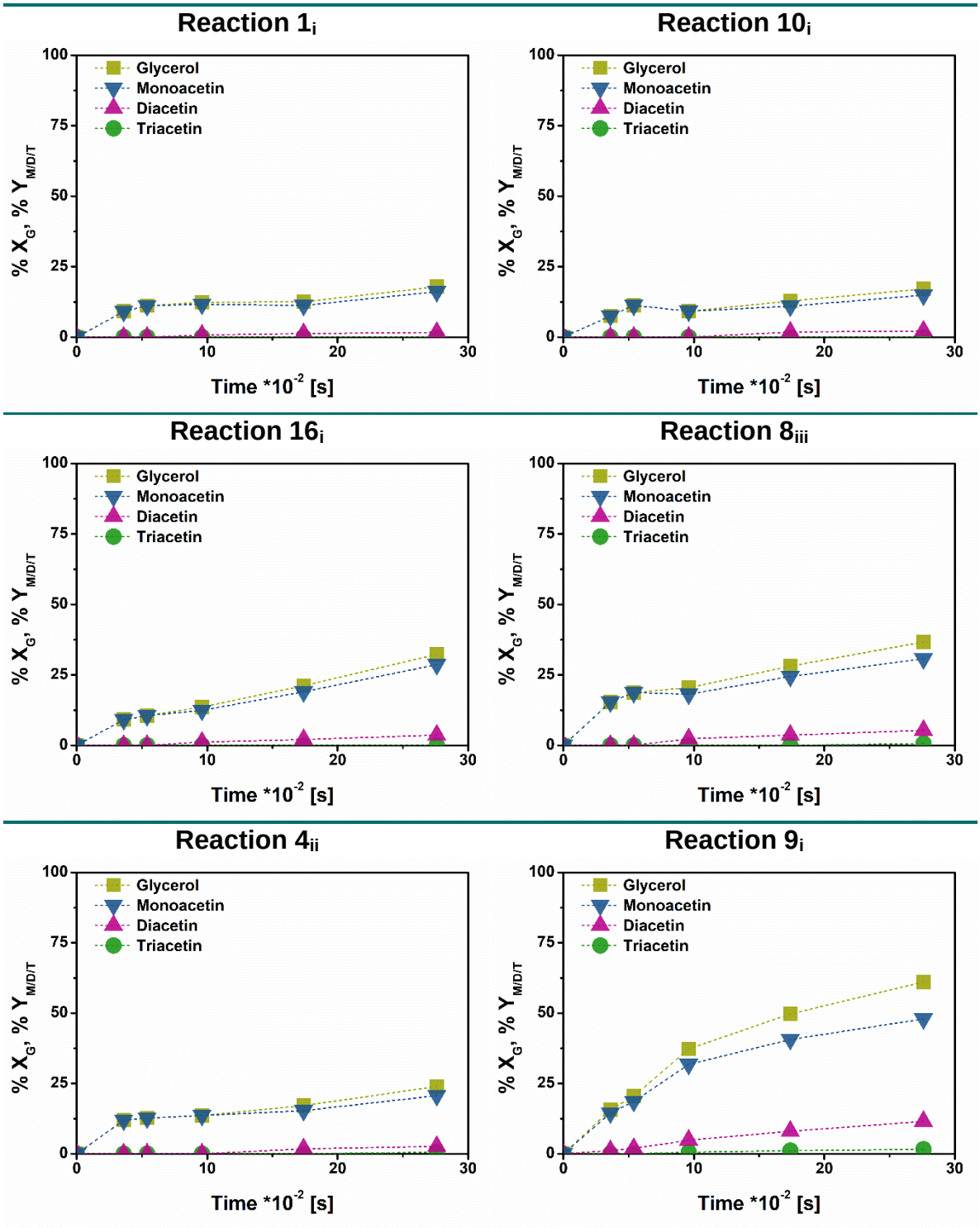
Reaction 1i
Reaction 10i
Reaction 16i
Reaction 8iii
Reaction 4ii
Reaction 9i
Glycerol
Monoacetin
Diacetin
Triacetin
% XG, % YM/D/T
Time *10-2 [s]
0
25
50
75
100
0
10
20
30

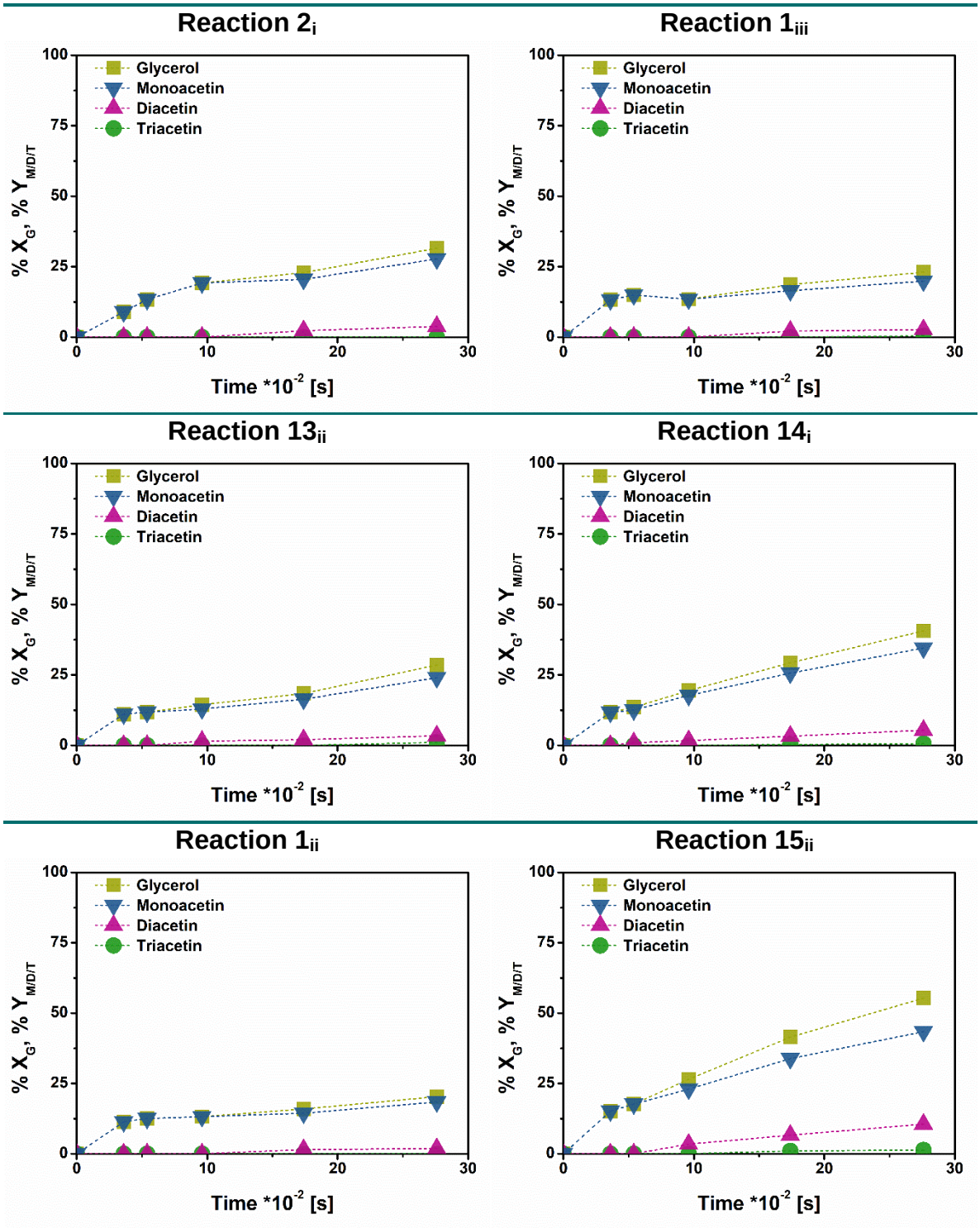
Reaction 2i
Reaction 1iii
Reaction 13ii
Reaction 14i
Reaction 1ii
Reaction 15ii
Glycerol
Monoacetin
Diacetin
Triacetin
% XG, % YM/D/T
Time *10-2 [s]
0
25
50
75
100
0
10
20
30

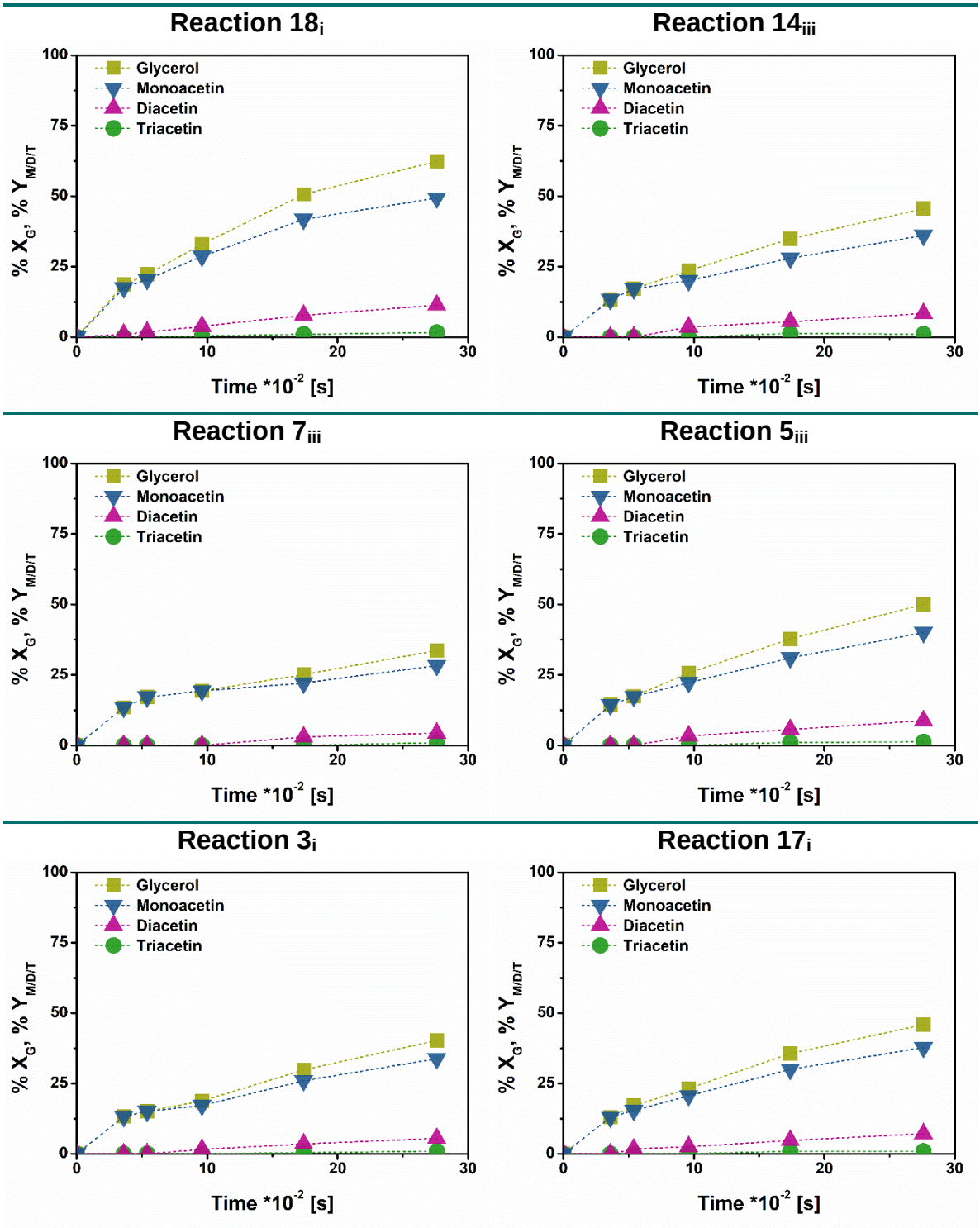
Reaction 18i
Reaction 14iii
Reaction 7iii
Reaction 5iii
Reaction 3i
Reaction 17i
Glycerol
Monoacetin
Diacetin
Triacetin
% XG, % YM/D/T
Time *10-2 [s]
0
25
50
75
100
0
10
20
30

Reaction 5_{ii}

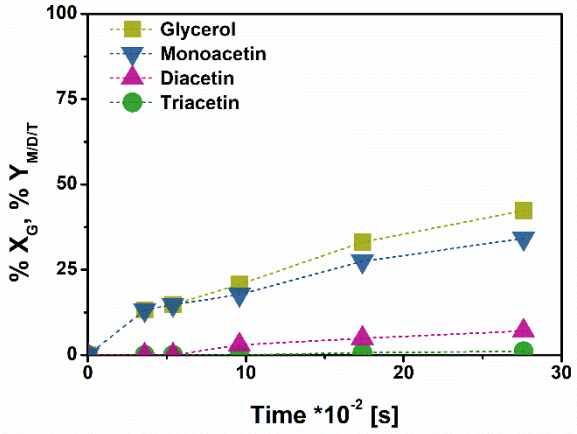

Reaction 6_{i}

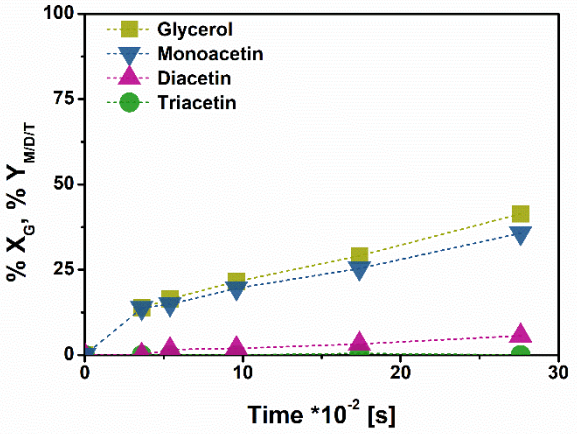

Reaction 18_{iii}

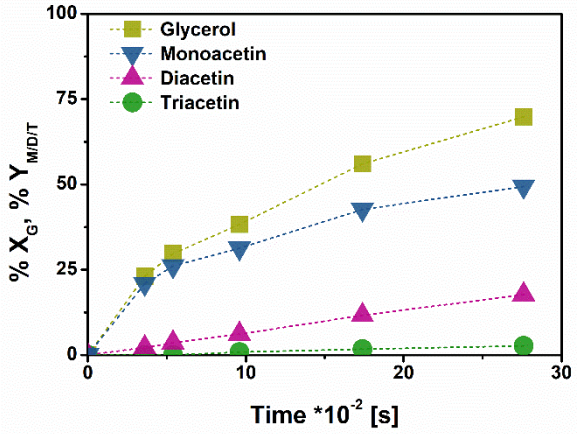

Reaction 3_{ii}

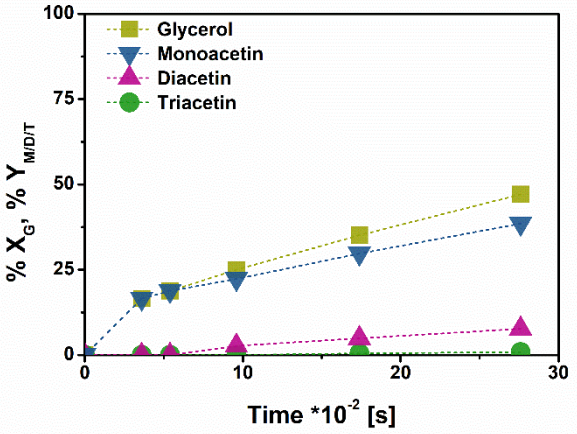

Reaction 13_{i}

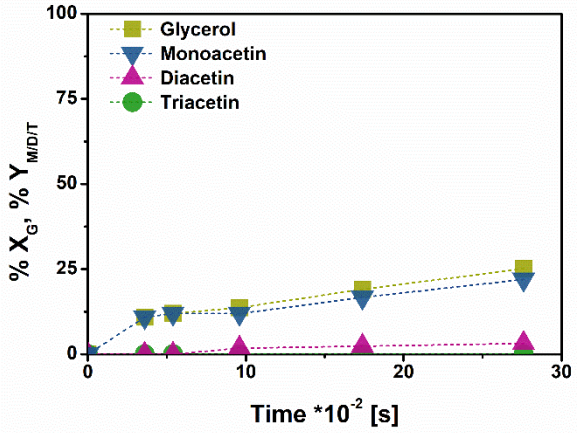

Reaction 4_{iii}

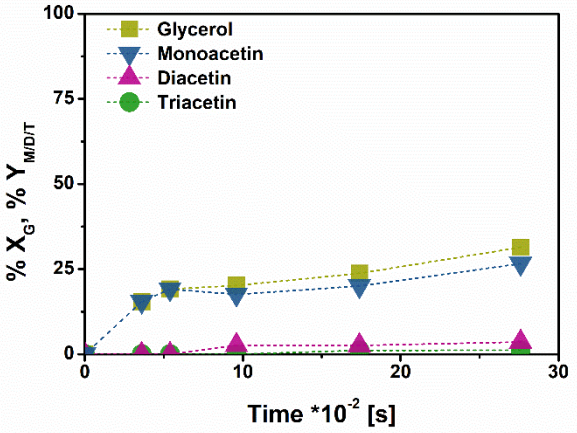

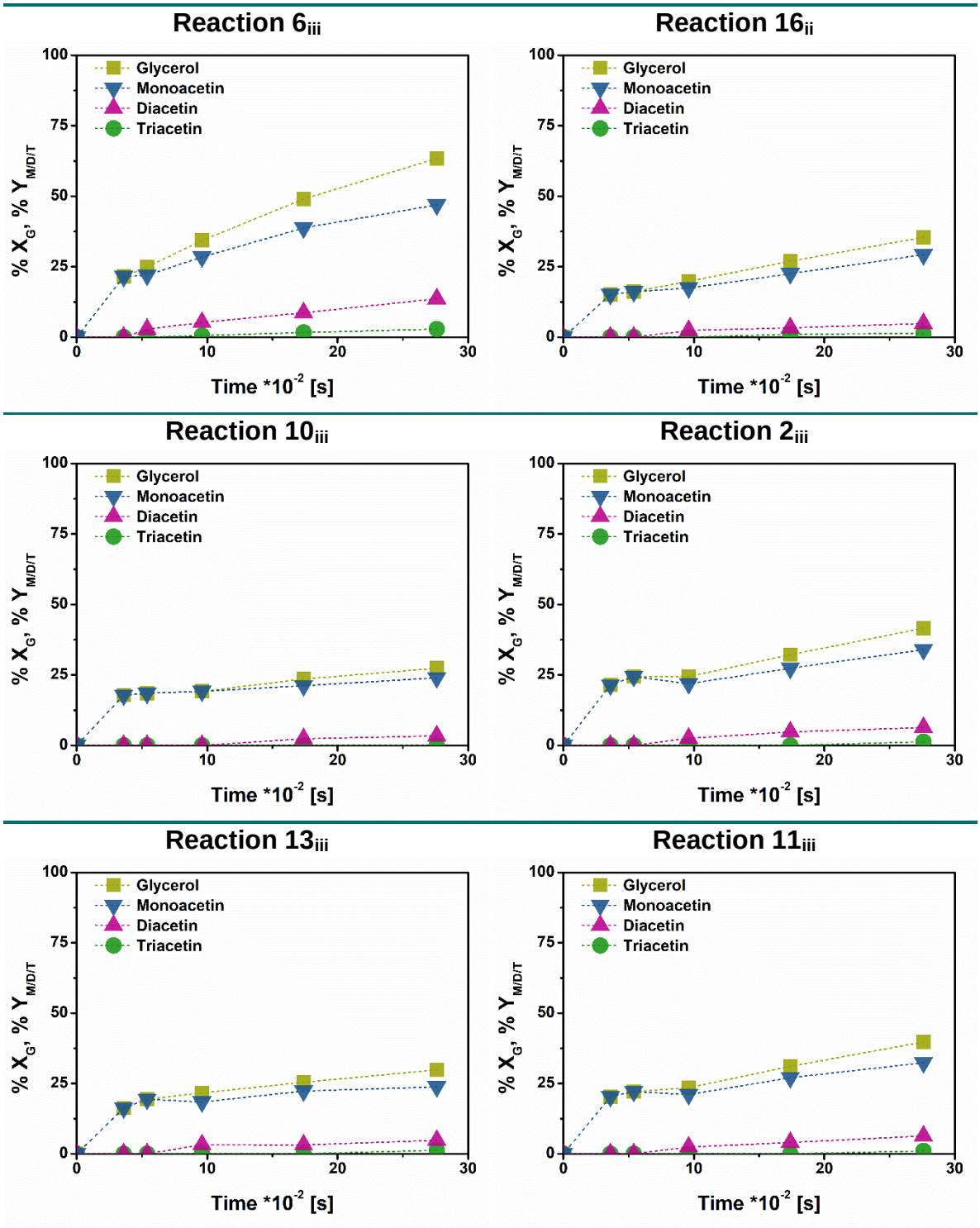
Reaction 6iii
Reaction 16ii
Reaction 10iii
Reaction 2iii
Reaction 13iii
Reaction 11iii
Glycerol
Monoacetin
Diacetin
Triacetin
% XG, % YM/D/T
Time *10-2 [s]
0
25
50
75
100
0
10
20
30

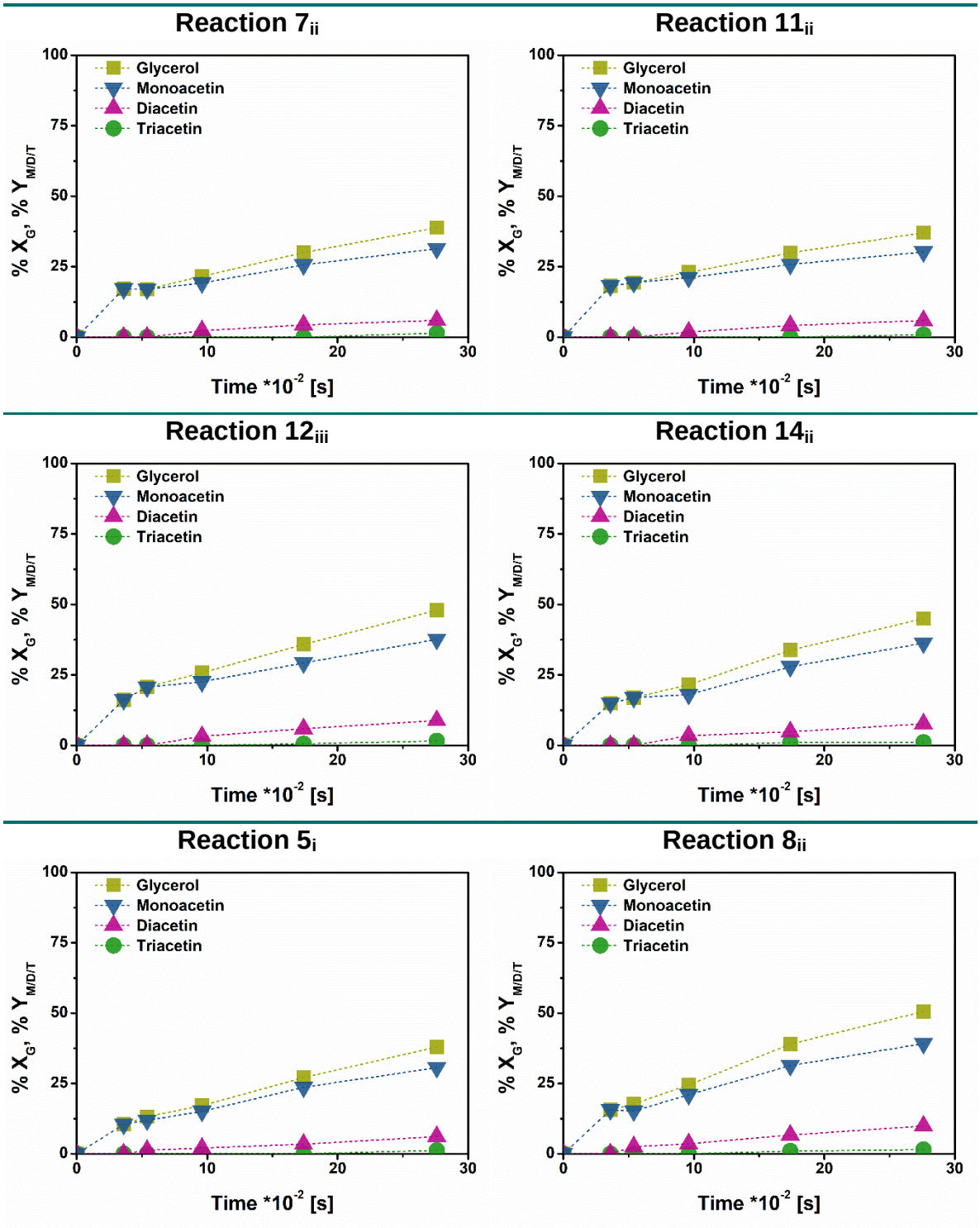
Reaction 7ii
Reaction 11ii
Reaction 12iii
Reaction 14ii
Reaction 5i
Reaction 8ii
Glycerol
Monoacetin
Diacetin
Triacetin
% XG, % YM/D/T
Time *10-2 [s]
0
25
50
75
100
0
10
20
30

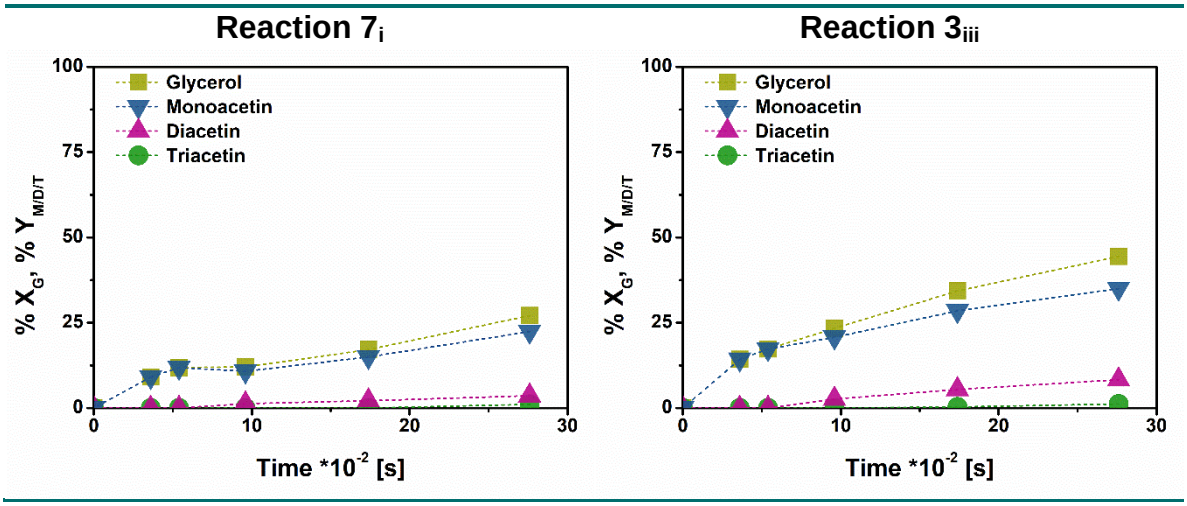
Reaction 7i
Reaction 3iii
Glycerol
Monoacetin
Diacetin
Triacetin
% XG, % YM/D/T
Time *10-2 [s]
0
25
50
75
100
0
10
20
30

Supplementary Information B. Analysis of the residuals and ANOVA models corresponding to the first experimental set to assess the transport limitations in glycerol esterification at the usual reaction conditions.

Figure S2. Assumption of constant variance for the different factors: i) μ^{*-1}, ii) T and iii) $\mu^{*-1}\times$T. iv) Independence plot, and v) Normality plot for the studentized residuals considered in the 3^2 full factorial experimental design executed for glycerol esterification with acetic acid over Amberlyst-35 with particle size of 600 – 1180 µm, and acetic acid to glycerol molar ratio of 1.8.

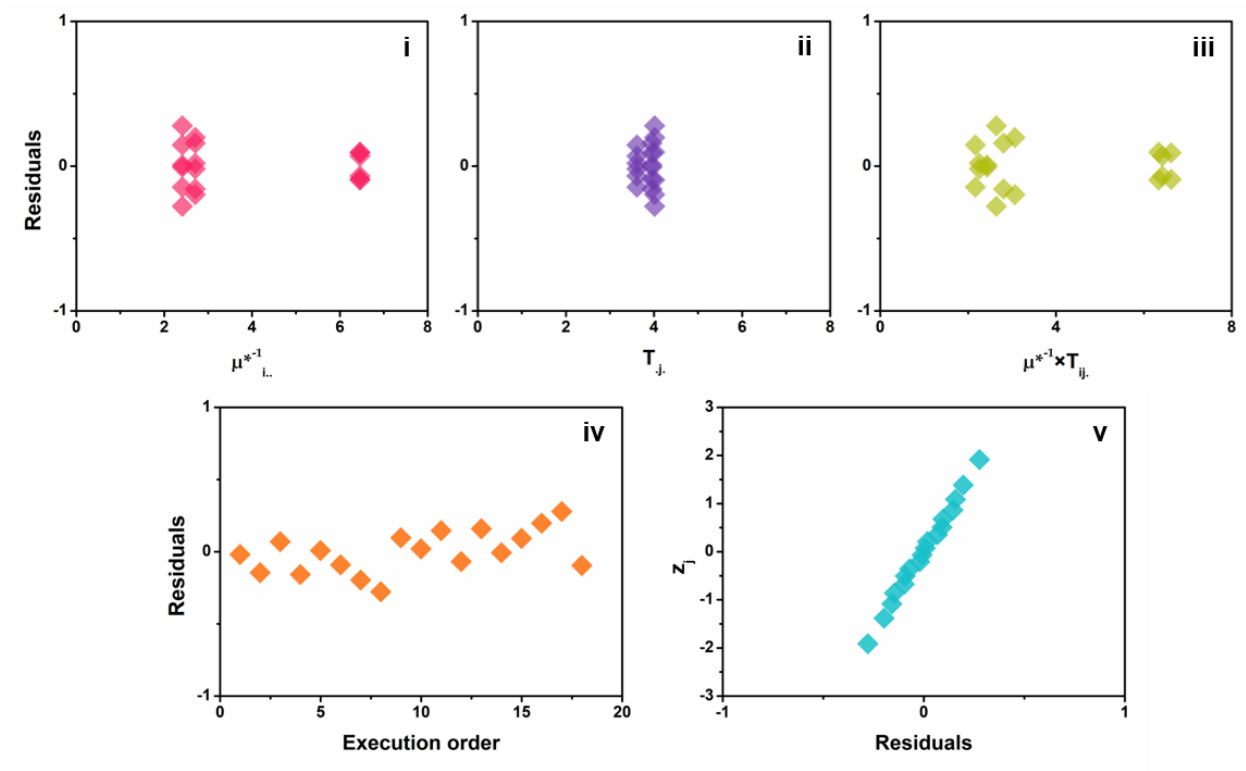

Section S3. Regression model developed based on the factors that were found to be statistically significant in the ANOVA test for the 3^2 full factorial experimental design executed for glycerol esterification with acetic acid over Amberlyst-35 with particle size of 600 – 1180 µm, and acetic acid to glycerol molar ratio of 1.8.

$$Turnover = 1.347 + 58.137\mu*^{-1}$$

Figure S4. Assumption of constant variance for the different factors: i) μ^{*-1}, ii) T and iii) $\mu^{*-1}\times T$. iv) Independence plot, and v) Normality plot for the studentized residuals considered in the 3^2 full factorial experimental design executed for glycerol esterification with acetic acid over Amberlyst-35 with particle size of 600 – 1180 µm, and acetic acid to glycerol molar ratio of 3.0.

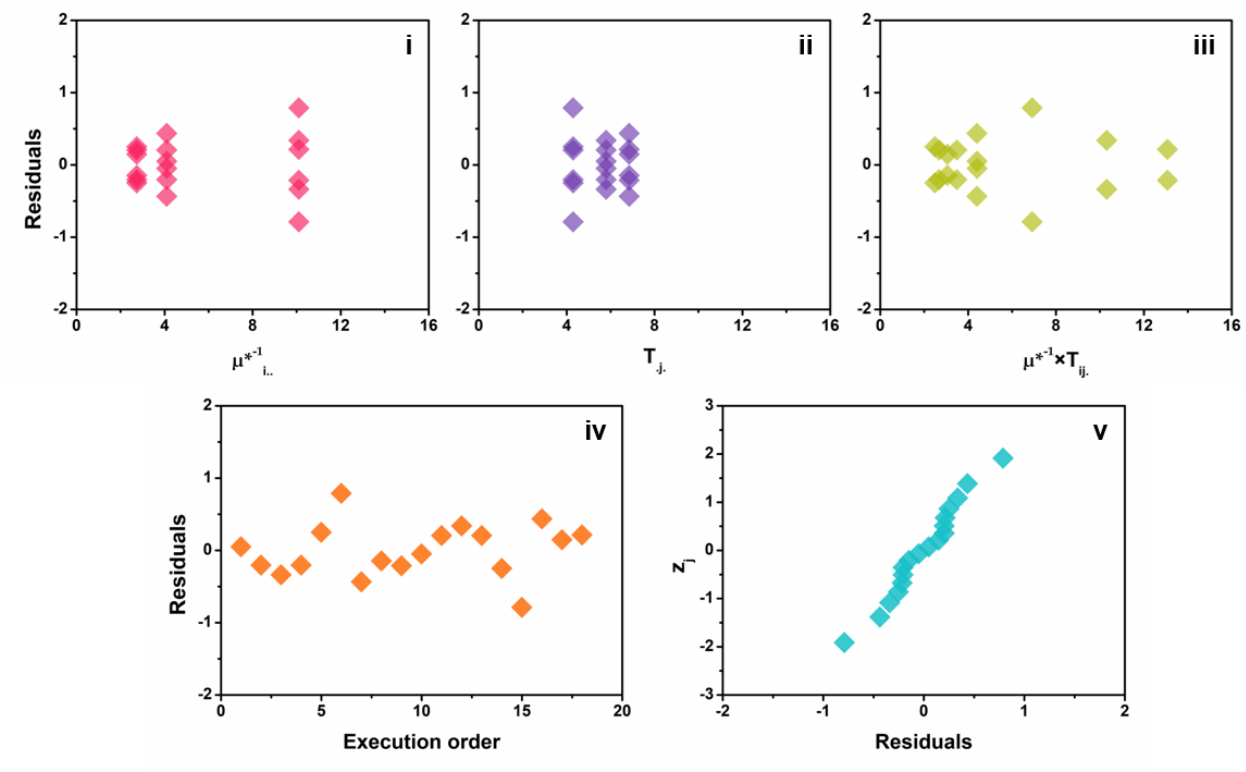

Section S5. Regression model developed based on the factors that were found to be statistically significant in the ANOVA test for the 3^2 full factorial experimental design executed for glycerol esterification with acetic acid over Amberlyst-35 with particle size of 600 – 1180 µm, and acetic acid to glycerol molar ratio of 3.0.

$$Turnover = 0.471 - 42.099\mu*^{-1} + 0.008T + 0.135\mu*^{-1} \times T$$

Figure S6. Assumption of constant variance for the different factors: i) μ^{*-1}, ii) T and iii) $\mu^{*-1}\times T$. iv) Independence plot, and v) Normality plot for the studentized residuals considered in the 3^2 full factorial experimental design executed for glycerol esterification with acetic acid over Amberlyst-35 with particle size of 600 – 1180 µm, and acetic acid to glycerol molar ratio of 4.4.

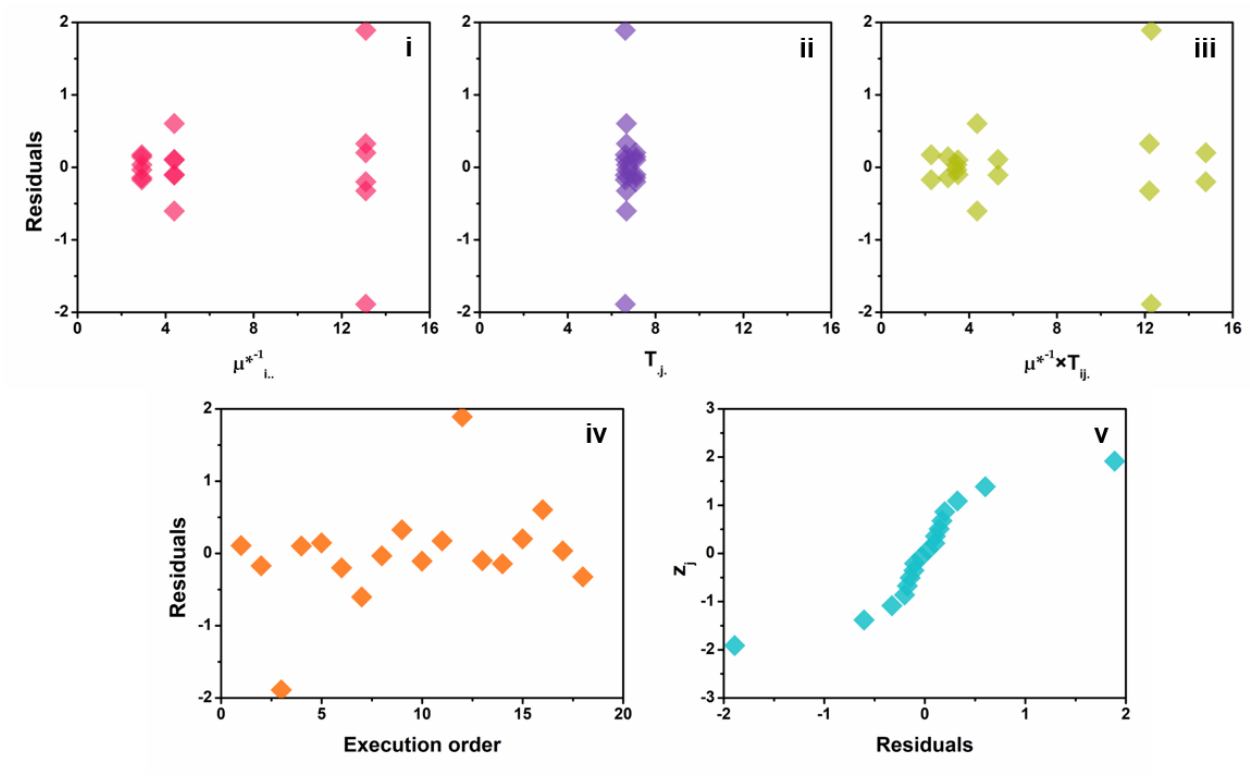

Section S7. Regression model developed based on the factors that were found to be statistically significant in the ANOVA test for the 3^2 full factorial experimental design executed for glycerol esterification with acetic acid over Amberlyst-35 with particle size of 600 – 1180 µm, and acetic acid to glycerol molar ratio of 4.4.

$$Turnover = 0.657 + 77.020\mu*^{-1}$$

Supplementary Information C. Reactions outcomes corresponding to the second experimental set to assess the transport limitations in glycerol esterification catalyzed by Amberlyst-35 with particle size reduced.

Table S8. Summary of the curves of glycerol conversion (X_G) and yield of each acetin ($Y_{M/D/T}$) in the reaction time from the second set of experiments, catalyzed by Amberlyst-35 with particle size of 25 – 75 µm. Block of 3^2 full factorial experimental design at the acetic acid to glycerol molar ratio of 4.4. These results are presented in order of execution.

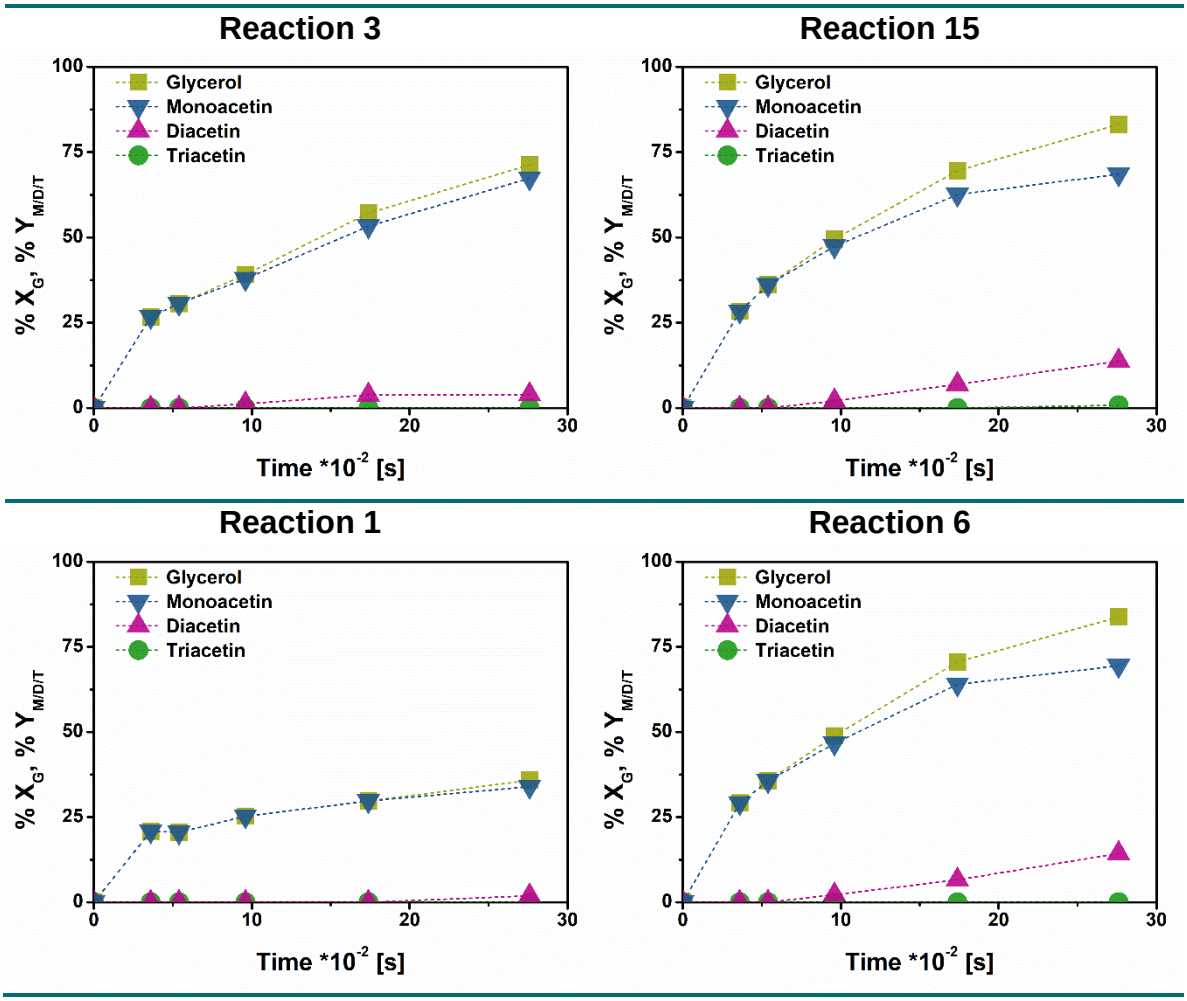

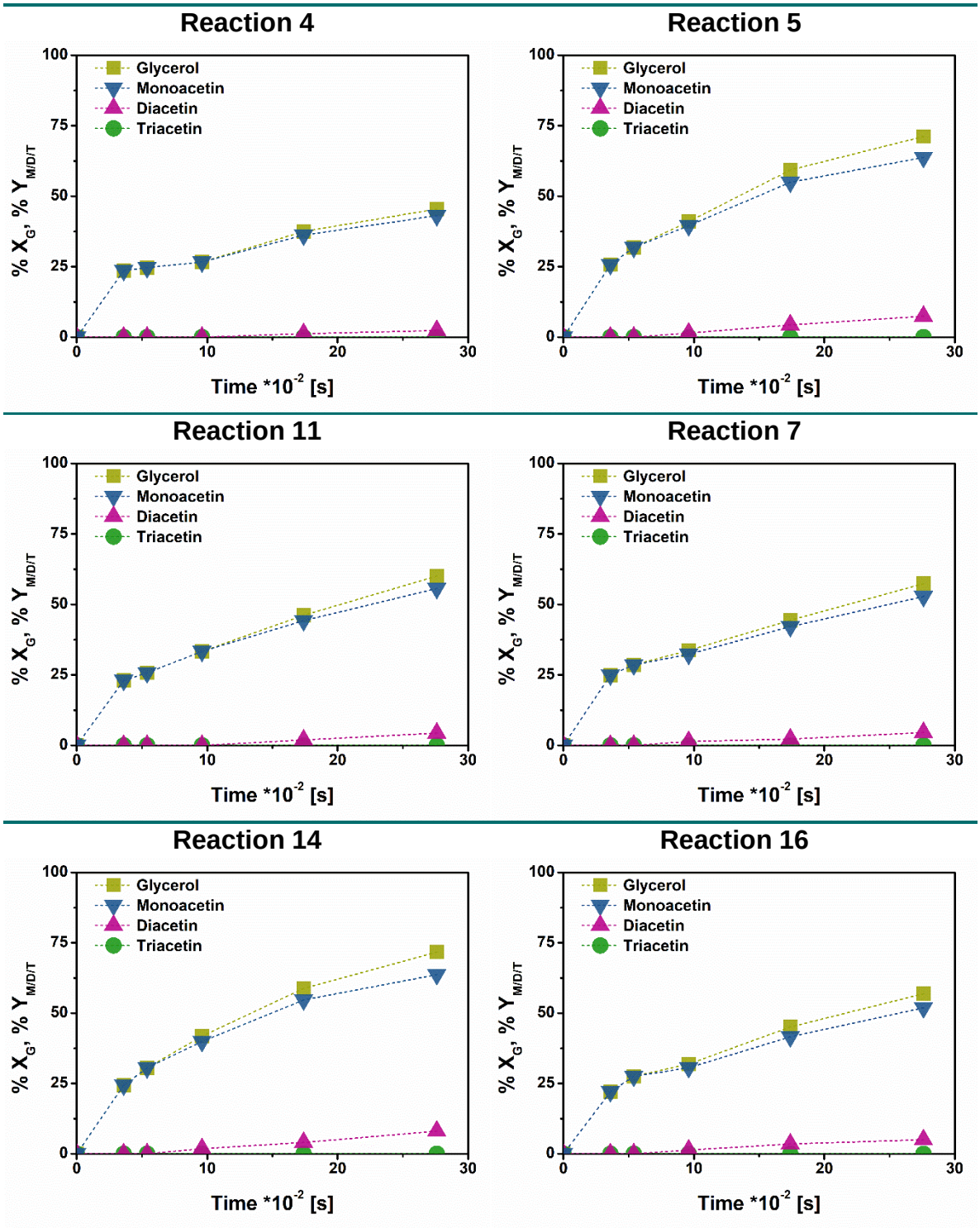
Reaction 4
Reaction 5
Reaction 11
Reaction 7
Reaction 14
Reaction 16
Glycerol
Monoacetin
Diacetin
Triacetin
% X_G, % Y_M/D/T
Time *10^-2 [s]
0
25
50
75
100
0
10
20
30

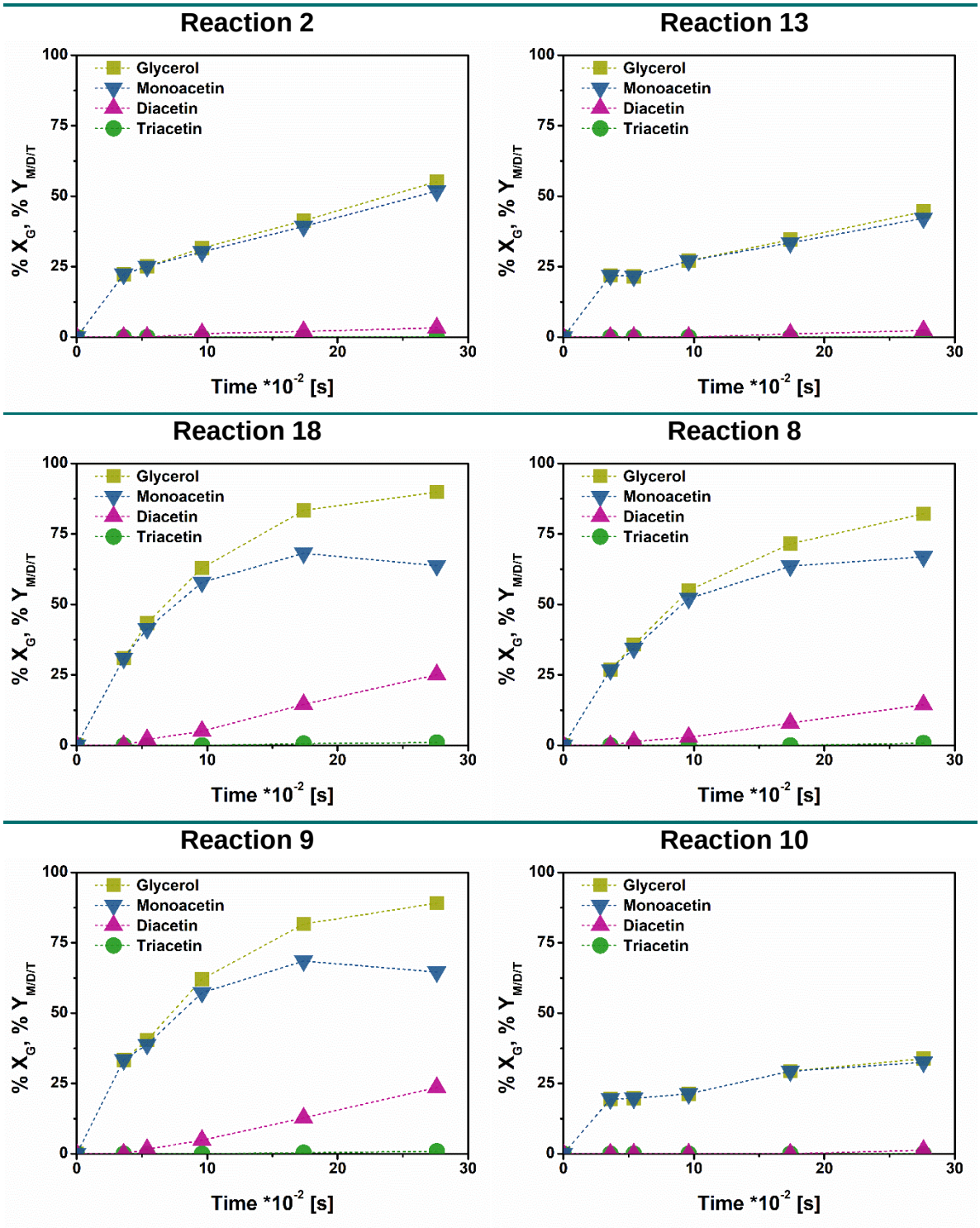
Reaction 2
Reaction 13
Reaction 18
Reaction 8
Reaction 9
Reaction 10
Glycerol
Monoacetin
Diacetin
Triacetin
% X_G, % Y_M/D/T
Time *10^-2 [s]
0
25
50
75
100
0
10
20
30

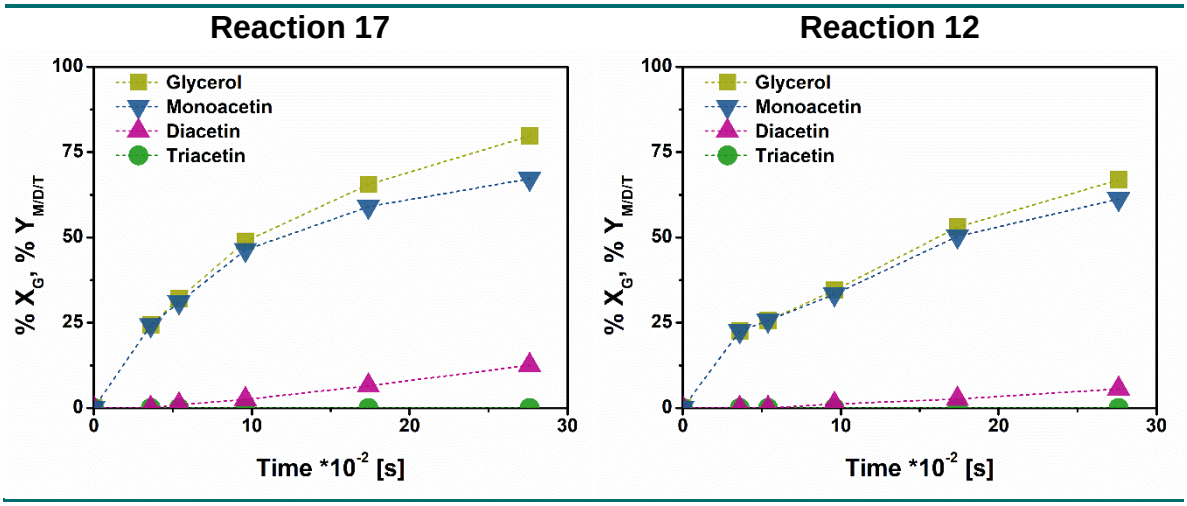
Reaction 17
Reaction 12
Glycerol
Monoacetin
Diacetin
Triacetin
% X_G, % Y_M/D/T
Time *10^-2 [s]
0
25
50
75
100
0
10
20
30

Supplementary Information D. Analysis of the residuals and ANOVA models corresponding to the first experimental set to assess the transport limitations in glycerol esterification catalyzed by Amberlyst-35 with particle size reduced.

Figure S9. Assumption of constant variance for the different factors: i) μ^{*-1}, ii) T and iii) μ^{*-1}×T. iv) Independence plot, and v) Normality plot for the studentized residuals considered in the 3^2 full factorial experimental design executed for glycerol esterification with acetic acid over Amberlyst-35 with particle size of 25 – 75 µm, and acetic acid to glycerol molar ratio of 4.4.

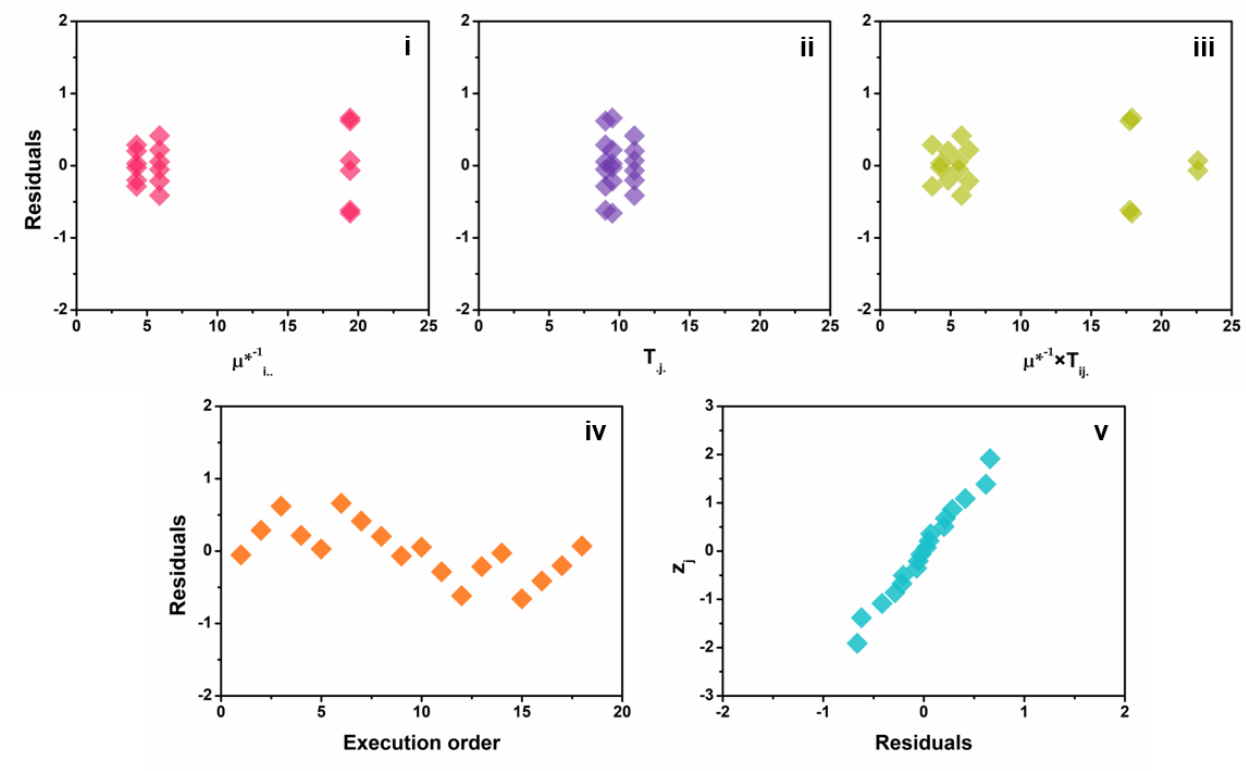

Section S10. Regression model developed based on the factors that were found to be statistically significant in the ANOVA test for the 3^2 full factorial experimental design executed for glycerol esterification with acetic acid over Amberlyst-35 with particle size of 25 – 75 µm, and acetic acid to glycerol molar ratio of 4.4.

$$Turnover = 12.490 - 601.021\mu*^{-1} - 0.034T + 2.032\mu*^{-1} \times T$$

Supplementary Information E. Effectiveness factor and Thiele modulus calculation.

Table S11. Effectiveness factor and Thiele modulus calculation from 18 pairs of tests at the same reaction conditions but different Amberlyst-35 particles sizes and acetic acid to glycerol molar ratio of 4.4. The ranges of particles size are 600 – 1180 μm, and 25 – 75 μm for the first and second set of experiments, respectively.

$Reaction_1$	$Reaction_2$	$-r'_1$	$-r'_2$	Φ_1	Φ_2	η_1	η_2
		$*10^4$ [mol/g_{cat} s]					
1_{iii}	1	5.41	9.56	4.753	0.267	0.499	0.995
2_{iii}	2	2.82	2.88	1.549	0.087	0.870	0.999
3_{iii}	3	1.10	2.07	5.162	0.290	0.469	0.994
4_{iii}	4	7.58	9.66	2.416	0.136	0.748	0.999
5_{iii}	5	1.87	3.40	5.162	0.290	0.469	0.994
6_{iii}	6	1.66	2.25	2.682	0.151	0.712	0.998
7_{iii}	7	6.52	11.72	4.108	0.231	0.553	0.996
8_{iii}	8	1.96	3.23	3.626	0.204	0.600	0.997
9_{iii}	9	1.78	2.62	3.062	0.172	0.664	0.998
10_{iii}	10	7.38	8.92	2.200	0.124	0.778	0.999
11_{iii}	11	2.71	2.94	1.800	0.101	0.834	0.999
12_{iii}	12	1.27	1.78	2.806	0.158	0.696	0.998
13_{iii}	13	7.79	8.97	2.026	0.114	0.802	0.999
14_{iii}	14	1.77	3.18	4.108	0.231	0.553	0.996
15_{iii}	15	1.51	2.22	3.052	0.171	0.665	0.998
16_{iii}	16	6.18	11.79	5.162	0.290	0.469	0.994
17_{iii}	17	2.59	2.80	1.790	0.101	0.836	0.999
18_{iii}	18	1.81	2.41	2.590	0.146	0.724	0.999

*The subscripts 1 and 2 are referred to the data from the first and second set of experiments.

Supplementary Information F. Repeatability test.

Figure S12. Three catalytic tests were achieved at the same reaction conditions: temperature of 361 K, acetic acid to glycerol molar ration of 7, and quantity of the moles of active sites of 1.01 mmol. Amberlyst-35 particle size of 25 – 75 μm. Each average point presents a standard deviation < 6%.

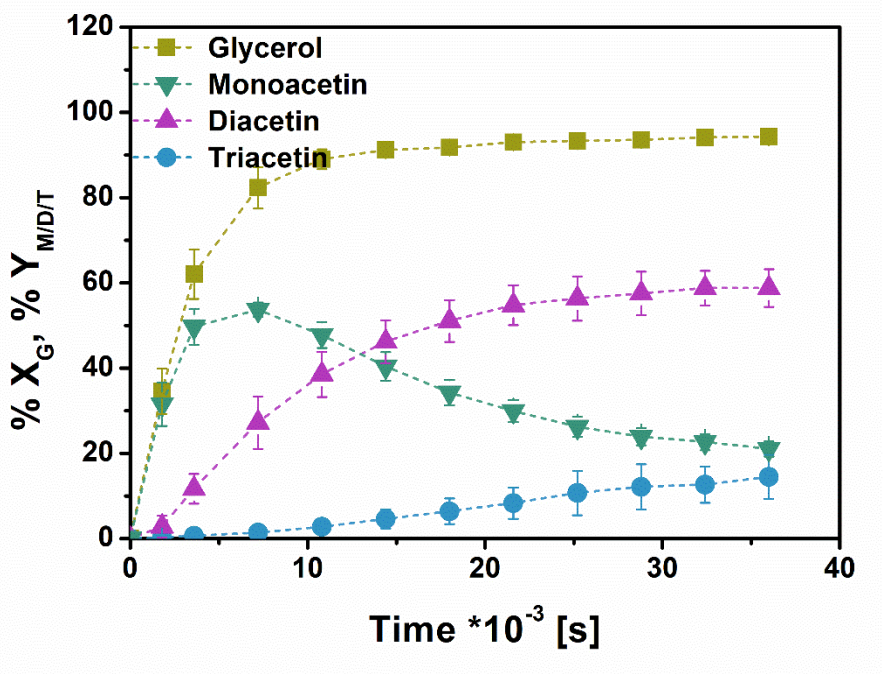

Supplementary Information G. Reactions outcomes corresponding to the sets of experiments designed to obtain the parameters of the kinetic models.

Figure S13. Evolution plots of the of each component in reaction 5. Glycerol esterification catalyzed by Amberlyst-35 with particle size of 25 – 75 μm. Initial acetic acid to glycerol molar ratio of 7, temperature of 361 K, and quantity of moles of active sites of 1.01 mmol. i) Acetins production. ii) water production. iii) Glycerol consumption. iv) Acetic acid consumption.

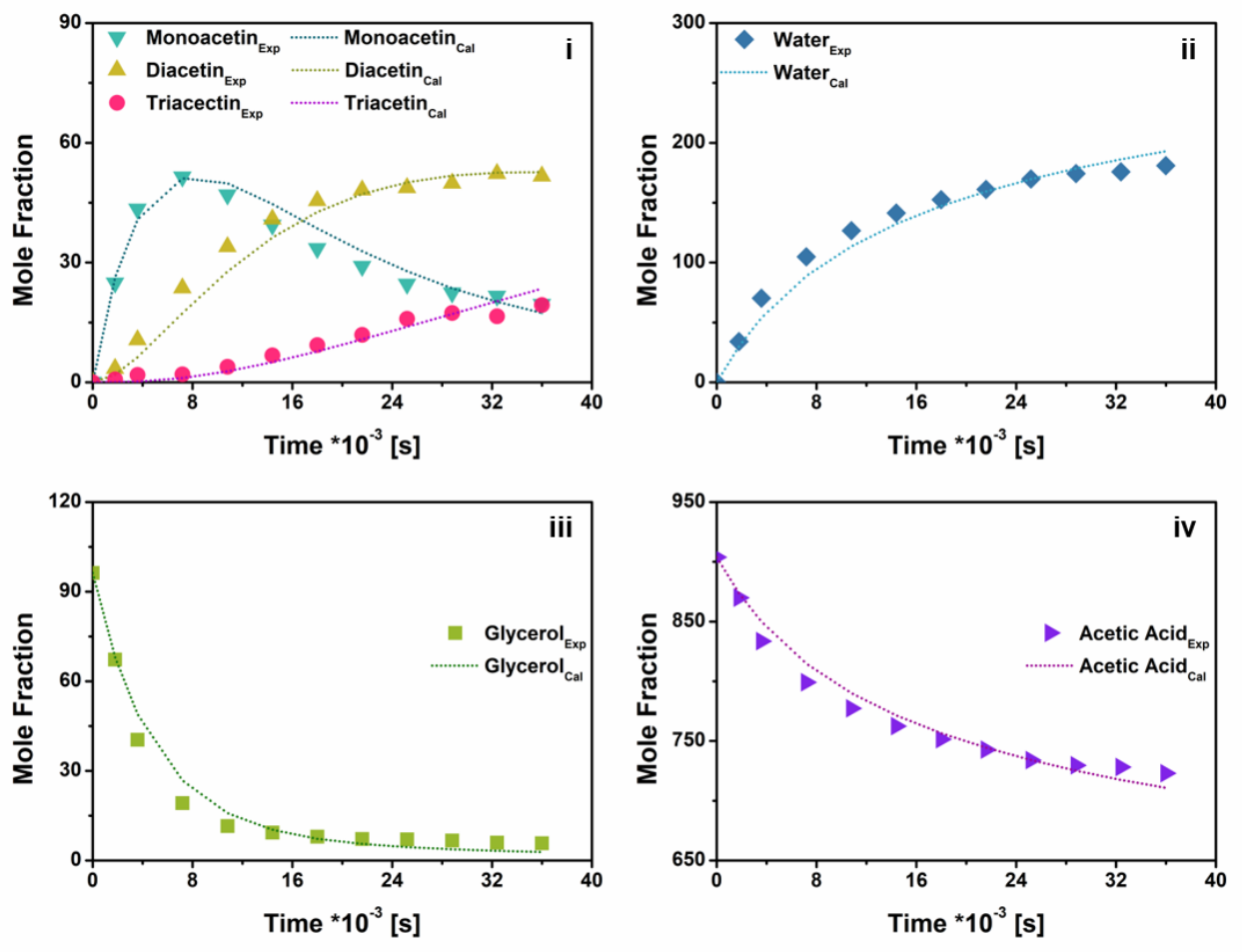

*Exp: experimental values from the experimental designs. Cal: calculated values from the developed kinetic models developed.

Figure S14. Evolution plots of the of each component in reaction 2. Glycerol esterification catalyzed by Amberlyst-35 with particle size of 25 – 75 µm. Initial acetic acid to glycerol molar ratio of 7, temperature of 347 K, and quantity of moles of active sites of 1.01 mmol. i) Acetins production. ii) water production. iii) Glycerol consumption. iv) Acetic acid consumption.

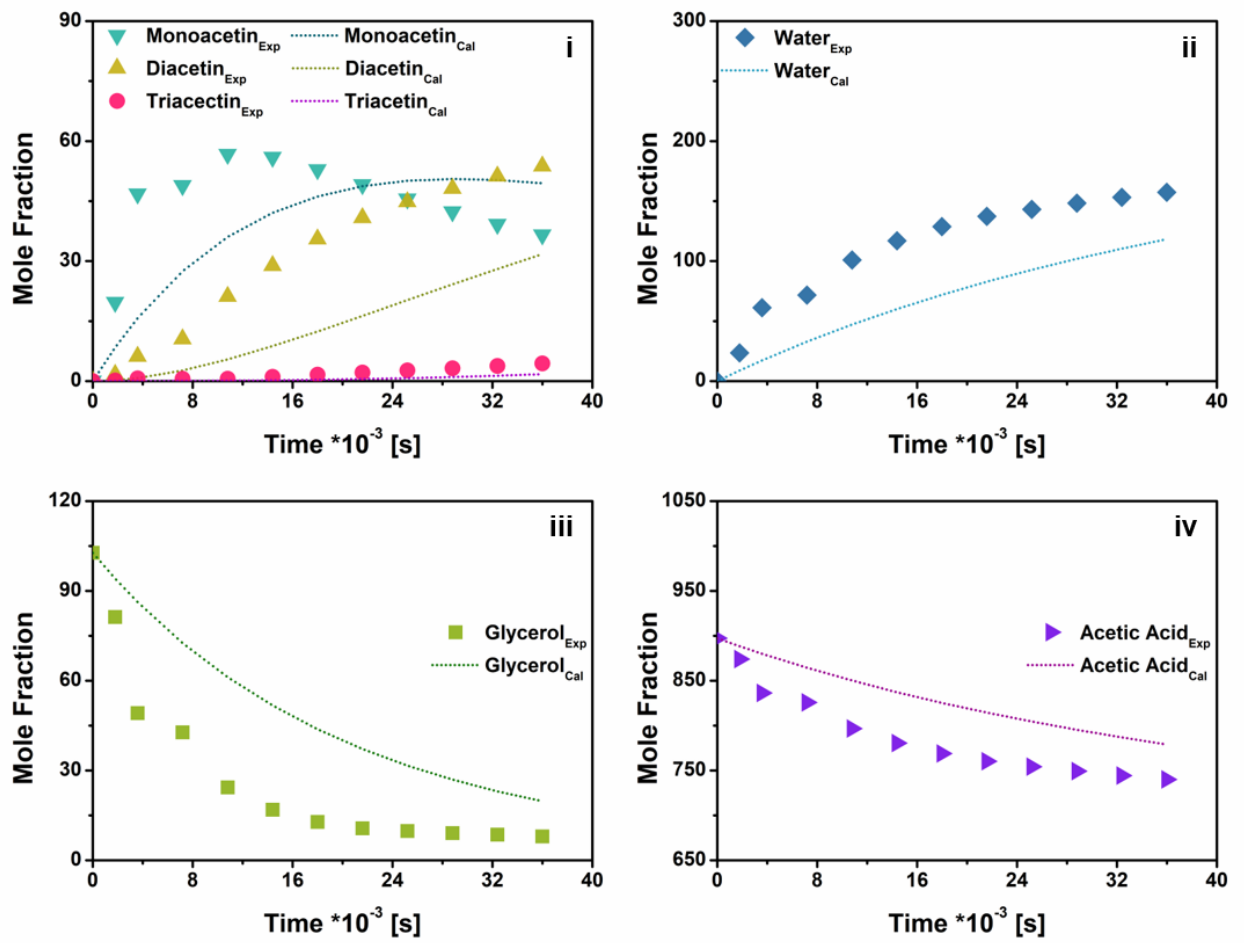

*Exp: experimental values from the experimental designs. Cal: calculated values from the developed kinetic models developed.

Figure S15. Evolution plots of the of each component in reaction 9. Glycerol esterification catalyzed by Amberlyst-35 with particle size of 25 – 75 µm. Initial acetic acid to glycerol molar ratio of 5, temperature of 373 K, and quantity of moles of active sites of 1.33 mmol. i) Acetins production. ii) water production. iii) Glycerol consumption. iv) Acetic acid consumption.

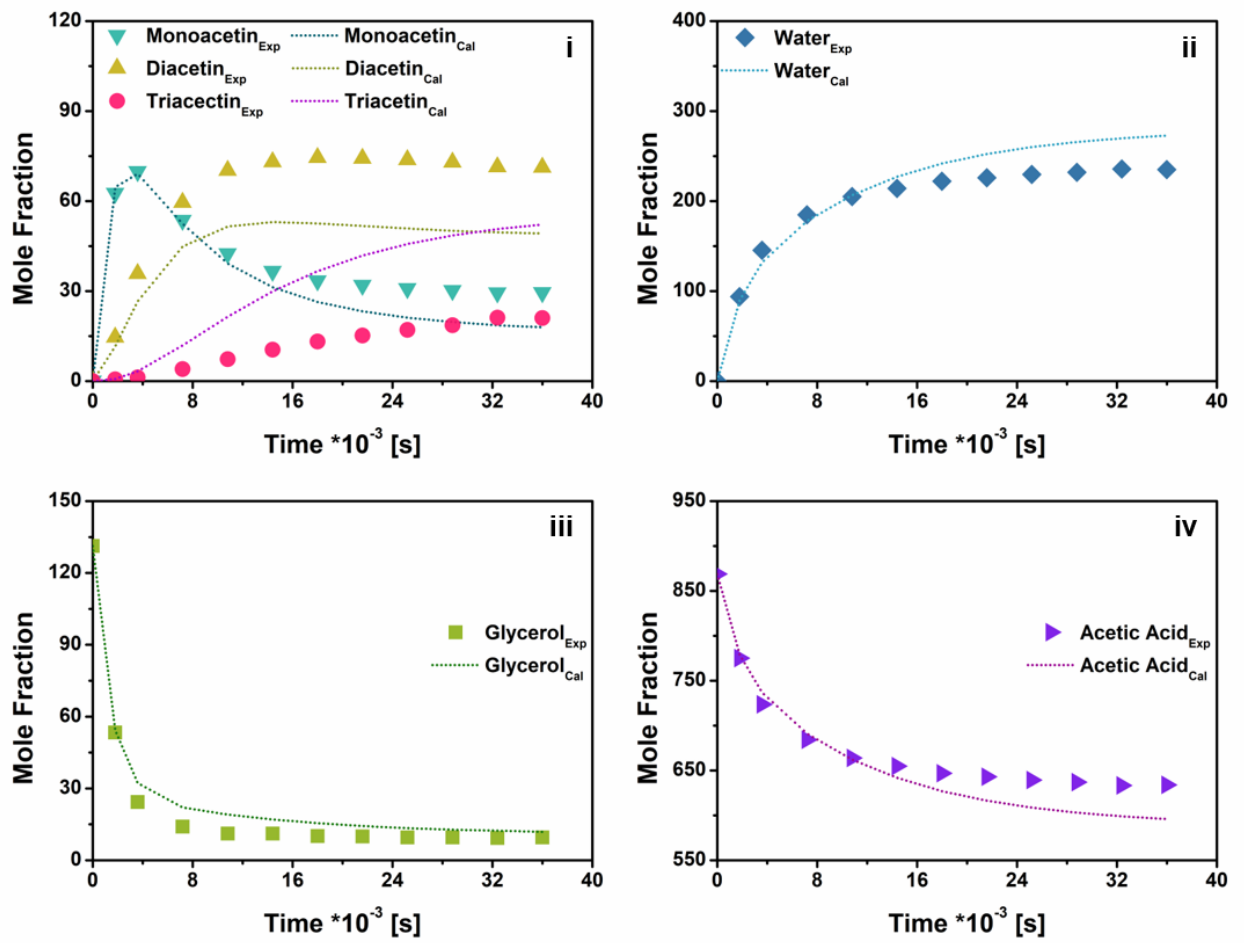

*Exp: experimental values from the experimental designs. Cal: calculated values from the developed kinetic models developed.

Figure S16. Evolution plots of the of each component in reaction 6. Glycerol esterification catalyzed by Amberlyst-35 with particle size of 25 – 75 µm. Initial acetic acid to glycerol molar ratio of 7, temperature of 361 K, and quantity of moles of active sites of 1.01 mmol. i) Acetins production. ii) water production. iii) Glycerol consumption. iv) Acetic acid consumption.

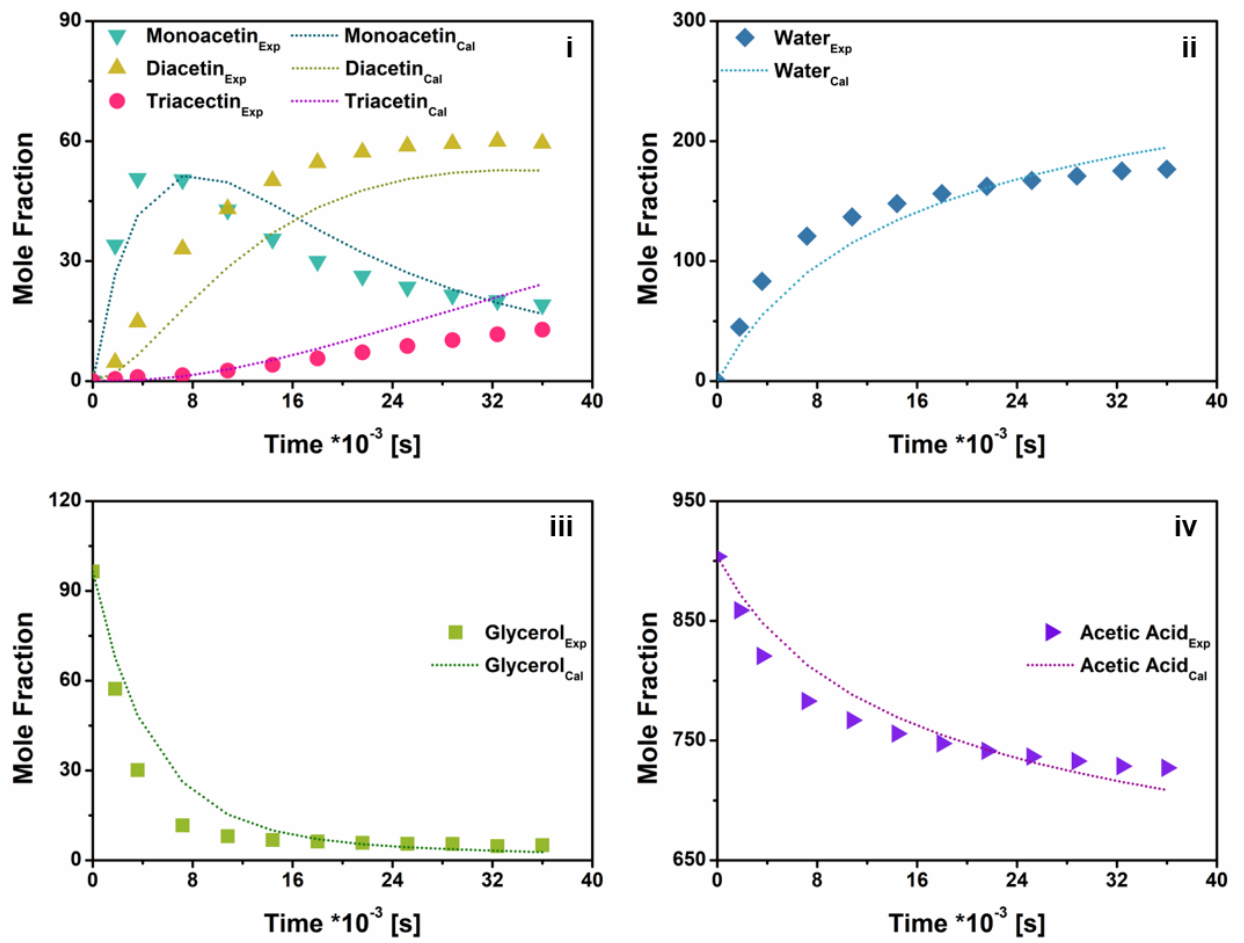

*Exp: experimental values from the experimental designs. Cal: calculated values from the developed kinetic models developed.

Figure S17. Evolution plots of the of each component in reaction 3. Glycerol esterification catalyzed by Amberlyst-35 with particle size of 25 – 75 μm. Initial acetic acid to glycerol molar ratio of 9, temperature of 347 K, and quantity of moles of active sites of 0.81 mmol. i) Acetins production. ii) water production. iii) Glycerol consumption. iv) Acetic acid consumption.

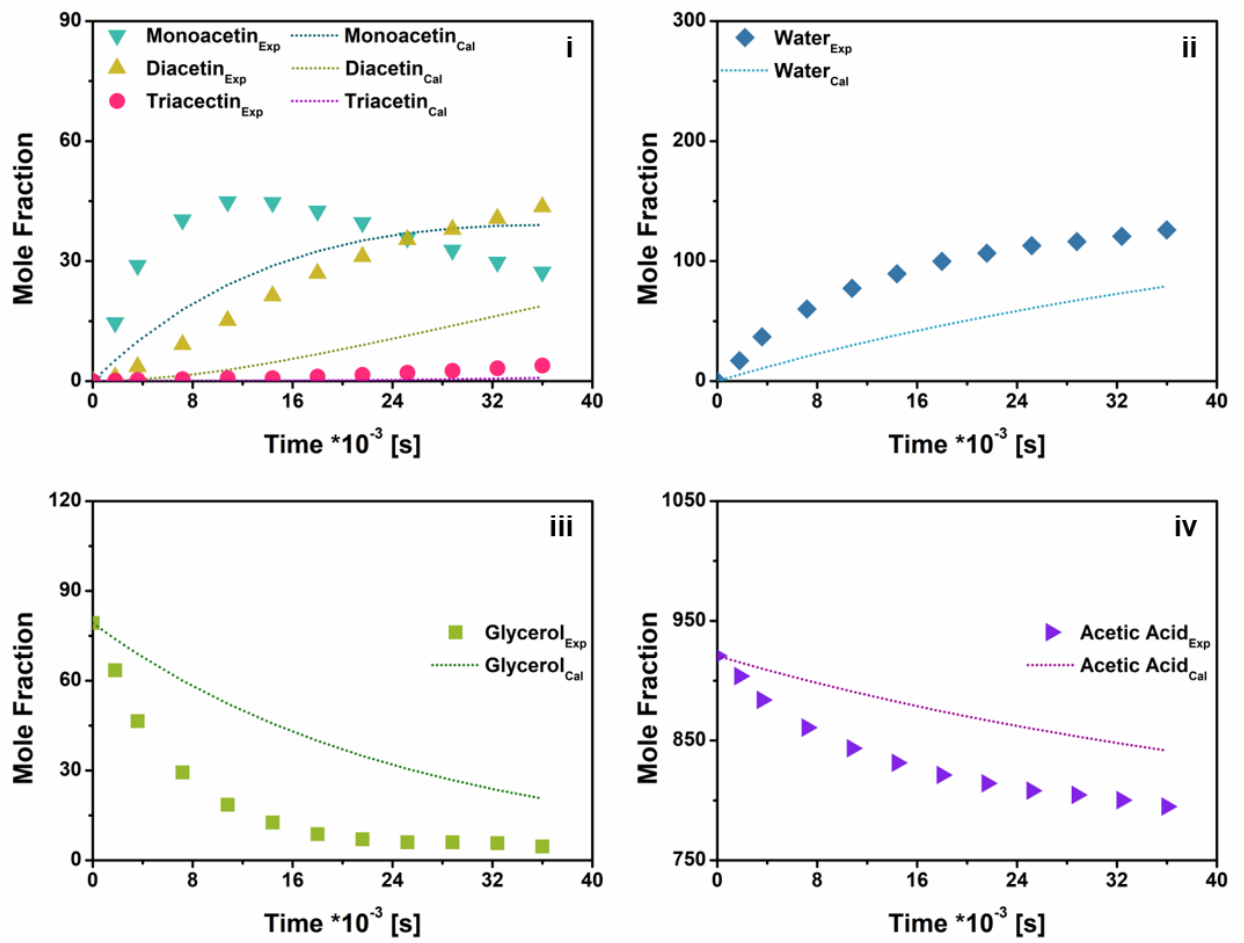

*Exp: experimental values from the experimental designs. Cal: calculated values from the developed kinetic models developed.

Figure S18. Evolution plots of the of each component in reaction 11. Glycerol esterification catalyzed by Amberlyst-35 with particle size of 25 – 75 µm. Initial acetic acid to glycerol molar ratio of 9, temperature of 373 K, and quantity of moles of active sites of 0.81 mmol. i) Acetins production. ii) water production. iii) Glycerol consumption. iv) Acetic acid consumption.

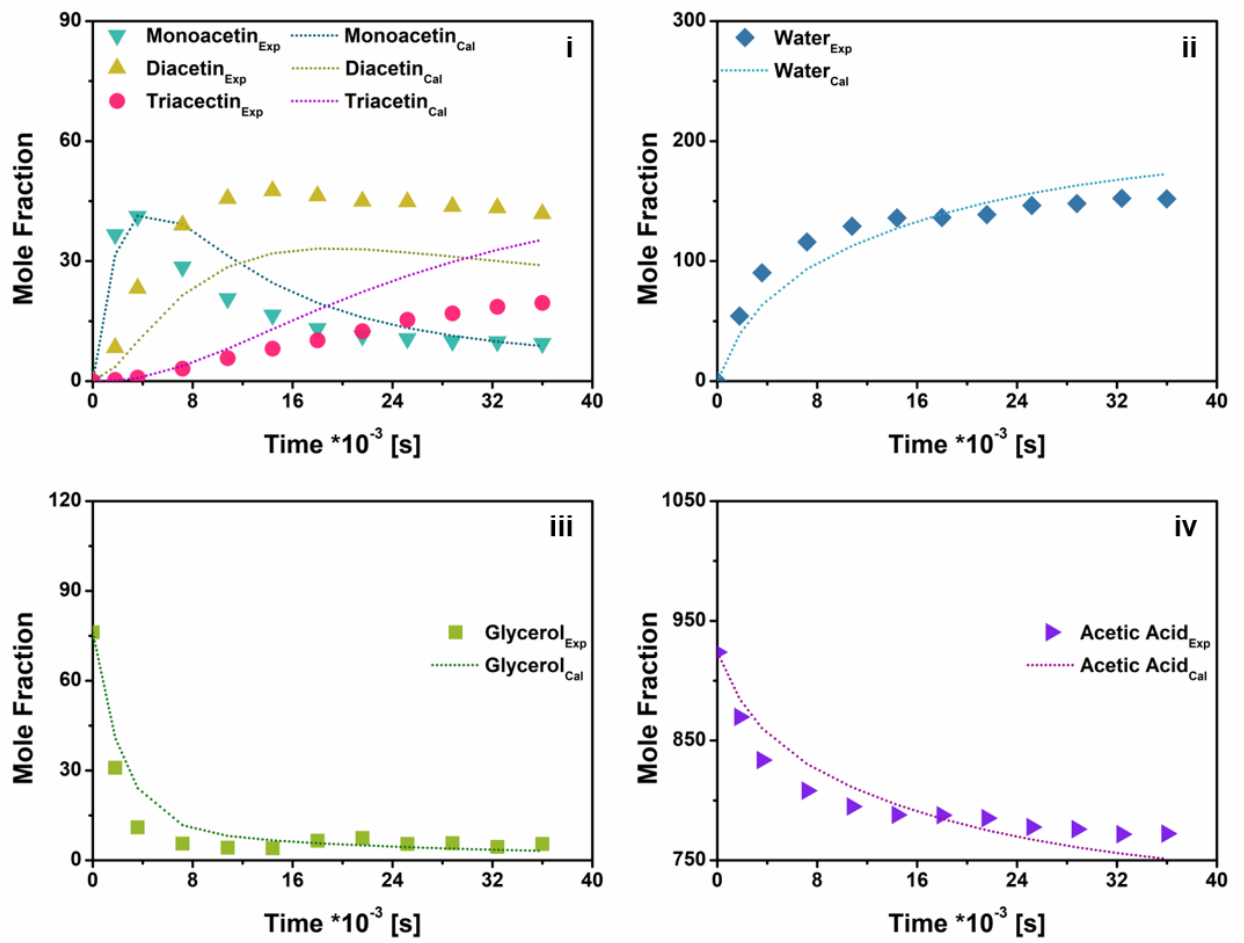

*Exp: experimental values from the experimental designs. Cal: calculated values from the developed kinetic models developed.

Figure S19. Evolution plots of the of each component in reaction 1. Glycerol esterification catalyzed by Amberlyst-35 with particle size of 25 – 75 µm. Initial acetic acid to glycerol molar ratio of 5, temperature of 347 K, and quantity of moles of active sites of 1.33 mmol. i) Acetins production. ii) water production. iii) Glycerol consumption. iv) Acetic acid consumption.

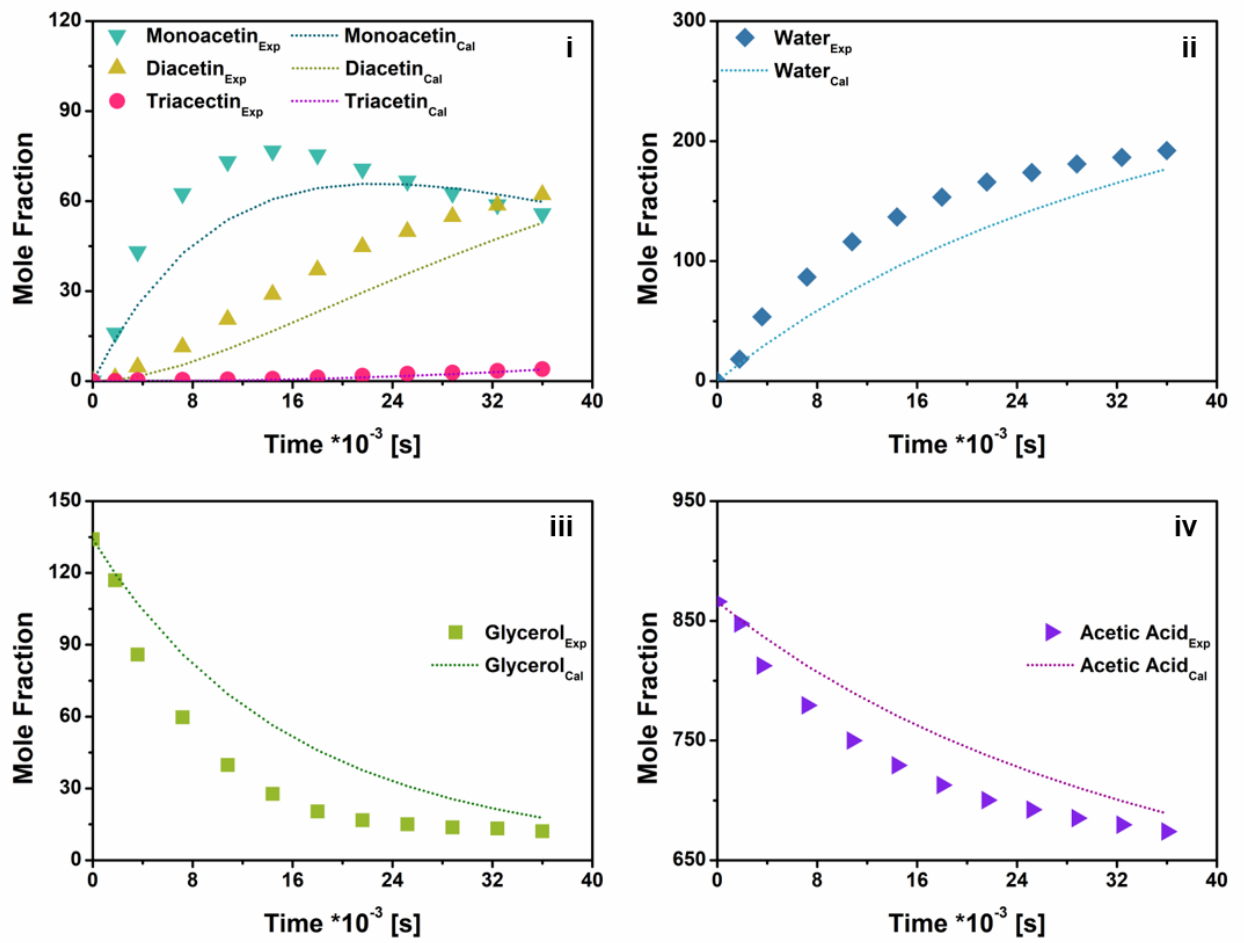

*Exp: experimental values from the experimental designs. Cal: calculated values from the developed kinetic models developed.

Figure S20. Evolution plots of the of each component in reaction 8. Glycerol esterification catalyzed by Amberlyst-35 with particle size of 25 – 75 µm. Initial acetic acid to glycerol molar ratio of 9, temperature of 361 K, and quantity of moles of active sites of 0.81 mmol. i) Acetins production. ii) water production. iii) Glycerol consumption. iv) Acetic acid consumption.

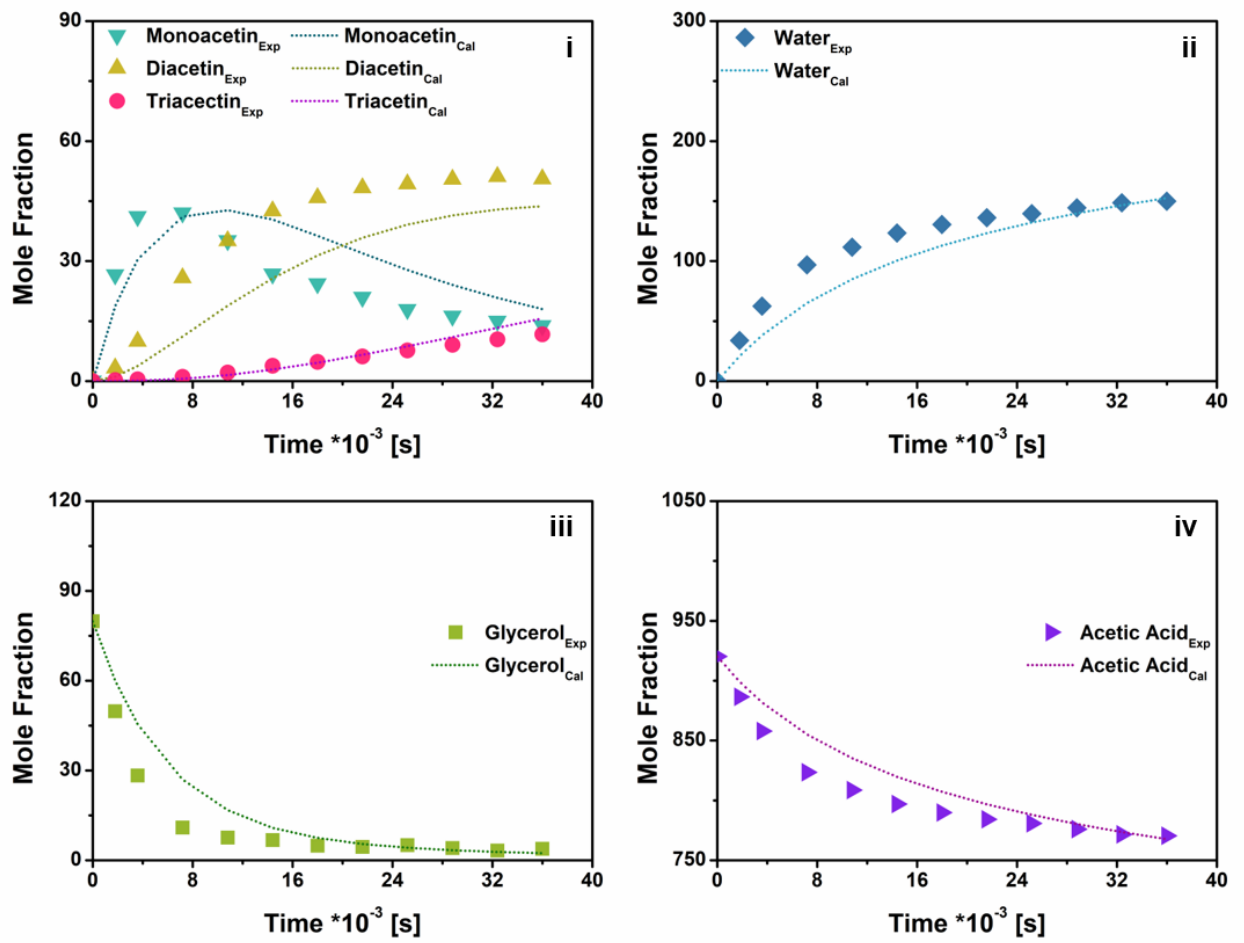

*Exp: experimental values from the experimental designs. Cal: calculated values from the developed kinetic models developed.

Figure S21. Evolution plots of the of each component in reaction 10. Glycerol esterification catalyzed by Amberlyst-35 with particle size of 25 – 75 µm. Initial acetic acid to glycerol molar ratio of 7, temperature of 373 K, and quantity of moles of active sites of 1.01 mmol. i) Acetins production. ii) water production. iii) Glycerol consumption. iv) Acetic acid consumption.

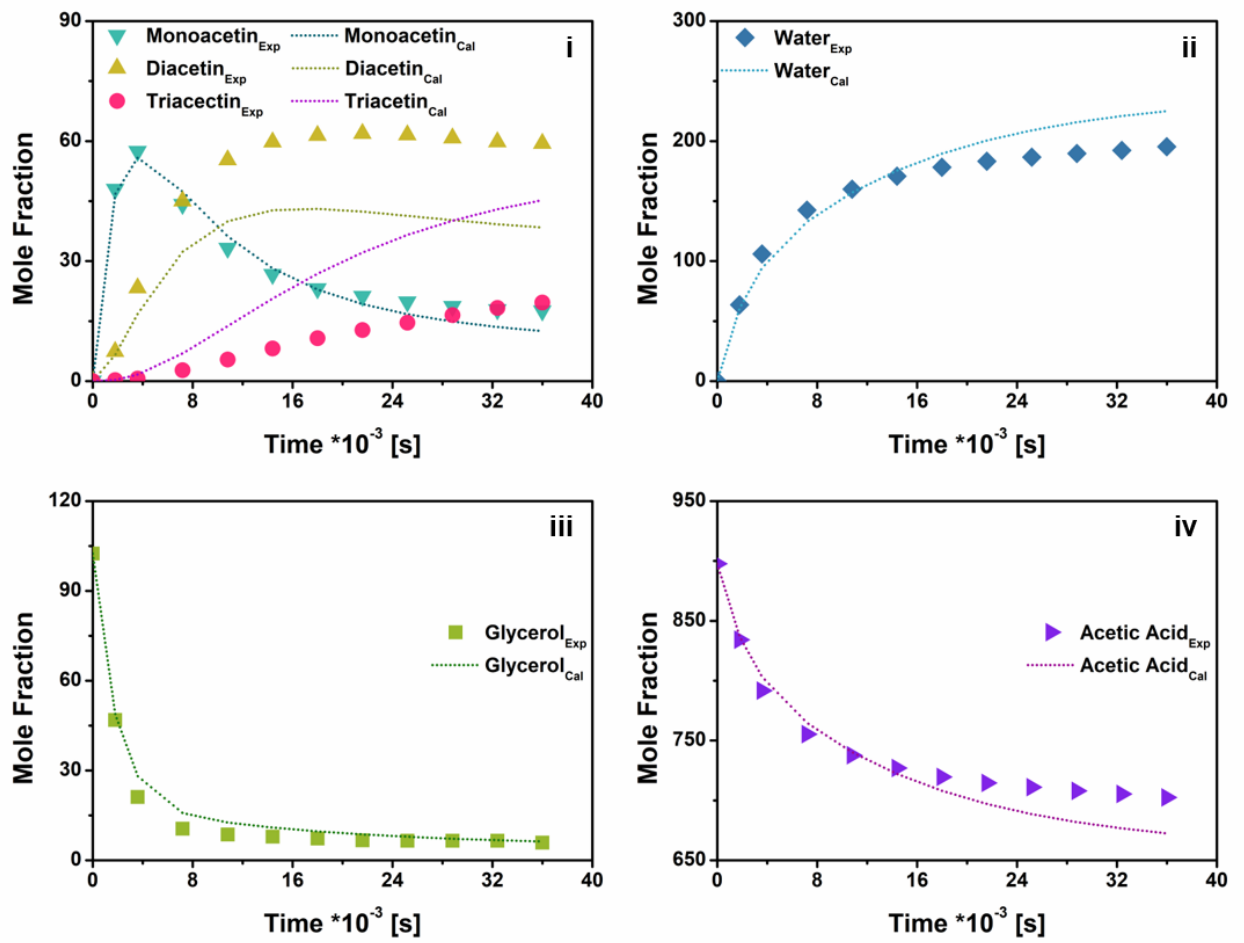

*Exp: experimental values from the experimental designs. Cal: calculated values from the developed kinetic models developed.

Figure S22. Evolution plots of the of each component in reaction 4. Glycerol esterification catalyzed by Amberlyst-35 with particle size of 25 – 75 µm. Initial acetic acid to glycerol molar ratio of 5, temperature of 361 K, and quantity of moles of active sites of 1.33 mmol. i) Acetins production. ii) water production. iii) Glycerol consumption. iv) Acetic acid consumption.

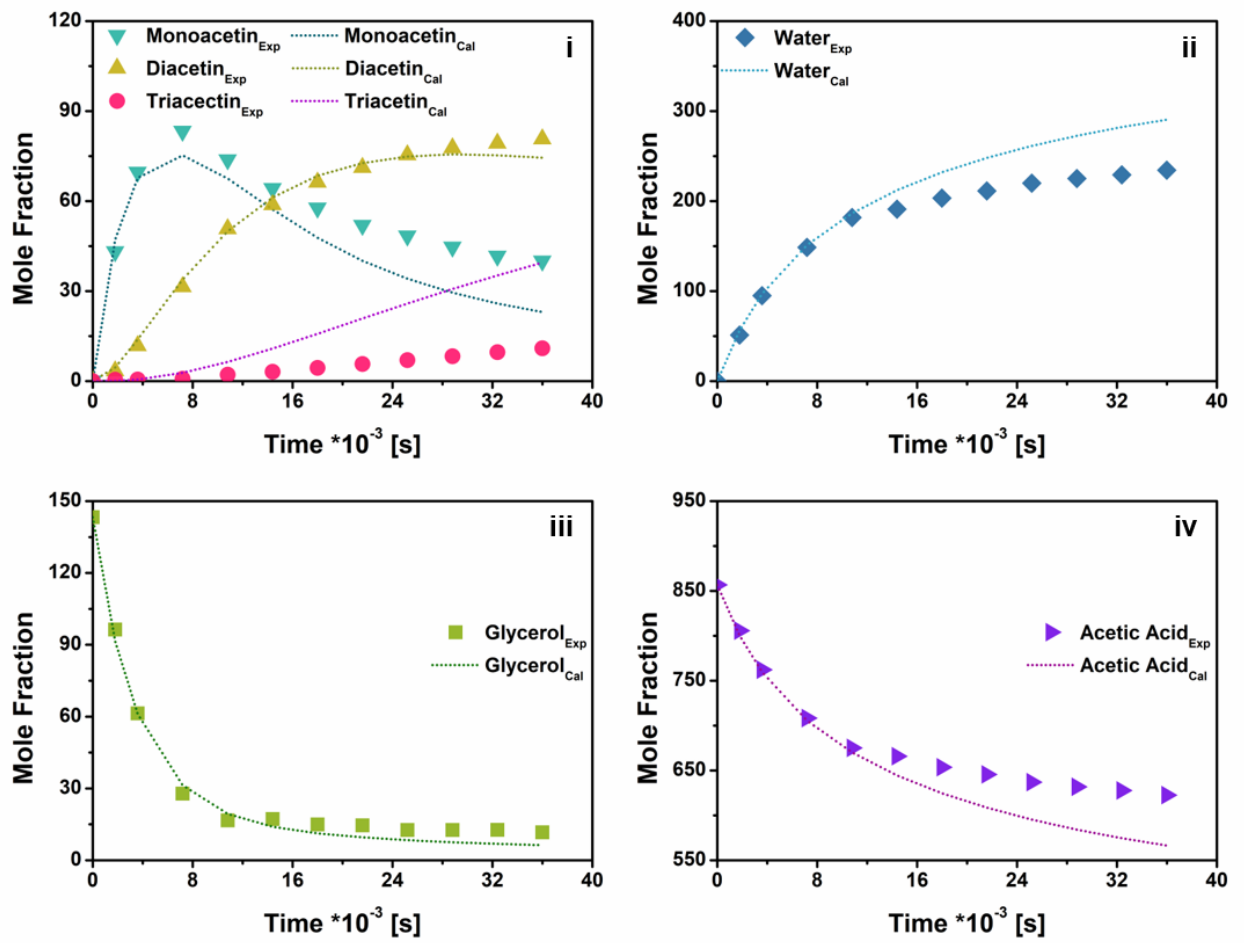

*Exp: experimental values from the experimental designs. Cal: calculated values from the developed kinetic models developed.

Figure S23. Evolution plots of the of each component in reaction 7. Glycerol esterification catalyzed by Amberlyst-35 with particle size of 25 – 75 µm. Initial acetic acid to glycerol molar ratio of 7, temperature of 361 K, and quantity of moles of active sites of 1.01 mmol. i) Acetins production. ii) water production. iii) Glycerol consumption. iv) Acetic acid consumption.

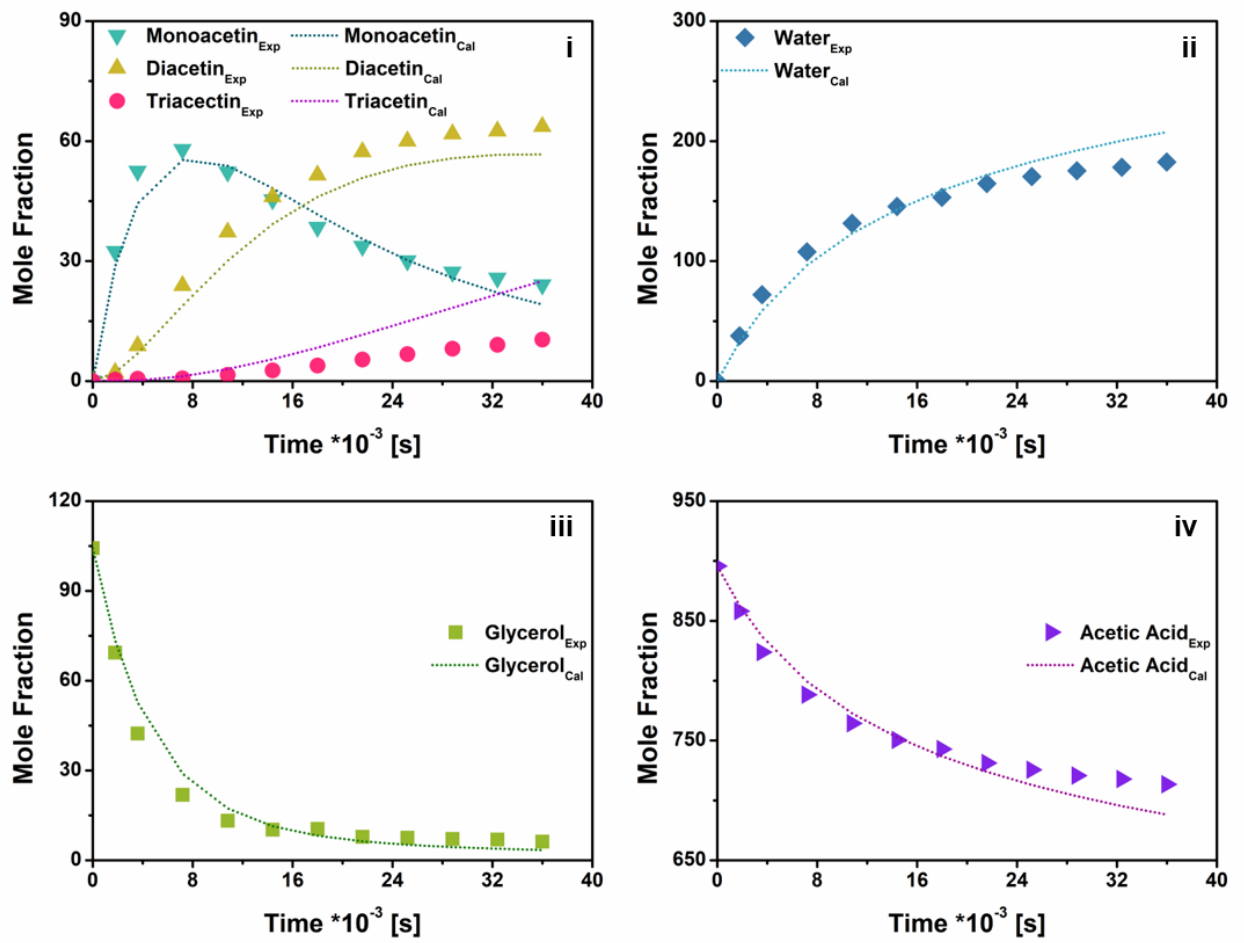

*Exp: experimental values from the experimental designs. Cal: calculated values from the developed kinetic models developed.

Figure S24. Evolution plots of the of each component in reaction 15. Glycerol esterification catalyzed by Amberlyst-35 with particle size of 25 – 75 µm. Initial acetic acid to glycerol molar ratio of 9, temperature of 361 K, and quantity of moles of active sites of 0.41 mmol. i) Acetins production. ii) water production. iii) Glycerol consumption. iv) Acetic acid consumption.

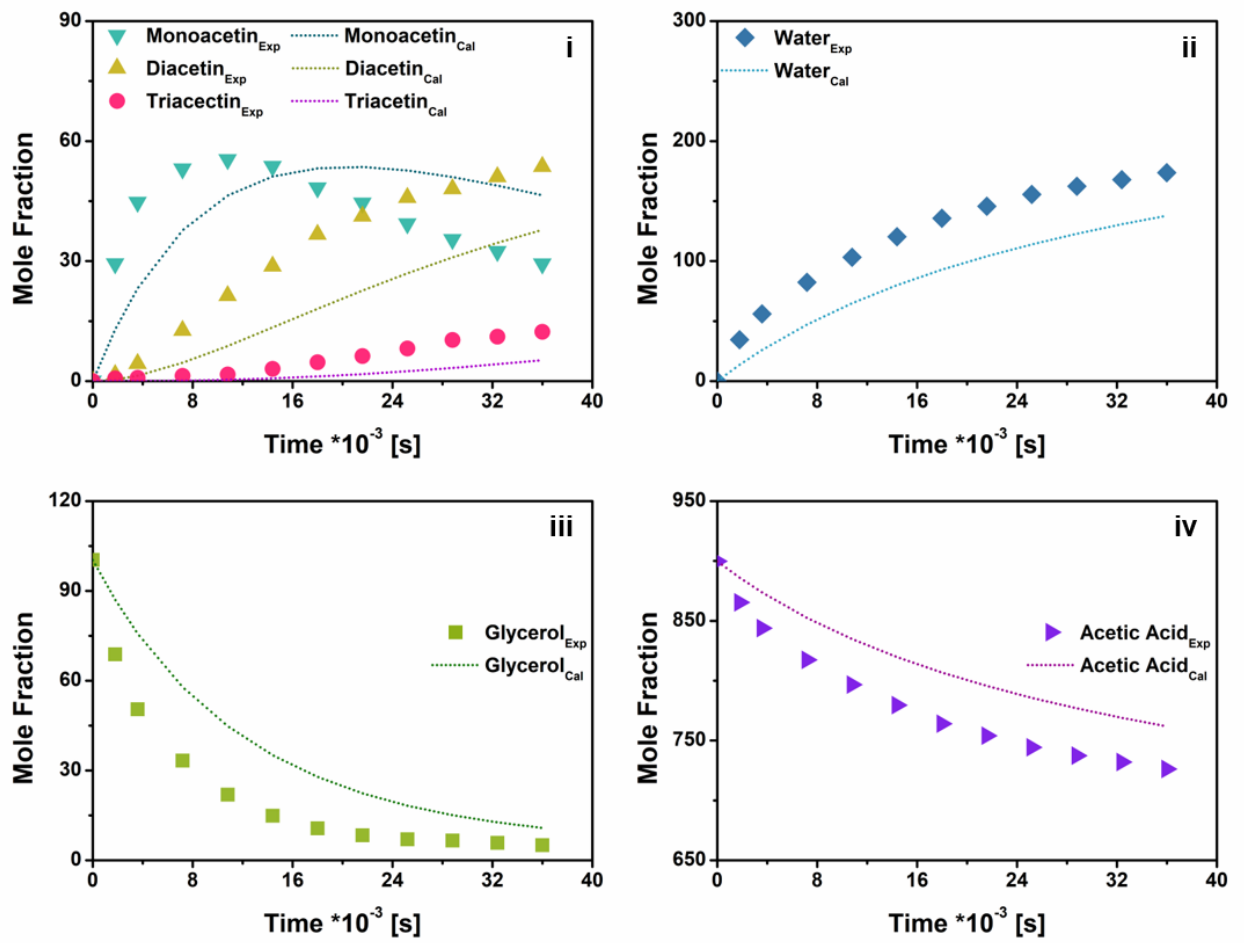

*Exp: experimental values from the experimental designs. Cal: calculated values from the developed kinetic models developed.

Figure S25. Evolution plots of the of each component in reaction 22. Glycerol esterification catalyzed by Amberlyst-35 with particle size of 25 – 75 µm. Initial acetic acid to glycerol molar ratio of 9, temperature of 373 K, and quantity of moles of active sites of 1.87 mmol. i) Acetins production. ii) water production. iii) Glycerol consumption. iv) Acetic acid consumption.

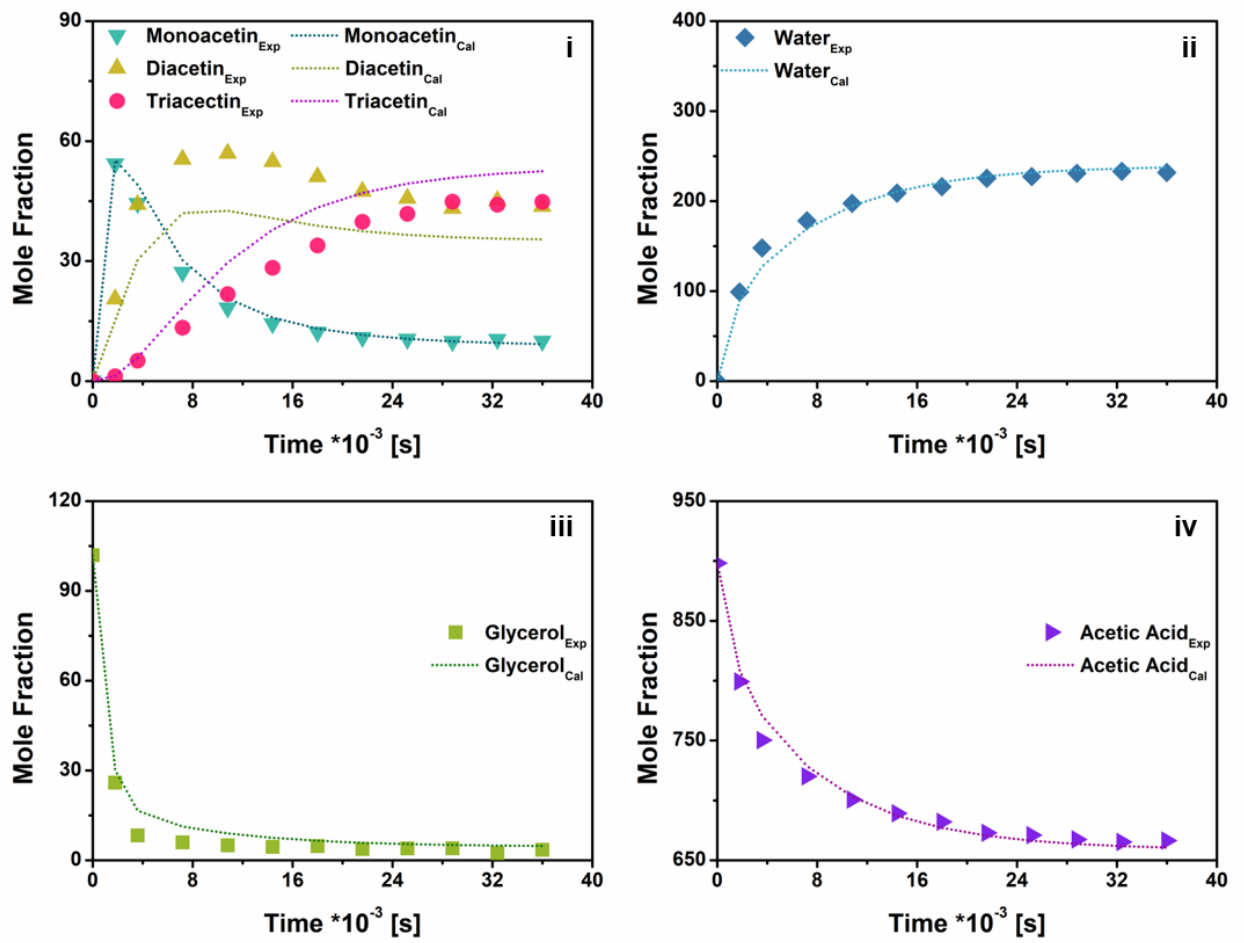

*Exp: experimental values from the experimental designs. Cal: calculated values from the developed kinetic models developed.

Figure S26. Evolution plots of the of each component in reaction 19. Glycerol esterification catalyzed by Amberlyst-35 with particle size of 25 – 75 μm. Initial acetic acid to glycerol molar ratio of 7, temperature of 373 K, and quantity of moles of active sites of 2.33 mmol. i) Acetins production. ii) water production. iii) Glycerol consumption. iv) Acetic acid consumption.

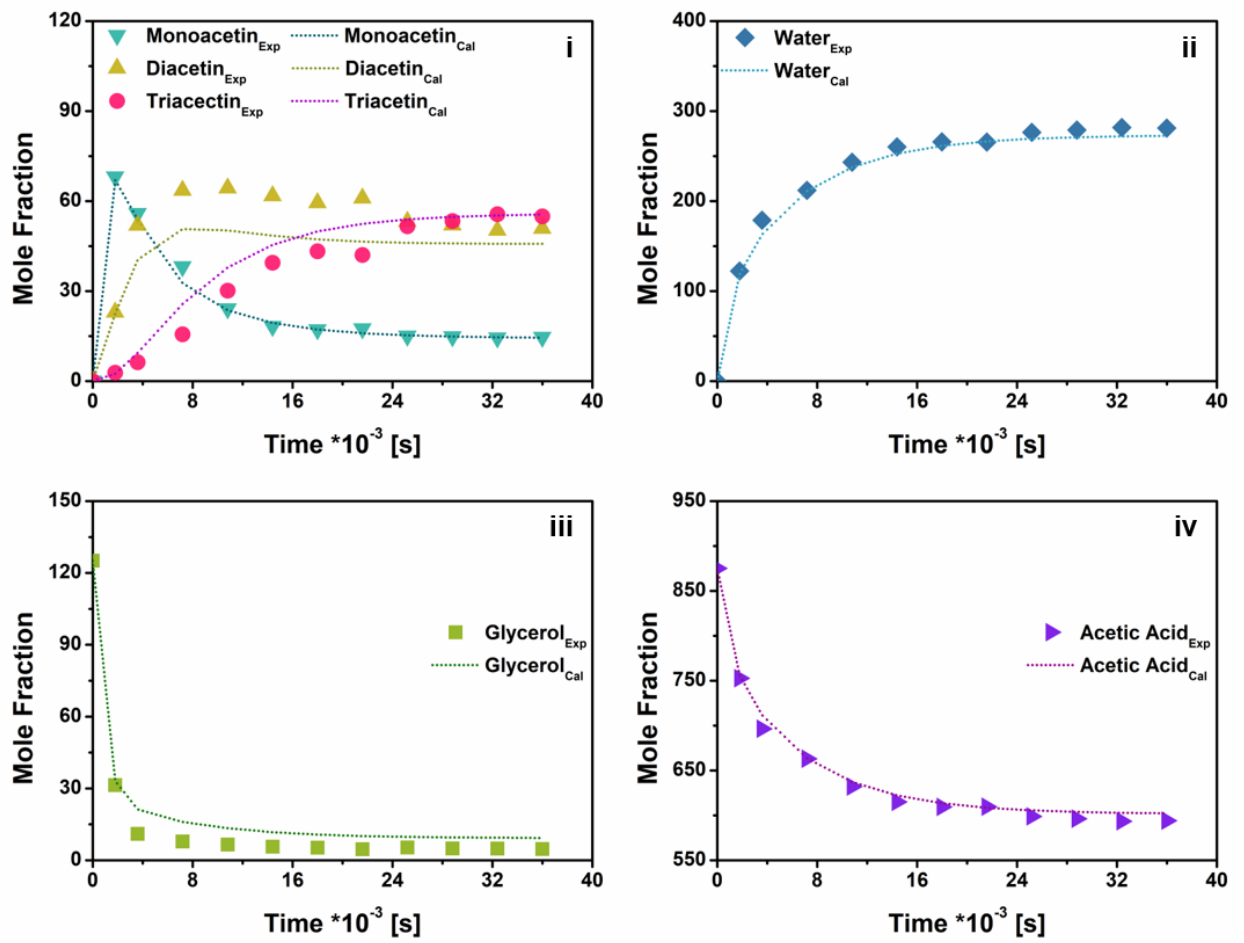

*Exp: experimental values from the experimental designs. Cal: calculated values from the developed kinetic models developed.

Figure S27. Evolution plots of the of each component in reaction 13. Glycerol esterification catalyzed by Amberlyst-35 with particle size of 25 – 75 µm. Initial acetic acid to glycerol molar ratio of 7, temperature of 361 K, and quantity of moles of active sites of 2.33 mmol. i) Acetins production. ii) water production. iii) Glycerol consumption. iv) Acetic acid consumption.

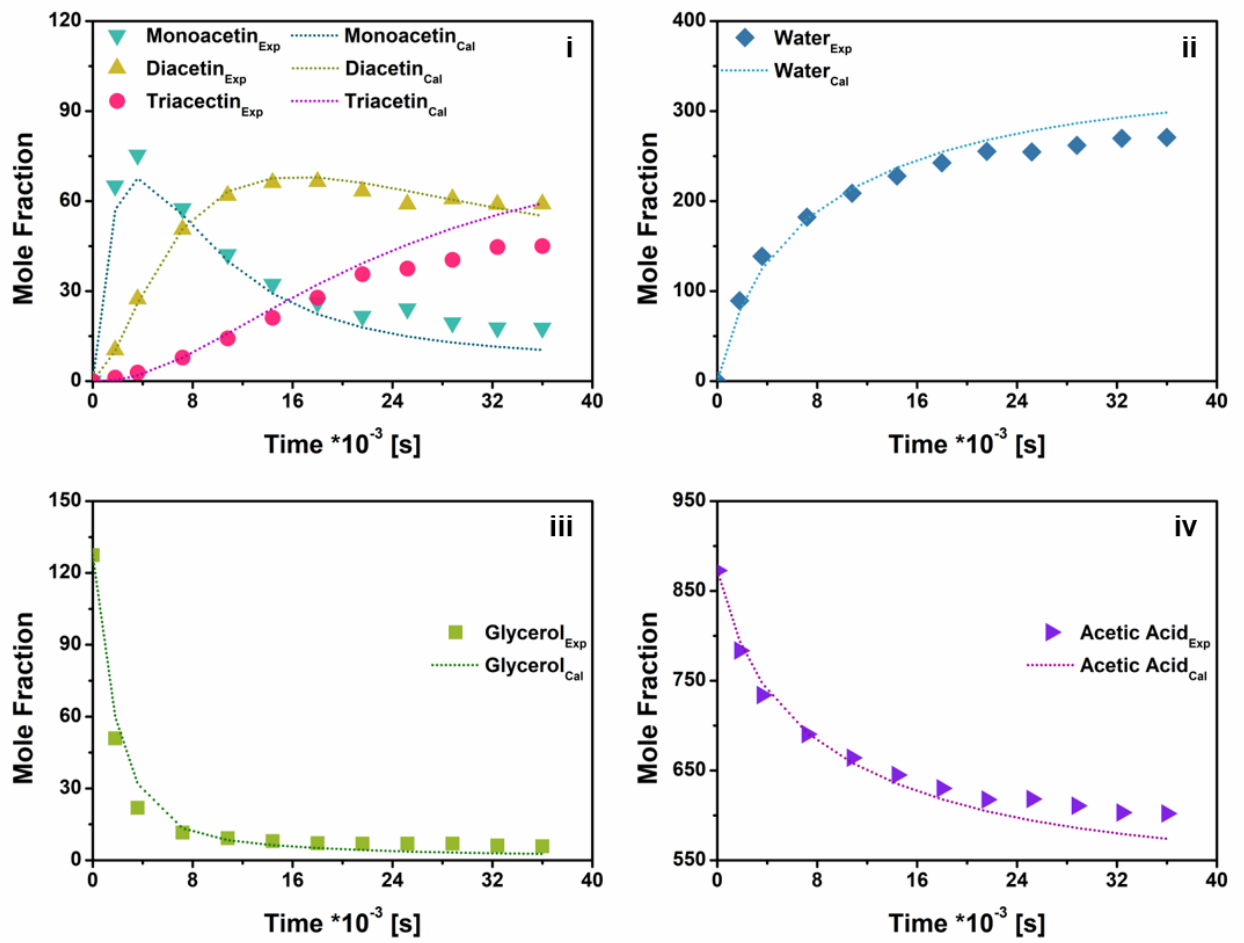

*Exp: experimental values from the experimental designs. Cal: calculated values from the developed kinetic models developed.

Figure S28. Evolution plots of the of each component in reaction 12. Glycerol esterification catalyzed by Amberlyst-35 with particle size of 25 – 75 µm. Initial acetic acid to glycerol molar ratio of 7, temperature of 361 K, and quantity of moles of active sites of 0.51 mmol. i) Acetins production. ii) water production. iii) Glycerol consumption. iv) Acetic acid consumption.

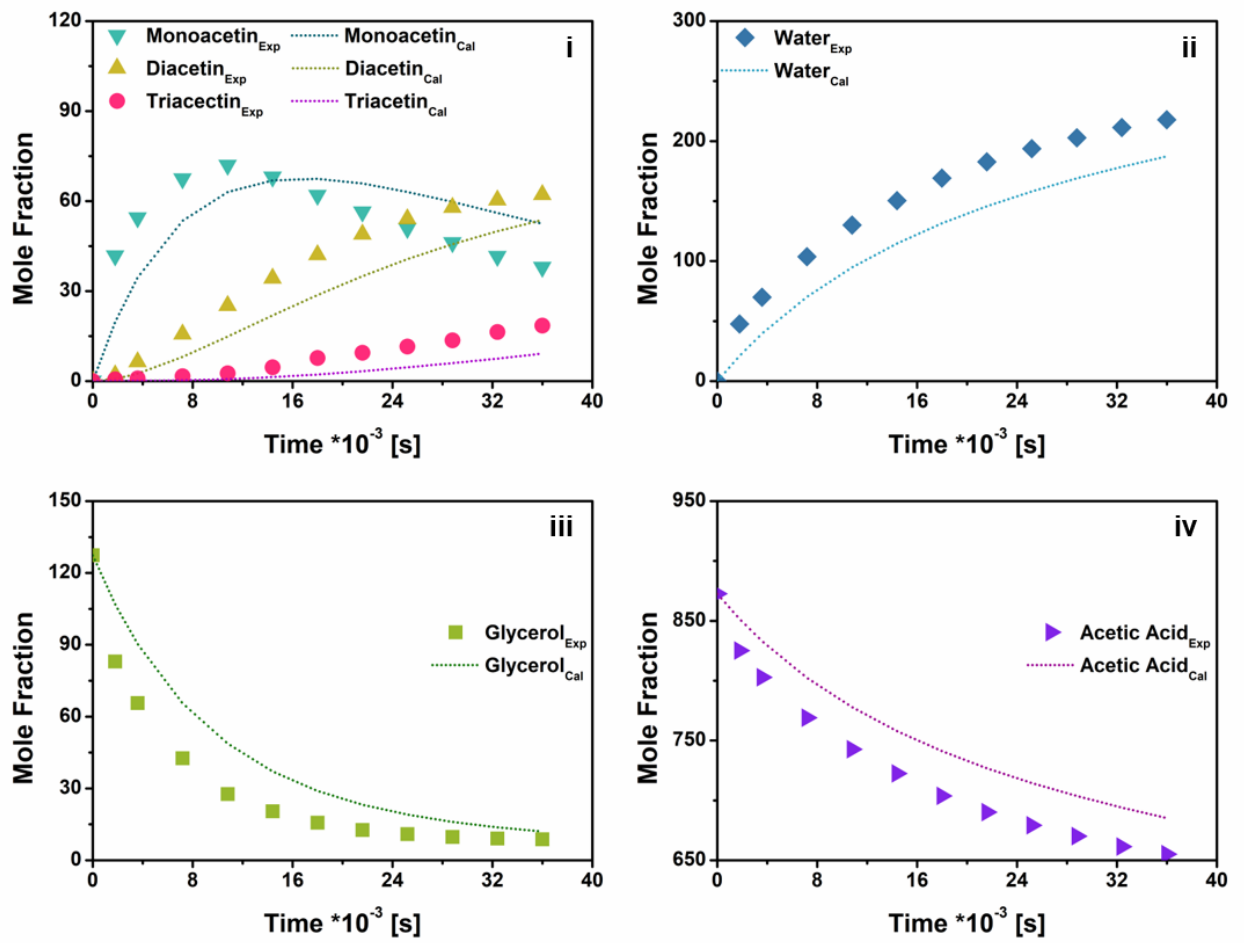

*Exp: experimental values from the experimental designs. Cal: calculated values from the developed kinetic models developed.

Figure S29. Evolution plots of the of each component in reaction 17. Glycerol esterification catalyzed by Amberlyst-35 with particle size of 25 – 75 µm. Initial acetic acid to glycerol molar ratio of 9, temperature of 361 K, and quantity of moles of active sites of 3.18 mmol. i) Acetins production. ii) water production. iii) Glycerol consumption. iv) Acetic acid consumption.

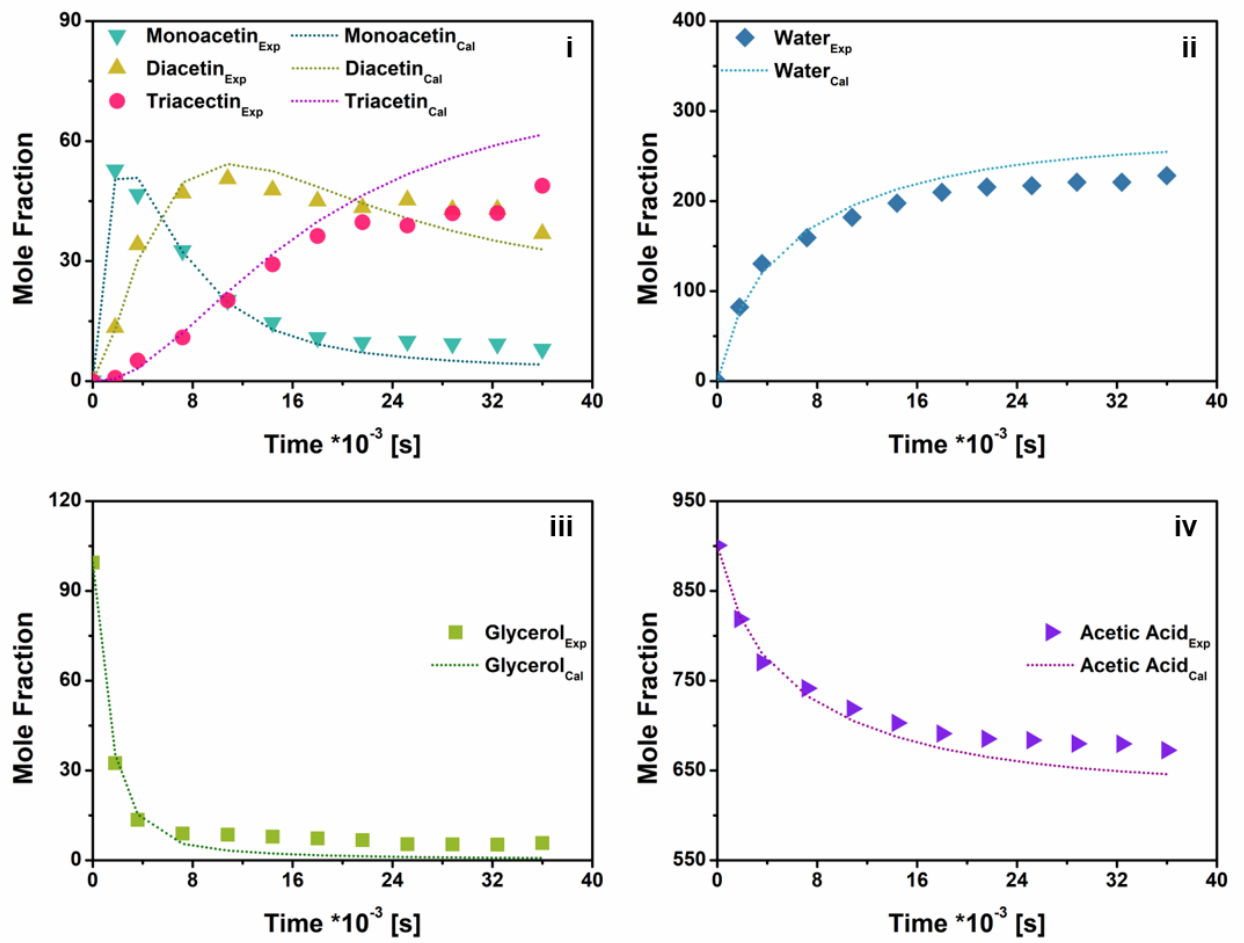

*Exp: experimental values from the experimental designs. Cal: calculated values from the developed kinetic models developed.

Figure S30. Evolution plots of the of each component in reaction 21. Glycerol esterification catalyzed by Amberlyst-35 with particle size of 25 – 75 µm. Initial acetic acid to glycerol molar ratio of 9, temperature of 373 K, and quantity of moles of active sites of 0.41 mmol. i) Acetins production. ii) water production. iii) Glycerol consumption. iv) Acetic acid consumption.

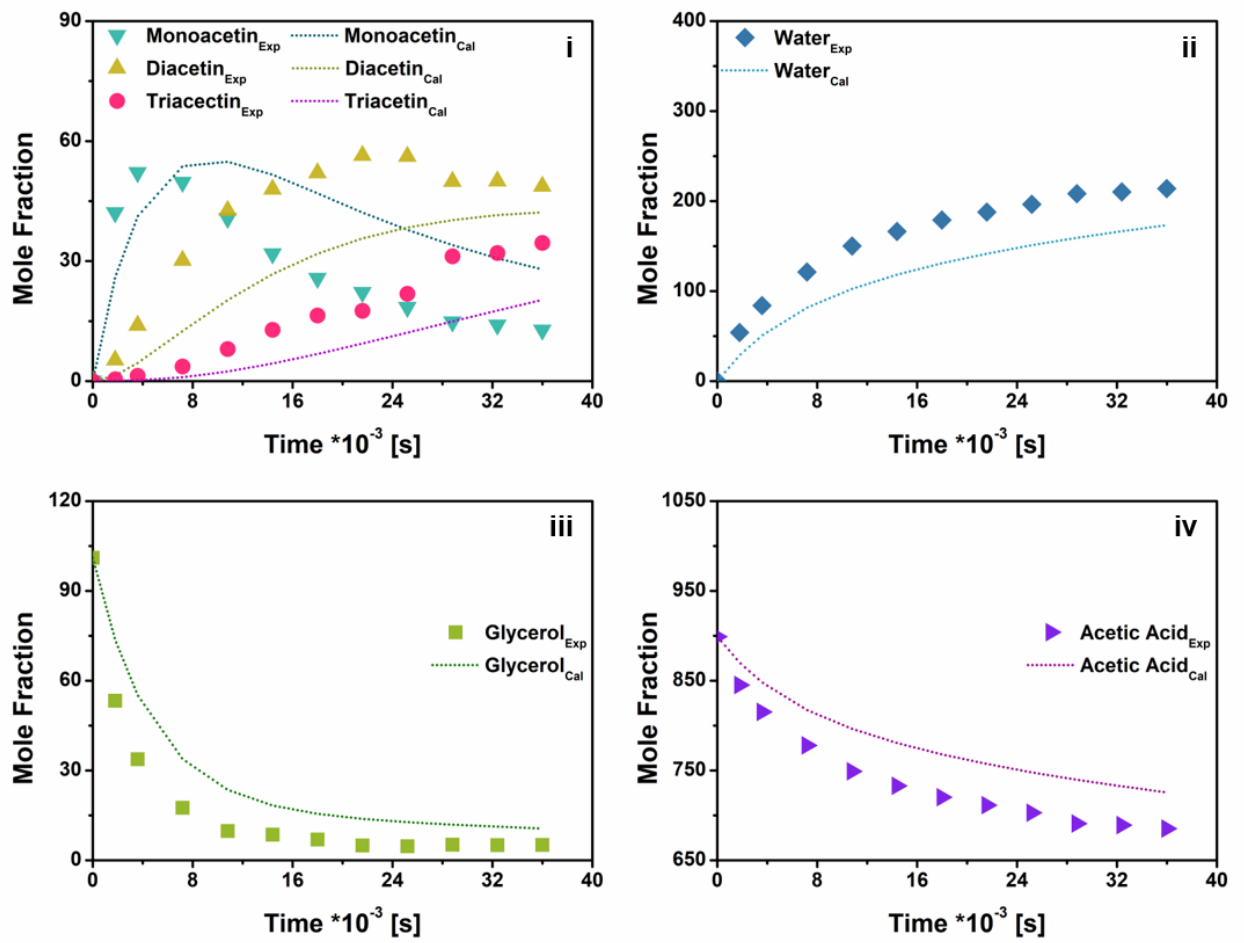

*Exp: experimental values from the experimental designs. Cal: calculated values from the developed kinetic models developed.

Figure S31. Evolution plots of the of each component in reaction 23. Glycerol esterification catalyzed by Amberlyst-35 with particle size of 25 – 75 μm. Initial acetic acid to glycerol molar ratio of 9, temperature of 373 K, and quantity of moles of active sites of 3.18 mmol. i) Acetins production. ii) water production. iii) Glycerol consumption. iv) Acetic acid consumption.

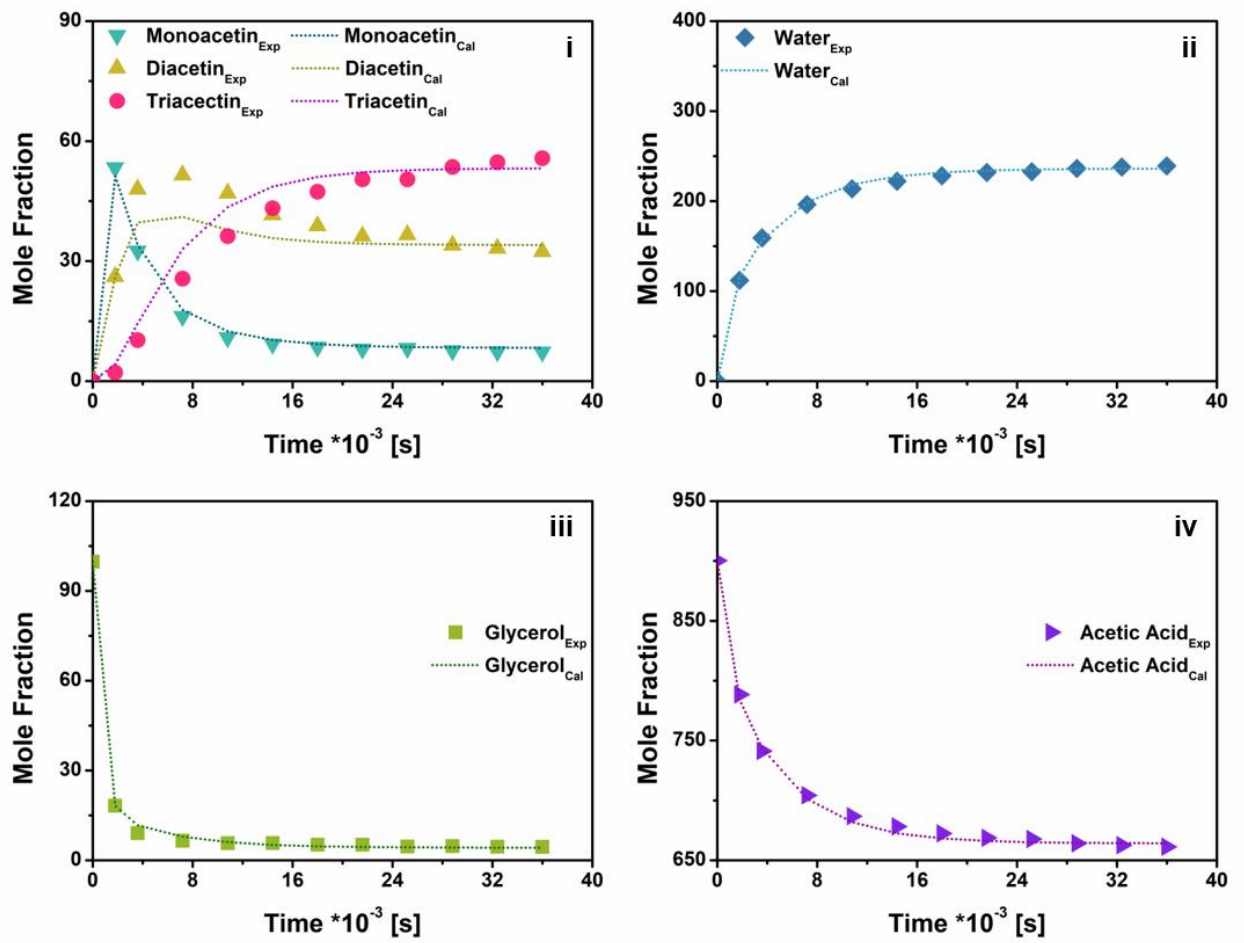

*Exp: experimental values from the experimental designs. Cal: calculated values from the developed kinetic models developed.

Figure S32. Evolution plots of the of each component in reaction 20. Glycerol esterification catalyzed by Amberlyst-35 with particle size of 25 – 75 µm. Initial acetic acid to glycerol molar ratio of 7, temperature of 373 K, and quantity of moles of active sites of 3.95 mmol. i) Acetins production. ii) water production. iii) Glycerol consumption. iv) Acetic acid consumption.

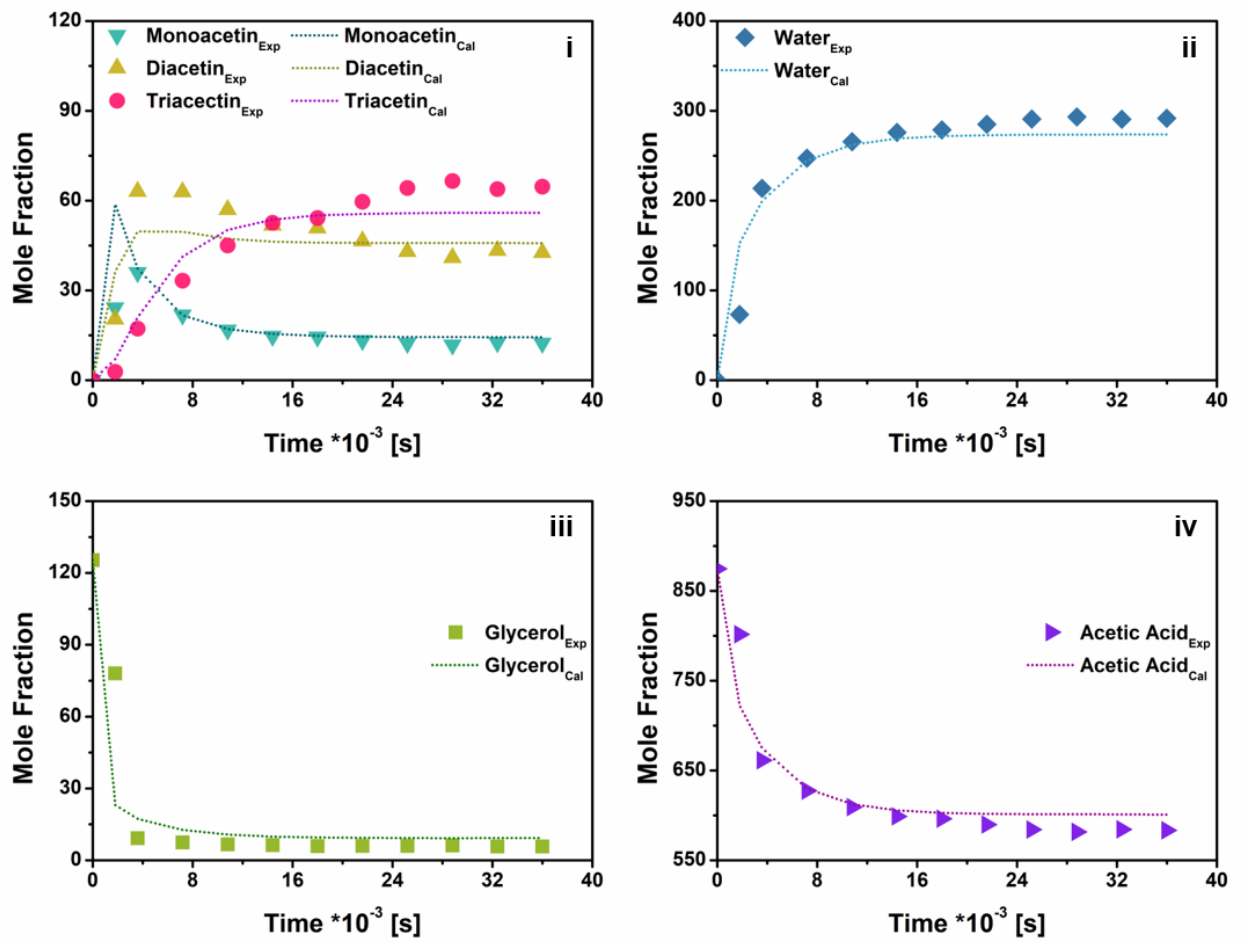

*Exp: experimental values from the experimental designs. Cal: calculated values from the developed kinetic models developed.

Figure S33. Evolution plots of the of each component in reaction 18. Glycerol esterification catalyzed by Amberlyst-35 with particle size of 25 – 75 µm. Initial acetic acid to glycerol molar ratio of 7, temperature of 373 K, and quantity of moles of active sites of 0.51 mmol. i) Acetins production. ii) water production. iii) Glycerol consumption. iv) Acetic acid consumption.

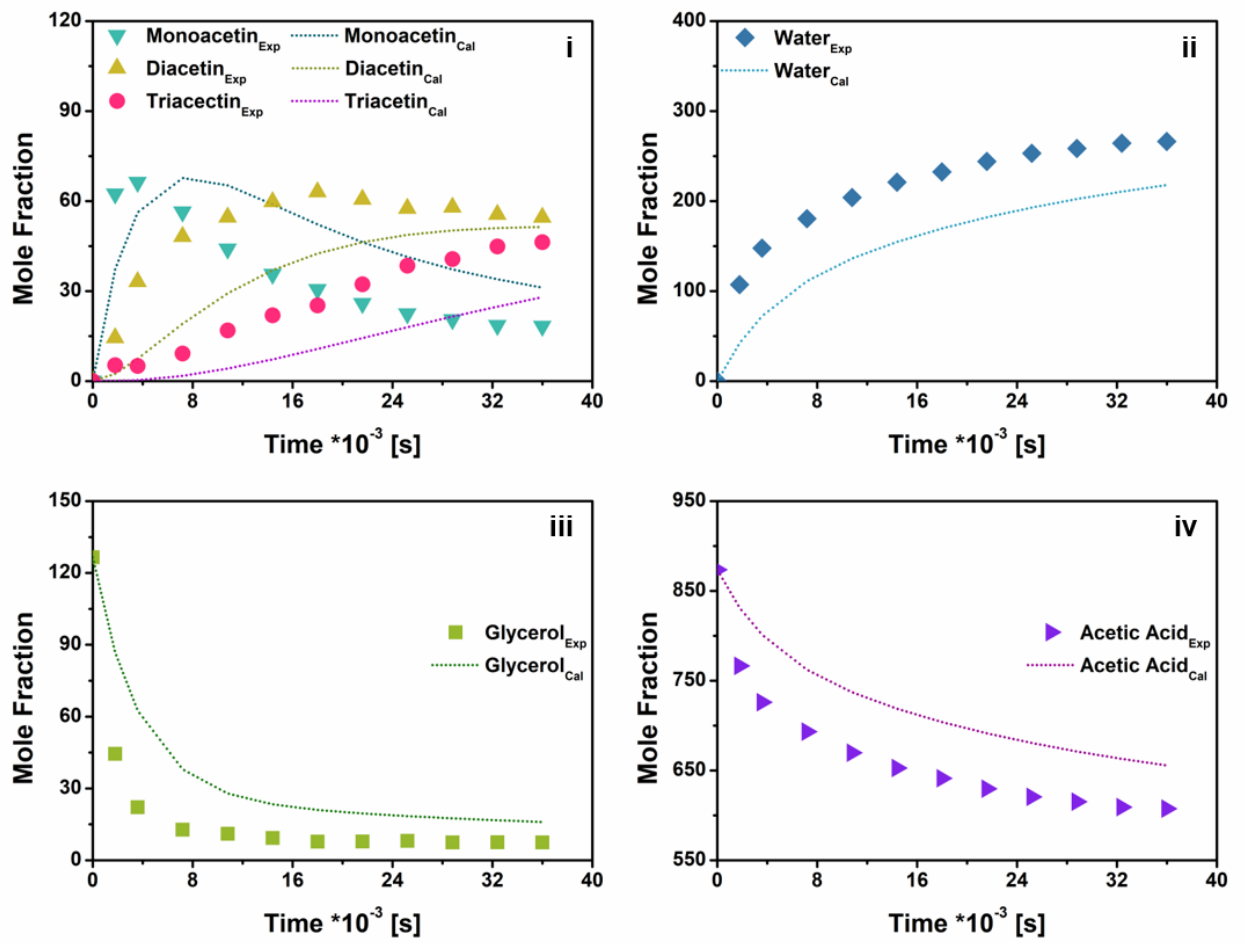

*Exp: experimental values from the experimental designs. Cal: calculated values from the developed kinetic models developed.

Figure S34. Evolution plots of the of each component in reaction 14. Glycerol esterification catalyzed by Amberlyst-35 with particle size of 25 – 75 µm. Initial acetic acid to glycerol molar ratio of 7, temperature of 361 K, and quantity of moles of active sites of 3.95 mmol. i) Acetins production. ii) water production. iii) Glycerol consumption. iv) Acetic acid consumption.

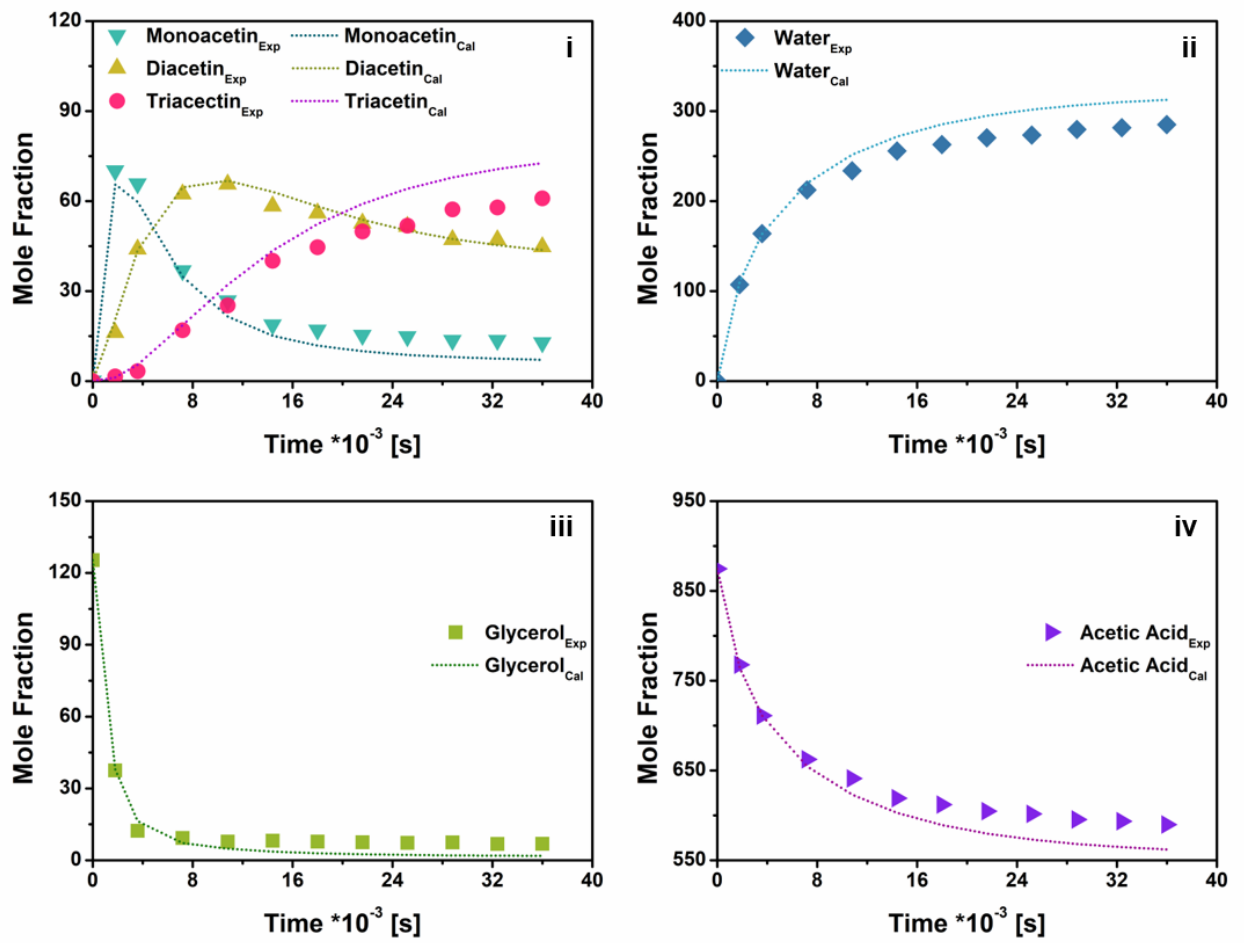

*Exp: experimental values from the experimental designs. Cal: calculated values from the developed kinetic models developed.

Figure S35. Evolution plots of the of each component in reaction 16. Glycerol esterification catalyzed by Amberlyst-35 with particle size of 25 – 75 µm. Initial acetic acid to glycerol molar ratio of 9, temperature of 361 K, and quantity of moles of active sites of 1.81 mmol. i) Acetins production. ii) water production. iii) Glycerol consumption. iv) Acetic acid consumption.

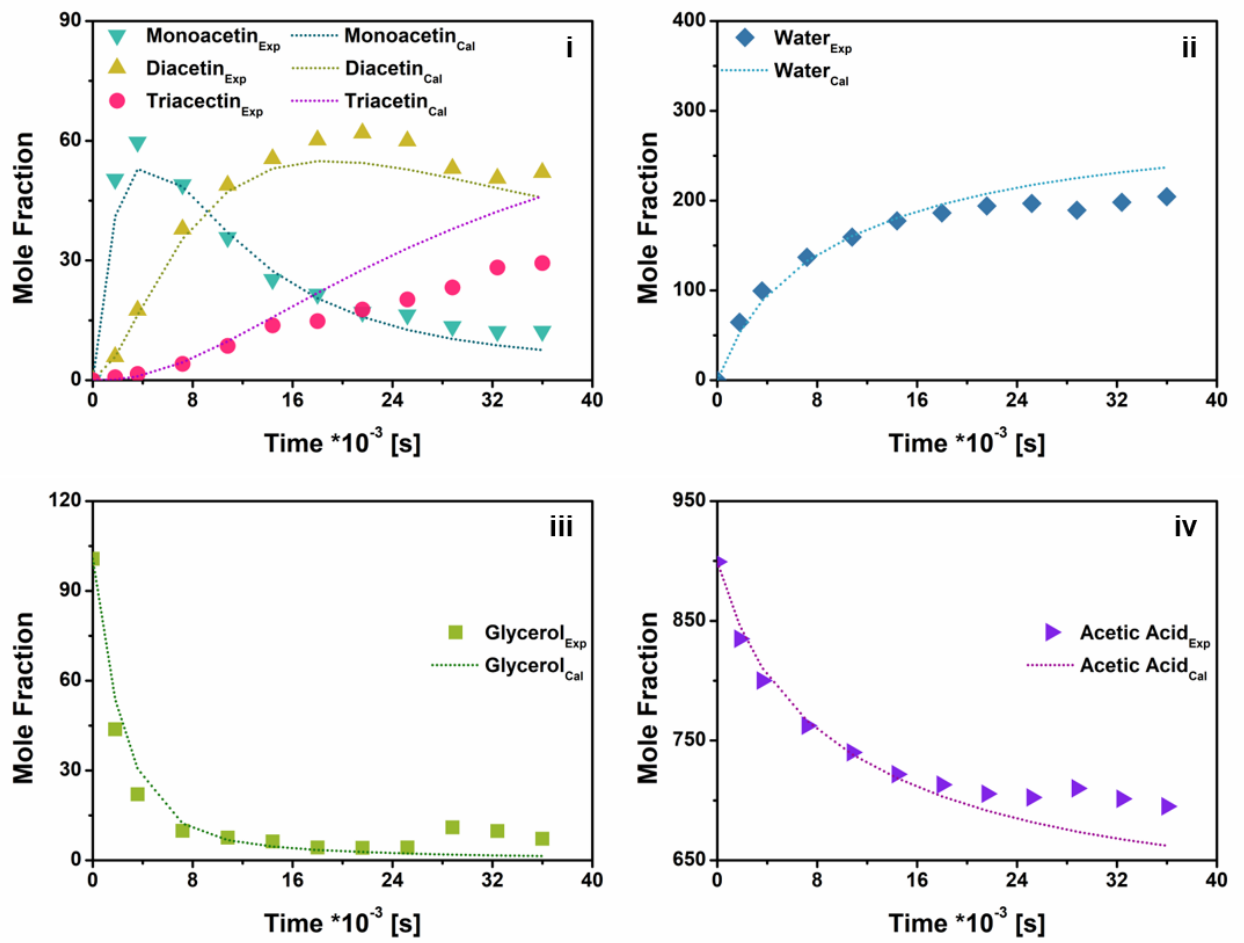

*Exp: experimental values from the experimental designs. Cal: calculated values from the developed kinetic models developed.

Figure S36. Evolution plots of the of each component in reaction 24. Glycerol esterification catalyzed by Amberlyst-35 with particle size of 25 – 75 µm. Initial acetic acid to glycerol molar ratio of 5, temperature of 373 K, and quantity of moles of active sites of 0.67 mmol. i) Acetins production. ii) water production. iii) Glycerol consumption. iv) Acetic acid consumption.

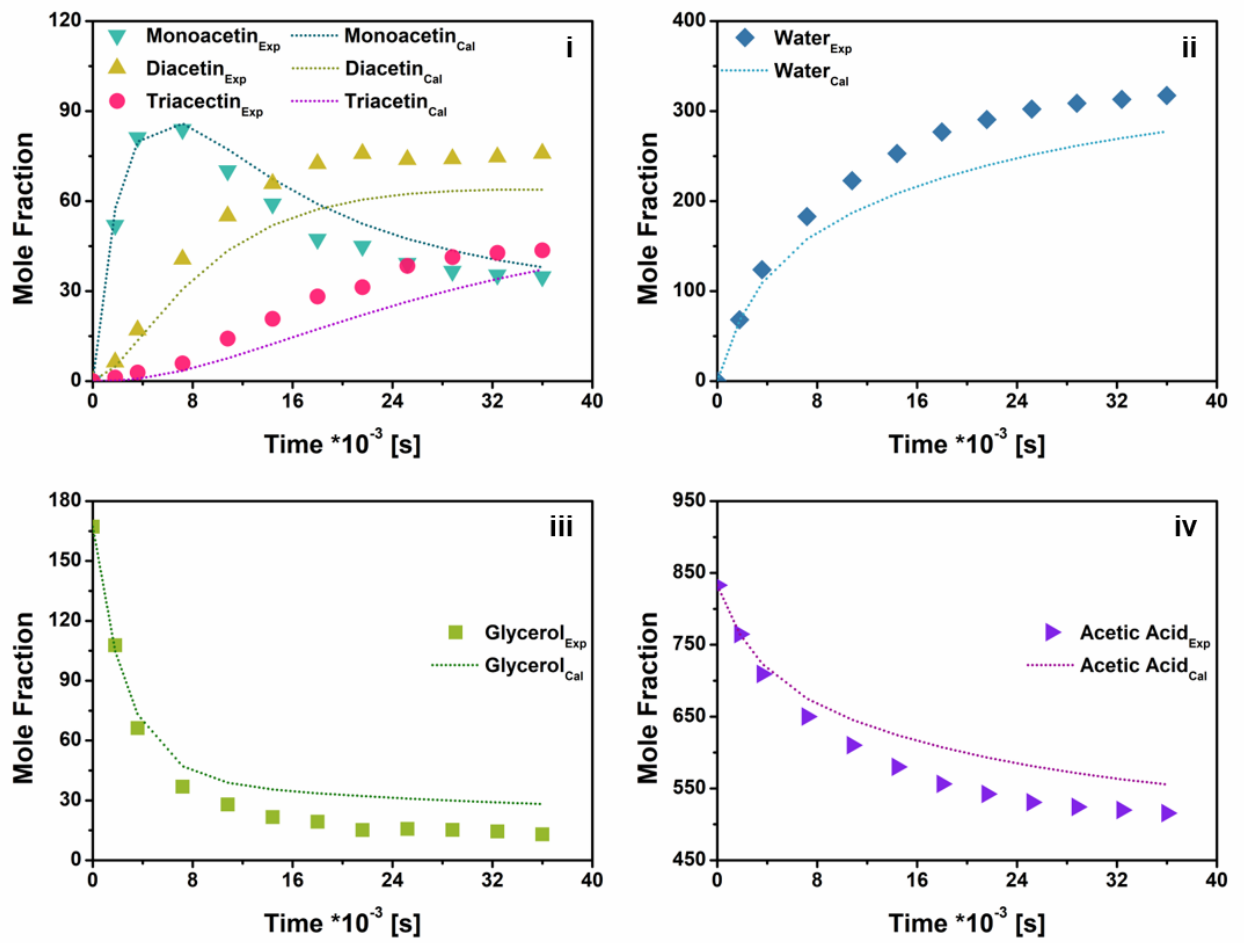

*Exp: experimental values from the experimental designs. Cal: calculated values from the developed kinetic models developed.

Figure S37. Evolution plots of the of each component in reaction 25. Glycerol esterification catalyzed by Amberlyst-35 with particle size of 25 – 75 µm. Initial acetic acid to glycerol molar ratio of 5, temperature of 361 K, and quantity of moles of active sites of 0.67 mmol. i) Acetins production. ii) water production. iii) Glycerol consumption. iv) Acetic acid consumption.

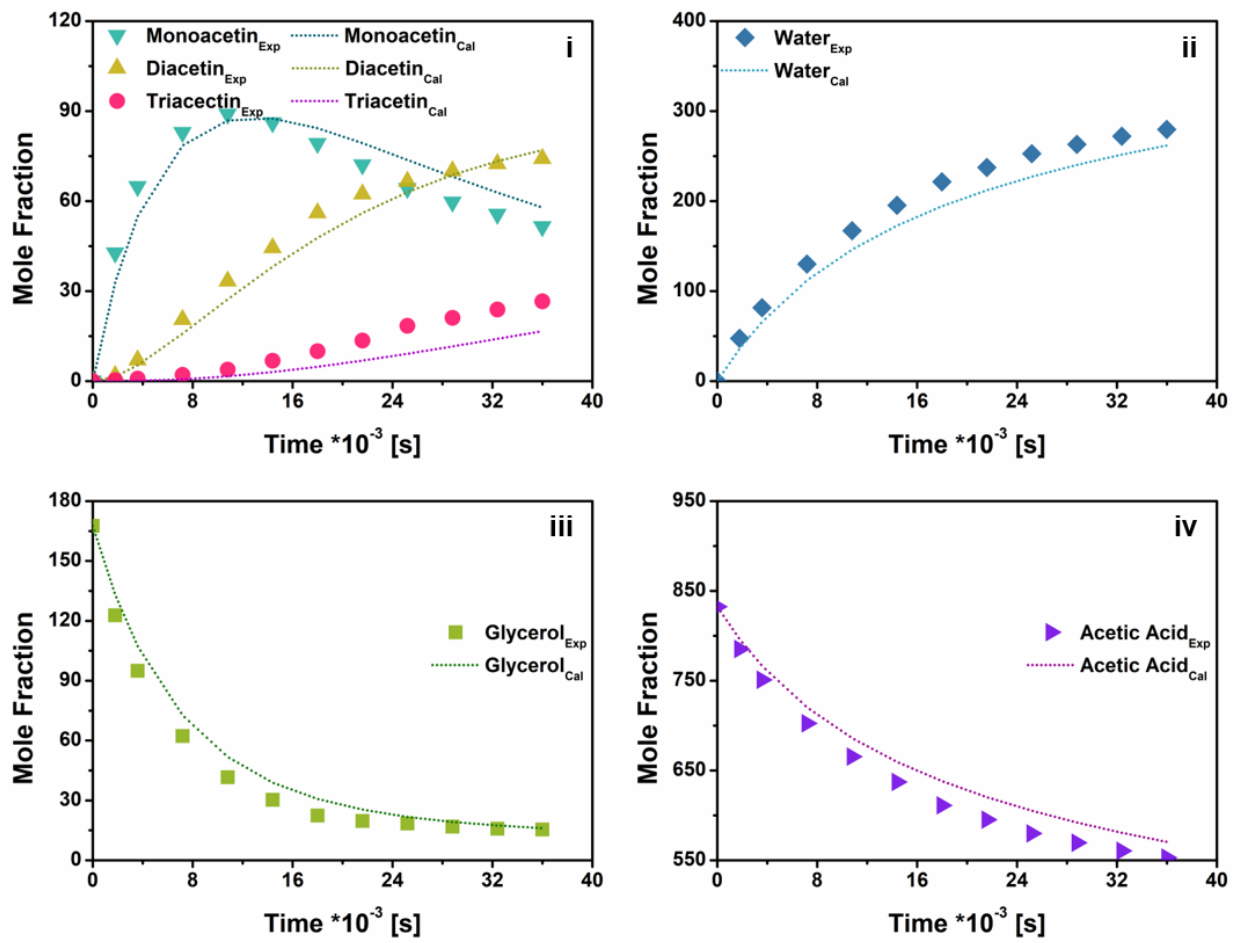

*Exp: experimental values from the experimental designs. Cal: calculated values from the developed kinetic models developed.

Figure S38. Evolution plots of the of each component in reaction 26. Glycerol esterification catalyzed by Amberlyst-35 with particle size of 25 – 75 µm. Initial acetic acid to glycerol molar ratio of 5, temperature of 373 K, and quantity of moles of active sites of 3.07 mmol. i) Acetins production. ii) water production. iii) Glycerol consumption. iv) Acetic acid consumption.

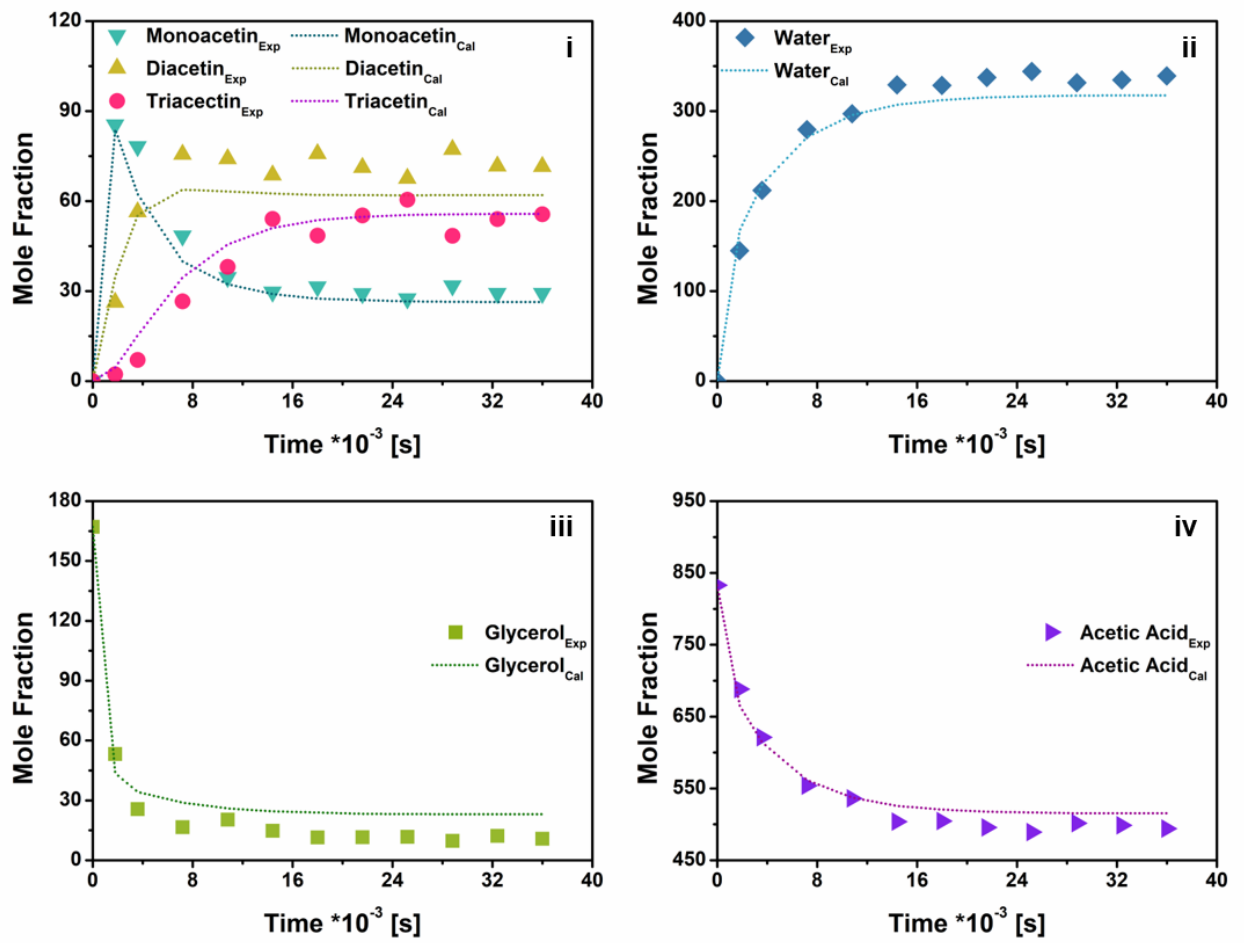

*Exp: experimental values from the experimental designs. Cal: calculated values from the developed kinetic models developed.

Figure S39. Evolution plots of the of each component in reaction 27. Glycerol esterification catalyzed by Amberlyst-35 with particle size of 25 – 75 µm. Initial acetic acid to glycerol molar ratio of 5, temperature of 361 K, and quantity of moles of active sites of 3.07 mmol. i) Acetins production. ii) water production. iii) Glycerol consumption. iv) Acetic acid consumption.

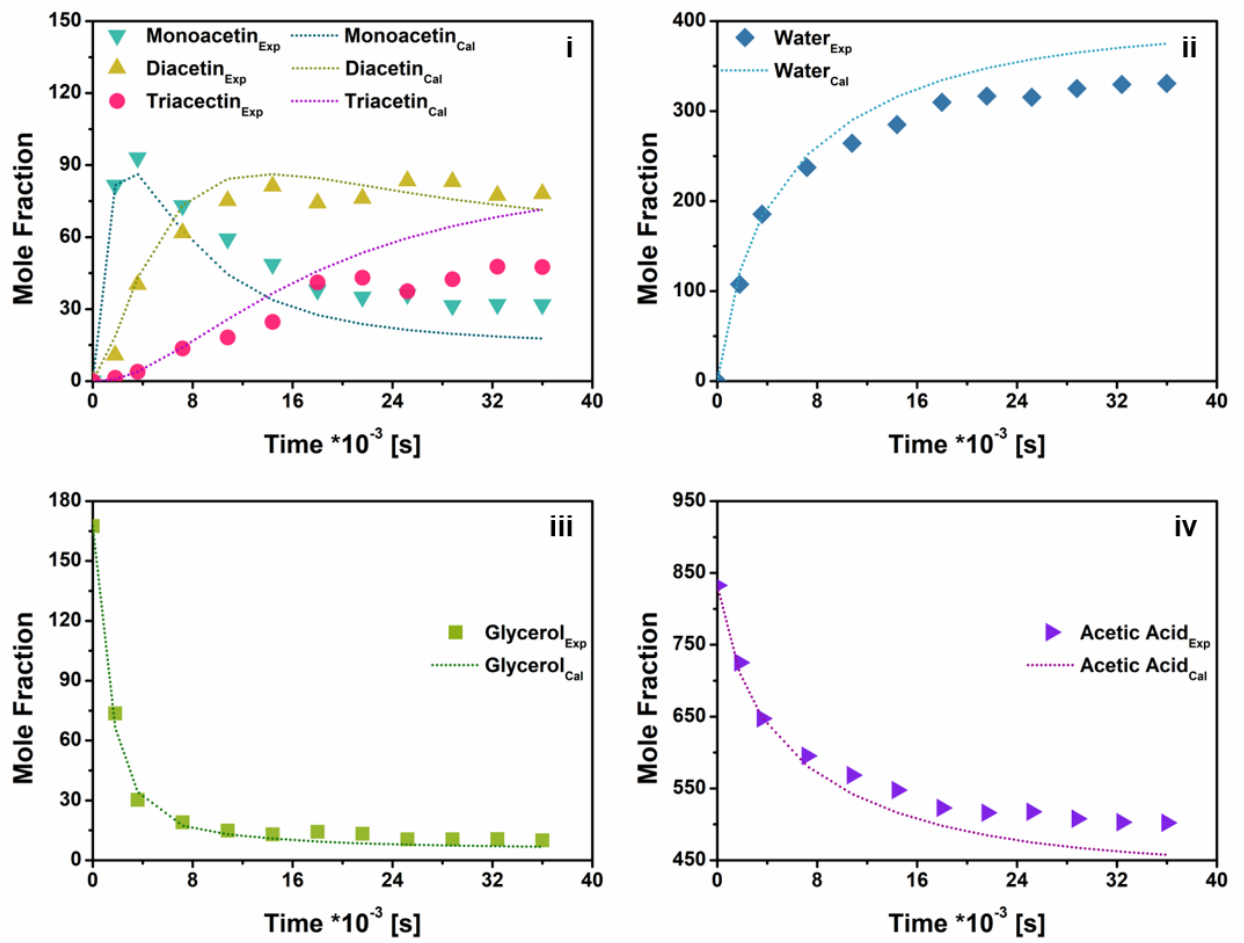

*Exp: experimental values from the experimental designs. Cal: calculated values from the developed kinetic models developed.

Supplementary Information H. Iterative process for the parameter estimation.

Scheme S40. General scheme of the Iterative process for the parameter estimation using the ODRPACK software.

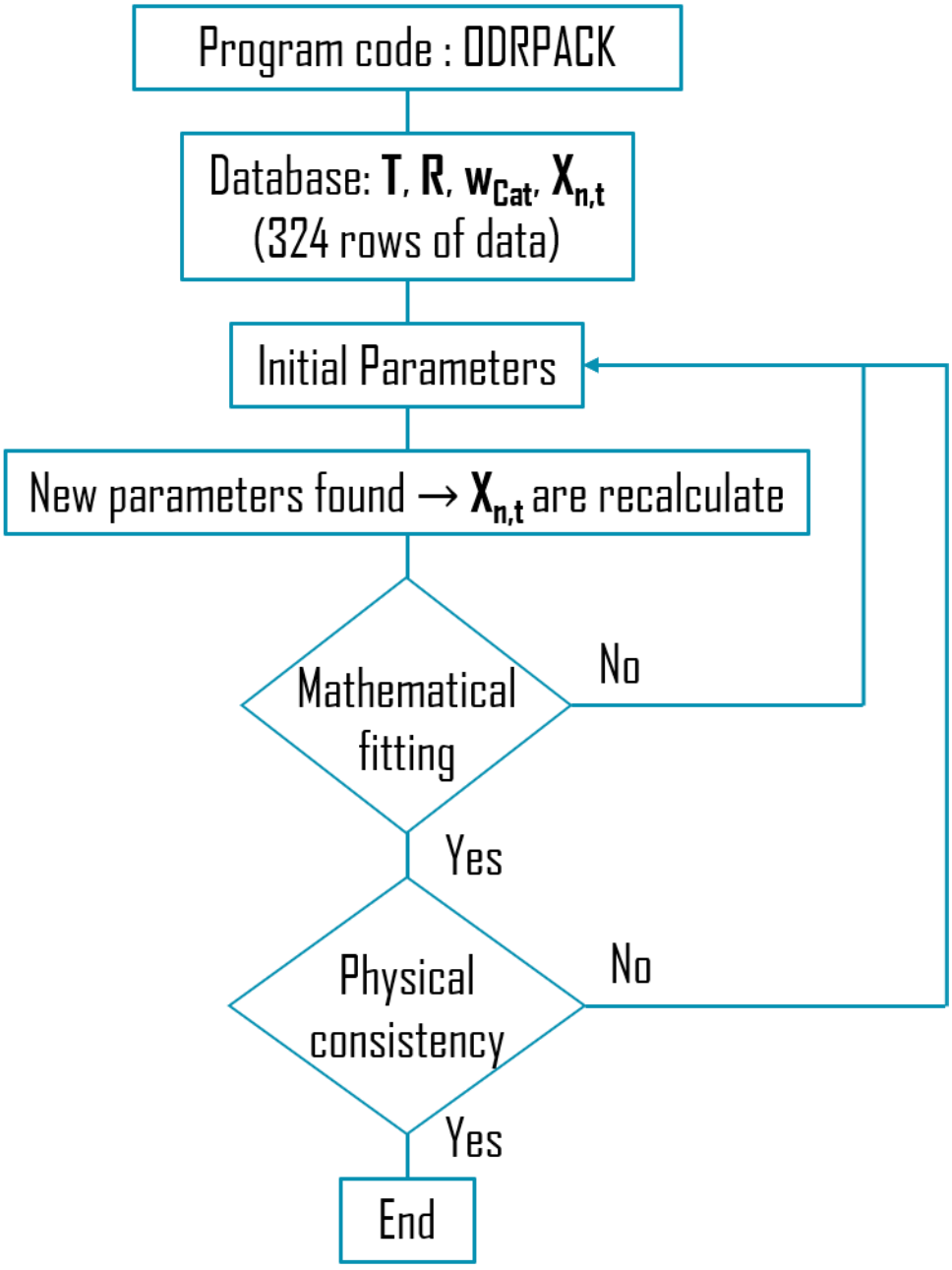

Supplementary Information I. Kinetic constants, equilibrium constants and equilibrium adsorption constants definitions.

Section S41. Kinetic constant of monoacetin formation. Forward reaction.

$$k_2 = A_2^F * exp\left[-\frac{E_{a2}^F}{R}\left(\frac{1}{T}-\frac{1}{T^*}\right)\right]$$

Section S42. Kinetic constant of diacetin formation. Forward reaction.

$$k_4 = A_4^F * exp\left[-\frac{E_{a4}^F}{R}\left(\frac{1}{T}-\frac{1}{T^*}\right)\right]$$

Section S43. Kinetic constant of triacetin formation. Forward reaction.

$$k_6 = A_6^F * exp\left[-\frac{E_{a6}^F}{R}\left(\frac{1}{T}-\frac{1}{T^*}\right)\right]$$

Section S44. Equilibrium constant of monoacetin formation.

$$K_2 = \frac{k_2}{k_{-2}}$$

Section S45. Equilibrium constant of diacetin formation.

$$K_4 = \frac{k_4}{k_{-4}}$$

Section S46. Equilibrium constant of triacetin formation.

$$K_6 = \frac{k_6}{k_{-6}}$$

Section S47. Kinetic constant of monoacetin formation. Backward reaction.

$$k_{-2} = A_2^B * exp\left[-\frac{E_{a2}^B}{R}\left(\frac{1}{T}-\frac{1}{T^*}\right)\right]$$

Section S48. Kinetic constant of diacetin formation. Backward reaction.

$$k_{-4} = A_4^B * exp\left[-\frac{E_{a4}^B}{R}\left(\frac{1}{T}-\frac{1}{T^*}\right)\right]$$

Section S49. Kinetic constant of triacetin formation. Backward reaction.

$$k_{-6} = A_6^B * exp\left[-\frac{E_{a6}^B}{R}\left(\frac{1}{T} - \frac{1}{T^*}\right)\right]$$

Section S50. Equilibrium adsorption constant of acetic acid.

$$K_A = exp\left[\frac{\Delta S_A^o}{R} - \frac{\Delta H_A^o}{R}\left(\frac{1}{T} - \frac{1}{T^*}\right)\right]$$

Section S51. Equilibrium adsorption constant of monoacetin.

$$K_M = exp\left[\frac{\Delta S_M^o}{R} - \frac{\Delta H_M^o}{R}\left(\frac{1}{T} - \frac{1}{T^*}\right)\right]$$

Section S52. Equilibrium adsorption constant of diacetin.

$$K_D = exp\left[\frac{\Delta S_D^o}{R} - \frac{\Delta H_D^o}{R}\left(\frac{1}{T} - \frac{1}{T^*}\right)\right]$$

Section S53. Equilibrium adsorption constant of triacetin.

$$K_T = exp\left[\frac{\Delta S_T^o}{R} - \frac{\Delta H_T^o}{R}\left(\frac{1}{T} - \frac{1}{T^*}\right)\right]$$

Section S54. Equilibrium adsorption constant of water.

$$K_W = exp\left[\frac{\Delta S_W^o}{R} - \frac{\Delta H_W^o}{R}\left(\frac{1}{T} - \frac{1}{T^*}\right)\right]$$